Composite Structures 335 (2024) 117995

Contents lists available at ScienceDirect

Composite Structures

journal homepage: www.elsevier.com/locate/compstruct

Thermo-Mechanical analysis of laminated Doubly-Curved Shells: Higher order Equivalent Layer-Wise formulation

Francesco Tornabene *, Matteo Viscoti, Rossana Dimitri

Department of Innovation Engineering, School of Engineering, University of Salento, 73100 Lecce, Italy

ARTICLE INFO

Keywords:
Composite materials
Equivalent layer-wise
Generalized differential quadrature
Multifield analysis
Navier solution
Stress and strain recovery
Smart structures

ABSTRACT

The paper presents a refined two-dimensional formulation for the thermo-mechanical analysis of laminated doubly-curved shell structures under thermodynamic equilibrium conditions. Both the kinematic configuration variables and the temperature variation with respect to the natural equilibrium state are described with a generalized formulation, following the Equivalent Layer-Wise (ELW) approach employing higher order polynomials, along with some proper zigzag functions. The governing equations are derived from the stationary configuration of the Helmholtz free energy of the system, and a semi-analytical solution is found. In the post-processing phase, the Fourier-based Generalized Differential Quadrature (F-GDQ) is applied to recover the actual three-dimensional response of the doubly-curved shell solid, and very accurate results are obtained for the quantities of both mechanical and heat conduction problems. In addition, the integrals occurring in the theory are performed numerically with the Taylor-based Generalized Integral Quadrature (GTIQ), showing a high level of accuracy with a reduced number of sample points. The model is validated in some case studies, where the accuracy of the model is shown, and the numerical predictions are successfully compared with those ones from refined three-dimensional numerical simulations. After that, an extensive set of parametric investigations is reported, pointing out the effects of the panel curvature, lamination schemes and different levels of coupling on the thermo-mechanical structural behavior of the investigated panels.

1. Introduction

In recent years, new applications have emerged in which structures of complex shapes are subjected to various external loads, including mechanical, thermal, electric and magnetic external forces [1,2]. For this reason, new advanced materials are adopted which can withstand to all these actions. For instance, in aerospace applications, the structural response of mechanical components must not be affected by the thermal environment, which may otherwise introduce additional stresses due to the thermal expansion phenomenon [3,4]. In the same way, the presence of an external electric or magnetic field can induce bending, potentially giving rise to some issues in the whole structural system [5–7]. Consequently, classical mechanical models are being enhanced to better predict both the structural response and the influence of other external fields.

When a smart structure is in a thermal environment, both coupled and uncoupled theoretical formulations can be employed [8–10]. In uncoupled simulations, the heat conduction problem is solved independently, and the temperature distribution is derived within the three-dimensional solid. This distribution is then used to obtain the corresponding volumetric forces which are computed as external mechanical loads applied to the structure [11–13]. On the other hand, in coupled thermo-mechanical simulations both the mechanical elasticity and heat conduction problems are simultaneously solved within the same system of equations. Therefore, additional terms are introduced into the total energy expression of the system accounting for the coupling effects between the involved physical problems [14–17].

Thermo-mechanical models can be developed using either two-dimensional (2D) and three-dimensional (3D) approaches. However, a closed form solution cannot be obtained for all possible geometries, lamination schemes and boundary conditions. Therefore, an approximate numerical solution is usually derived which can be computationally expensive, especially in 3D simulations, due to the high number of Degrees of Freedom (DOFs) involved [18–21]. For this reason, among two-dimensional theories refined formulations for doubly-curved shells are developed, incorporating Higher Order Shear Deformation Theories (HSDTs) [22–24], which account for a higher order description of the unknown field variables. In this way, an axiomatic assumption along the

* Corresponding author.
E-mail address: francesco.tornabene@unisalento.it (F. Tornabene).

https://doi.org/10.1016/j.compstruct.2024.117995
Received 10 January 2024; Received in revised form 13 February 2024; Accepted 21 February 2024
Available online 1 March 2024

thickness directions for the problem variables are made using thickness functions, dependent on the thickness coordinate, which can be either polynomial or non-polynomial [25,26]. Among two-dimensional theories, Equivalent Single Layer (ESL) and Layer-Wise (LW) approaches are adopted [25,27–30]. In addition, the Equivalent Layer-Wise (ELW) theory is introduced, which is a hybrid approach combining aspects of ESL and LW formulations, allows one to assess kinematic boundary conditions, as happens in LW models, but it requires a limited computational cost like the ESL theory [31]. In ESL and ELW theories the interaction between two adjacent laminae is kinematically described by zigzag functions [32–35] that provide a slope change in the deflection profile. Refined zigzag theories [36,37] are developed based on the mechanical properties of the actual lamination scheme, yielding very accurate results even though for a limited number of cases. In applications with complex lamination schemes with a softcore layer a generalized model is required in which variable kinematic assumptions can be made. For this reason, the unified formulation, presented for the first time in the works of Washizu and Reddy [38,39], is adopted. According to this methodology, the structural theory is developed for an arbitrary set of thickness functions. In this way, several structural theories, including the classic approaches, can be embedded within the same model [40–42]. Governing equations are derived from the computation of the total energy of the system. In thermo-mechanical problems both the mechanical and thermal energy must be evaluated [43]. In addition, the coupling effects are considered through the introduction of some additional terms. In the same way, multifield structural theories account for the computation of the total free energy of the system [44], which turns out to be made of the energy associated with all fields, and the contributions coming from coupling effects between the physical problems. In other words, the total free energy can be seen as the virtual work of all generalized forces acting on the system. The solution of a multifield problem can be found if the total energy is a thermodynamic potential, thus enabling the application of the Master Balance principle. In the same way, the fundamental equations can be derived for the thermo-mechanical case once the Helmholtz energy is derived, which depends on the deformation gradient and absolute temperature [45]. Similarly, the heat conduction equations, depending on the temperature gradient, can be derived using the same principle, yielding the well-known Fourier equations in a stationary configuration of the system [46,47].

As far as the solution of the problem is concerned, from the pioneering works by Pagano [48,49] closed-form analytical procedures have been developed to validate two-dimensional and three-dimensional models. Most of these solutions is based on the Classical Plate Theory (CPT) and the First Order Shear Deformation Theory (FSDT). These solutions are expanded in semi-analytical procedures such as those by Navier and Levy in order to provide some relevant results in practical applications [50,51]. On the other hand, the three-dimensional profiles of primary and secondary variables derived from a two-dimensional model may not satisfy a priori the equilibrium conditions along the thickness direction [52]. For this reason, a post-processing procedure has been developed [53–55], based on the three-dimensional equilibrium equations. It allows for an accurate prediction of the three-dimensional structural response starting from a refined two-dimensional solution. The correction of primary and secondary variables profiles can be performed using a numerical technique, which should not be computationally expensive. In this context, the Generalized Differential Quadrature (GDQ) [56–59], a spectral collocation method, has been proven to be a valuable alternative to the Finite Element Method (FEM), which is widely adopted in literature, and it is implemented in most commercial software [60,61]. The GDQ method provides a quadrature approximation of derivatives, enabling the solution of a differential problem directly in the strong form without relying on shape functions [62,63]. Based on a global interpolation of the field variables, it evaluates the derivative of a function as a weighted sum of the values assumed by the function itself in a computational grid. The weighting coefficients are evaluated once the interpolating basis functions of the polynomial vector space are declared. Starting from the first pioneering works by Shu, the GDQ method is based on a quadrature formula that adopts Lagrange interpolating polynomials. When Taylor's series are adopted as basis functions, the Taylor-based Differential Quadrature is obtained. In the same way, the Harmonic Differential Quadrature (HDQ) accounts for a Fourier series expansion of the given functions [64–67]. Finally, when trigonometric functions are used, the Fourier-based Generalized Differential Quadrature (F-GDQ) comes out.

Derived from the F-GDQ method, the Generalized Taylor-based Integral Quadrature (GTIQ) method provides an efficient evaluation of integrals, taking into account a reduced number of DOFs. Several previous studies demonstrate that both GDQ and GTIQ methods reach the highest level of accuracy when non-uniform computational grids are used [68,69]. These numerical methods have found extensive application in various structural problems, including bending and vibration analysis of innovative structural components [70–73], time integration formulations [74–77], and fracture and contact problems, among others. In addition, some interesting papers can be found in literature involving multifield simulations based on the GDQ method [78–83].

In this paper, an innovative ELW formulation, employing higher order theories, is presented for the evaluation of the thermo-mechanical stationary response of laminated doubly-curved shell structures made of advanced materials. The geometry of the solid is described using the differential geometry with curvilinear principal coordinates, while the mechanical behavior is modelled under the assumption of linear elastic materials. On the other hand, the heat conduction problem is addressed with the Fourier equations, expressed in principal coordinates. The present theory is built employing the unified formulation, and the ELW thickness functions enables the imposition of prescribed values on the displacement field components and temperature variation. A semi-analytical solution is derived under the assumption of an harmonic expansion of the unknown field variables. A post-processing procedure is then employed to recover the actual three-dimensional response of the structure from the higher order two-dimensional solution. The procedure in hand is performed using the F-GDQ numerical technique for derivative computation, yielding highly accurate results with a reduced number of DOFs. An extensive set of case studies is presented, evaluating the thermo-mechanical response of panels with different curvatures and lamination schemes. Results are successfully compared with predictions from refined three-dimensional simulations developed using a commercial software. Various load cases and the influence of a two-parameter elastic foundation [84], based on the Winkler-Pasternak model [85,86], are investigated. This ELW formulation is shown to predict accurately the response of structures subjected to either prescribed values of configuration variables, as well as to external pressures and thermal fluxes. Furthermore, it allows one to accurately predict the thermo-mechanical three-dimensional response of these structural components under various load shapes with a semi-analytical method. The recovery procedure, along with the F-GDQ numerical method, is shown to be an essential tool for deriving the actual distribution of primary and secondary variables from the analytical solution, even in a two-dimensional formulation, especially when lamination schemes containing softcore layers are considered. The present higher order theory is a valuable tool for thermo-mechanical simulations of curved and layered panels, providing results in line with predictions from computationally expensive models. This enables rapid and accurate parametric investigations for the design of laminated structures in thermal environment, saving the computational time.

2. Esl geometric description of a laminated shell structure

A laminated doubly-curved shell is a solid in the three-dimensional Euclidean space. Therefore, its position vector, denoted by $\mathbf{R}$, can be expressed through three different parameters $(\alpha_1, \alpha_2, \alpha_3) \in \left[\alpha_1^0, \alpha_1^1\right] \times \left[\alpha_2^0, \alpha_2^1\right] \times \left[\alpha_3^0, \alpha_3^1\right]$ as follows:

$$\mathbf{R}(\alpha_1,\alpha_2,\alpha_3)=f_1(\alpha_1,\alpha_2,\alpha_3)\mathbf{e}_1+f_2(\alpha_1,\alpha_2,\alpha_3)\mathbf{e}_2+f_3(\alpha_1,\alpha_2,\alpha_3)\mathbf{e}_3 \tag{1}$$

being $\mathbf{e}_1,\mathbf{e}_2$ and $\mathbf{e}_3$ the unit vectors of the global Cartesian coordinate system. Following to the ELW methodology, the description of the shell solid can be achieved through the geometric properties of the reference surface, located in the middle thickness of the solid. If the position vector of the surface is denoted by $\mathbf{r}(\alpha_1,\alpha_2)$, the previous relation can be expressed as [22]:

$$\mathbf{R}(\alpha_1,\alpha_2,\zeta)=\mathbf{r}(\alpha_1,\alpha_2)+\frac{h(\alpha_1,\alpha_2)}{2}z\ \mathbf{n}(\alpha_1,\alpha_2) \tag{2}$$

Here, h is the total thickness of the shell, while $z=2\zeta/h$ is a dimensionless parameter which is defined from the thickness coordinate ζ. The outward normal unit vector $\mathbf{n}(\alpha_1,\alpha_2)$ is evaluated by applying the principles of differential geometry to the reference surface $\mathbf{r}$, leading to [22]:

$$\mathbf{n}(\alpha_1,\alpha_2)=\frac{\mathbf{r}_{,1}\wedge\mathbf{r}_{,2}}{\left|\mathbf{r}_{,1}\wedge\mathbf{r}_{,2}\right|} \tag{3}$$

being $\mathbf{r}_{,i}=\partial\mathbf{r}/\partial\alpha_i$ the partial derivative of the position vector $\mathbf{r}$ with respect to $\alpha_i=\alpha_1,\alpha_2$. The total thickness of the laminated shell solid is computed as the sum of widths h_k of each layer in the stacking sequence, setting $k=1,...,l$:

$$h(\alpha_1,\alpha_2)=\sum_{k=1}^{l}h_k(\alpha_1,\alpha_2)=\sum_{k=1}^{l}(\zeta_{k+1}-\zeta_k) \tag{4}$$

where l is the total number of layers. In the previous relation, the quantities ζ_k and ζ_{k+1} denote the location along the thickness direction of the lower and the upper skin of an arbitrary k-th layer, respectively. On the other hand, the well-known Lamè parameters $A_i=A_1,A_2$ as well as the principal radii of curvature $R_i=R_1,R_2$ referred to $\alpha_i=\alpha_1,\alpha_2$ principal directions, are evaluated at each point of the reference surface as follows [22]:

$$\begin{aligned}R_i(\alpha_1,\alpha_2)&=-\frac{\mathbf{r}_{,i}\cdot\mathbf{r}_{,i}}{\mathbf{r}_{,ii}\cdot\mathbf{n}}\\ A_i(\alpha_1,\alpha_2)&=\sqrt{\mathbf{r}_{,i}\cdot\mathbf{r}_{,i}}\end{aligned} \tag{5}$$

In addition, the principal curvatures $k_{ni}=k_{n1},k_{n2}$ of the reference surface are evaluated as $k_{ni}=1/R_i$ with $i=1,2$. The curvature effect is considered along the thickness direction via the definition of the scaling quantities $H_i=H_1,H_2$ defined at each point of the three-dimensional solid in terms of the principal radii of curvature R_i introduced in Eqn. (5):

$$H_i(\alpha_1,\alpha_2,\zeta)=1+\frac{\zeta}{R_i} \tag{6}$$

In the same way, the quantities A_i of Eqn. (5) are adopted to compute the length, denoted by $ds_i=ds_1,ds_2$, of an infinitesimal arc along $\alpha_i=\alpha_1,\alpha_2$ directions:

$$ds_i=A_i d\alpha_i \tag{7}$$

The integration of the previous equation allows one to derive the curvilinear abscissa $s_i=s_1,s_2$ along $\alpha_i=\alpha_1,\alpha_2$ principal direction, defined so that $s_i\in\left[s_i^0,s_i^1\right]$. In this way, a measure of the arc length along α_i is provided within the laminated doubly-curved shell.

3. ELW assessment of the thermo-mechanical definition equations

In this section, a two-dimensional ELW model is introduced, incorporating the configuration variables of both the mechanical elasticity problem and the heat conduction problem within a solid. To this end, the vector $\mathbf{\Delta}^{(k)}(\alpha_1,\alpha_2,\zeta)$ is introduced at each point of an arbitrary k-th layer of the stacking sequence. This vector collects the three-dimensional displacement field components $U_1^{(k)},U_2^{(k)},U_3^{(k)}$, referred to the curvilinear reference system of the shell, and the temperature variation $\Delta T^{(k)}=T^{(k)}-T_0$ with respect to the natural equilibrium conditions, characterized by the absolute temperature T_0:

$$\mathbf{\Delta}^{(k)}(\alpha_1,\alpha_2,\zeta)=\begin{bmatrix}U_1^{(k)} & U_2^{(k)} & U_3^{(k)} & \Delta T^{(k)}\end{bmatrix}^T \tag{8}$$

Following the International Standard (S.I.) guidelines, the displacement field components are expressed in meters [m], whereas the kelvin [K] unit is adopted for the temperature variation. Following the ELW approach, each element of the vector $\mathbf{\Delta}^{(k)}$ is expanded up to the $N+1$-th order via the introduction of generalized thickness functions, denoted by $F_\tau^{(k)\alpha_i}=F_\tau^{(k)\alpha_i}(\zeta)$ with $\tau=0,...,N+1$ and $i=1,...,4$:

$$\begin{bmatrix}U_1^{(k)}\\U_2^{(k)}\\U_3^{(k)}\\\Delta T^{(k)}\end{bmatrix}=\sum_{\tau=0}^{N+1}\begin{bmatrix}F_\tau^{(k)\alpha_1}&0&0&0\\0&F_\tau^{(k)\alpha_2}&0&0\\0&0&F_\tau^{(k)\alpha_3}&0\\0&0&0&F_\tau^{(k)\alpha_4}\end{bmatrix}\begin{bmatrix}u_1^{(\tau)}\\u_2^{(\tau)}\\u_3^{(\tau)}\\\xi^{(\tau)}\end{bmatrix} \tag{9}$$

Here, $\mathbf{\delta}^{(\tau)}=\begin{bmatrix}u_1^{(\tau)} & u_2^{(\tau)} & u_3^{(\tau)} & \xi^{(\tau)}\end{bmatrix}^T$ is the vector of the generalized configuration variables for the thermo-mechanical problem, defined for each τ-th kinematic expansion order. Employing a compact notation, Eqn. (9) is expressed as follows [22]:

$$\mathbf{\Delta}^{(k)}=\sum_{\tau=0}^{N+1}\mathbf{F}_\tau^{(k)}\mathbf{\delta}^{(\tau)} \tag{10}$$

where $\mathbf{F}_\tau^{(k)}$ is the matrix of the generalized thickness functions associated with each τ-th order. Note that Eqn. (9) allows for the development of a generalized theory regardless of the actual expression of the thickness functions set. As a consequence, it embeds many classical theories like the FSDT and the TSDT. Furthermore, some advanced model can be considered, which can predict exotic deformations of the laminae, as well as the stretching effects that act along the thickness direction. In the present paper, higher order thickness functions are selected that can capture the zigzag effects acting between two adjacent laminae. More specifically, the following analytical expressions, taken from Ref. [22], are considered for $F_\tau^{(k)\alpha_i}$ with $\tau=0,...,N$ and $i=1,...,4$:

$$F_\tau^{(k)\alpha_i}=\begin{cases}\dfrac{1-z}{2} & \text{for } \tau=0\\ z^{\tau+1}-z^{\tau-1} & \text{for } \tau=1,..,N-1\\ \dfrac{1+z}{2} & \text{for } \tau=N\end{cases} \tag{11}$$

where the quantity z is a dimensionless parameter dependent on the thickness coordinate ζ according to the following expression:

$$z=\frac{2}{h}\zeta \tag{12}$$

The zigzag effects are modelled in Eqn. (9) by means of the thickness function reported below, referred to $\tau=N+1$, setting l the total number of laminae of the shell:

$$F_{N+1}^{(k)\alpha_i}=\begin{cases}(-1)^k\widehat{z}_k & \text{for } k=1\\ (-1)^k z_k & \text{for } k=2,...,l-1\\ (-1)^k\breve{z}_k & \text{for } k=l\end{cases} \tag{13}$$

The quantities $\widehat{z}_k,z_k$ and $\breve{z}_k$ are defined for each k-th layer of the stacking sequence as follows:

$$\begin{aligned} \widehat{z}_k &= \frac{\zeta-\zeta_k}{\zeta_{k+1}-\zeta_k} \\ z_k = \frac{2}{\zeta_{k+1}-\zeta_k}\zeta - \frac{\zeta_{k+1}+\zeta_k}{\zeta_{k+1}-\zeta_k} &= 2\overline{z}_k - 1 \\ \breve{z}_k &= \frac{\zeta-\zeta_{k+1}}{\zeta_{k+1}-\zeta_k} \end{aligned} \tag{14}$$

The following nomenclature is, thus, introduced in order to identify the thickness function set of the present generalized model:

$$\begin{matrix} \text{ELD}-N \\ \text{ELDZL}-N \end{matrix} \tag{15}$$

being N the maximum kinematic expansion order, while the symbol "ZL" is adopted when the zigzag function (13) is selected. On the other hand, the symbol "D" means that the displacement field components (D) and the temperature variation are the configuration variables of the theory, whereas "EL" indicates that these variables are modelled according to the ELW approach.

The thickness functions introduced in Eqns. (11) and (13) are defined so that the arbitrary elements $\Delta_i^{(k)}$ of the vector $\boldsymbol{\Delta}^{(k)}$ of the three-dimensional configuration variables referred to the points at heights $\zeta=-h/2$ and $\zeta=h/2$ are equal to the corresponding generalized variables $\delta_i^{(\tau)}$ of the vector $\boldsymbol{\delta}^{(\tau)}$ associated with $\tau=0$ and $\tau=N+1$, respectively. In aspect allows prescribing a value of the configuration variable at the top and the bottom surfaces of the panel within a two-dimensional model:

$$\begin{aligned} \Delta_i^{(1)}\left(\alpha_1,\alpha_2,\zeta=-\frac{h}{2}\right) &= \delta_i^{(0)}(\alpha_1,\alpha_2) \\ \Delta_i^{(l)}\left(\alpha_1,\alpha_2,\zeta=\frac{h}{2}\right) &= \delta_i^{(N)}(\alpha_1,\alpha_2) \end{aligned} \tag{16}$$

At this point, the definition equations for the present model are derived starting from the generalized kinematic assumption of Eqn. (10). To achieve this, the three-dimensional definition equations of the mechanical and heat conduction problem are considered for a doubly-curved laminated shell solid, expressed in a compact form as follows [22]:

$$\boldsymbol{\pi}^{(k)} = \mathbf{D}\boldsymbol{\Delta}^{(k)} \quad \Leftrightarrow \quad \begin{bmatrix} \boldsymbol{\varepsilon}^{(k)} \\ \widehat{\Delta\mathrm{T}}^{(k)} \\ \boldsymbol{\theta}^{(k)} \end{bmatrix} = \begin{bmatrix} \mathbf{D}_{(1)} & \mathbf{0} \\ \mathbf{0} & \mathbf{D}_{(3)} \\ \mathbf{0} & \mathbf{D}_{(2)} \end{bmatrix} \begin{bmatrix} \mathbf{U}^{(k)} \\ \Delta\mathrm{T}^{(k)} \end{bmatrix} \tag{17}$$

being $k=1,\ldots,l$, while $\boldsymbol{\varepsilon}^{(k)}, \widehat{\Delta\mathrm{T}}^{(k)}, \boldsymbol{\theta}^{(k)}$ are the vectors of the three-dimensional thermo-mechanical primary variables:

$$\begin{aligned} \boldsymbol{\varepsilon}^{(k)} &= \begin{bmatrix} \varepsilon_1^{(k)} & \varepsilon_3^{(k)} & \gamma_{12}^{(k)} & \gamma_{13}^{(k)} & \gamma_{23}^{(k)} & \varepsilon_3^{(k)} \end{bmatrix}^T \\ \widehat{\Delta\mathrm{T}}^{(k)} &= \widehat{\Delta\mathrm{T}}^{(k)}, \quad \boldsymbol{\theta}^{(k)} = \begin{bmatrix} \theta_1^{(k)} & \theta_2^{(k)} & \theta_3^{(k)} \end{bmatrix}^T \end{aligned} \tag{18}$$

As can be seen, the differential operator $\mathbf{D}$ of Eqn. (17) is defined in terms of the sub-operators $\mathbf{D}_{(1)}, \mathbf{D}_{(2)}$ and $\mathbf{D}_{(3)}$. In particular, $\mathbf{D}_{(1)}$ is the symmetric part of the definition operator of the mechanical problem, while $\mathbf{D}_{(2)}$ is the definition operator of an arbitrary scalar field. Finally, $\mathbf{D}_{(3)}=1$. The three-dimensional operator $\boldsymbol{D}$ is here modelled as the product of two matrices $\mathbf{D}_\zeta$ and $\mathbf{D}_\Omega$ according to the following expressions:

$$\mathbf{D} = \mathbf{D}_\zeta \mathbf{D}_\Omega \tag{19}$$

More specifically, the operator $\mathbf{D}_\Omega$ collects the terms involving the partial derivatives with respect to the principal coordinates of the shell α_1, α_2:

$$\mathbf{D}_\Omega = \begin{bmatrix} \mathbf{D}_{\Omega(1)} & \mathbf{0} \\ \mathbf{0} & \mathbf{D}_{\Omega(3)} \\ \mathbf{0} & \mathbf{D}_{\Omega(2)} \end{bmatrix} \tag{20}$$

The sub-operators $\mathbf{D}_{\Omega(1)}, \mathbf{D}_{\Omega(2)}$ and $\mathbf{D}_{\Omega(3)}$ occurring in the previous relation take the following form:

$$\begin{aligned} \mathbf{D}_{\Omega(1)} &= \begin{bmatrix} \overline{\mathbf{D}}_\Omega^{\alpha_1} & \overline{\mathbf{D}}_\Omega^{\alpha_2} & \overline{\mathbf{D}}_\Omega^{\alpha_3} \end{bmatrix} \\ \mathbf{D}_{\Omega(2)} &= \begin{bmatrix} -\frac{1}{A_1}\frac{\partial}{\partial\alpha_1} & -\frac{1}{A_2}\frac{\partial}{\partial\alpha_2} & -1 \end{bmatrix}^T \\ \mathbf{D}_{\Omega(3)} &= 1 \end{aligned} \tag{21}$$

where the quantities $\overline{\mathbf{D}}_\Omega^{\alpha_1}, \overline{\mathbf{D}}_\Omega^{\alpha_2}$ and $\overline{\mathbf{D}}_\Omega^{\alpha_3}$ read as:

$$\overline{\mathbf{D}}_\Omega^{\alpha_1} = \begin{bmatrix} \frac{1}{A_1}\frac{\partial}{\partial\alpha_1} \\ \frac{1}{A_1A_2}\frac{\partial A_2}{\partial\alpha_1} \\ -\frac{1}{A_1A_2}\frac{\partial A_1}{\partial\alpha_2} \\ \frac{1}{A_2}\frac{\partial}{\partial\alpha_2} \\ -\frac{1}{R_1} \\ 0 \\ 1 \\ 0 \\ 0 \end{bmatrix}, \quad \overline{\mathbf{D}}_\Omega^{\alpha_2} = \begin{bmatrix} \frac{1}{A_1A_2}\frac{\partial A_1}{\partial\alpha_2} \\ \frac{1}{A_2}\frac{\partial}{\partial\alpha_2} \\ \frac{1}{A_1}\frac{\partial}{\partial\alpha_1} \\ -\frac{1}{A_1A_2}\frac{\partial A_2}{\partial\alpha_1} \\ 0 \\ -\frac{1}{R_2} \\ 0 \\ 1 \\ 0 \end{bmatrix}, \quad \overline{\mathbf{D}}_\Omega^{\alpha_3} = \begin{bmatrix} \frac{1}{R_1} \\ \frac{1}{R_2} \\ 0 \\ 0 \\ \frac{1}{A_1}\frac{\partial}{\partial\alpha_1} \\ \frac{1}{A_2}\frac{\partial}{\partial\alpha_2} \\ 0 \\ 0 \\ 1 \end{bmatrix} \tag{22}$$

In the same way, $\mathbf{D}_\zeta$ accounts for the derivation with respect to the thickness coordinate ζ:

$$\mathbf{D}_\zeta = \begin{bmatrix} \mathbf{D}_{\zeta(1)} & \mathbf{0} & \mathbf{0} \\ \mathbf{0} & \mathbf{D}_{\zeta(3)} & \mathbf{0} \\ \mathbf{0} & \mathbf{0} & \mathbf{D}_{\zeta(2)} \end{bmatrix} \tag{23}$$

where the quantities $\mathbf{D}_{\zeta(1)}, \mathbf{D}_{\zeta(2)}$ and $\mathbf{D}_{\zeta(3)}$ are defined as follows:

$$\mathbf{D}_{\zeta(1)} = \begin{bmatrix} \frac{1}{H_1} & 0 & 0 & 0 & 0 & 0 & 0 & 0 & 0 \\ 0 & \frac{1}{H_2} & 0 & 0 & 0 & 0 & 0 & 0 & 0 \\ 0 & 0 & \frac{1}{H_1} & \frac{1}{H_2} & 0 & 0 & 0 & 0 & 0 \\ 0 & 0 & 0 & 0 & \frac{1}{H_1} & 0 & \frac{\partial}{\partial\zeta} & 0 & 0 \\ 0 & 0 & 0 & 0 & 0 & \frac{1}{H_2} & 0 & \frac{\partial}{\partial\zeta} & 0 \\ 0 & 0 & 0 & 0 & 0 & 0 & 0 & 0 & \frac{\partial}{\partial\zeta} \end{bmatrix}$$

$$\mathbf{D}_{\zeta(2)} = \begin{bmatrix} \frac{1}{H_1} & 0 & 0 \\ 0 & \frac{1}{H_2} & 0 \\ 0 & 0 & \frac{\partial}{\partial\zeta} \end{bmatrix}, \quad \mathbf{D}_{\zeta(3)} = 1 \tag{24}$$

Finally, the differential operator $\mathbf{D}_\Omega$ is conveniently expressed as the sum of the operators $\mathbf{D}_\Omega^{\alpha_i}$ with $i=1,\ldots,4$:

$$\mathbf{D}_\Omega = \sum_{i=1}^{4} \mathbf{D}_\Omega^{\alpha_i} \tag{25}$$

The quantities $\mathbf{D}_\Omega^{\alpha_i}$ assume the following extended matrix form, setting $\overline{\mathbf{D}}_\Omega^{\alpha_4} = \mathbf{D}_{\Omega(2)}$ and $\overline{\mathbf{D}}_\Omega^{\alpha_4} = \mathbf{D}_{\Omega(3)}$:

$$\mathbf{D}_{\Omega}^{\alpha_1}=\begin{bmatrix}\overline{\mathbf{D}}_{\Omega}^{\alpha_1} & \mathbf{0} & \mathbf{0} & \mathbf{0}\\ \mathbf{0} & \mathbf{0} & \mathbf{0} & \mathbf{0}\\ \mathbf{0} & \mathbf{0} & \mathbf{0} & \mathbf{0}\end{bmatrix},\quad \mathbf{D}_{\Omega}^{\alpha_2}=\begin{bmatrix}\mathbf{0} & \overline{\mathbf{D}}_{\Omega}^{\alpha_2} & \mathbf{0} & \mathbf{0}\\ \mathbf{0} & \mathbf{0} & \mathbf{0} & \mathbf{0}\\ \mathbf{0} & \mathbf{0} & \mathbf{0} & \mathbf{0}\end{bmatrix},$$
$$\mathbf{D}_{\Omega}^{\alpha_3}=\begin{bmatrix}\mathbf{0} & \mathbf{0} & \overline{\mathbf{D}}_{\Omega}^{\alpha_3} & \mathbf{0}\\ \mathbf{0} & \mathbf{0} & \mathbf{0} & \mathbf{0}\\ \mathbf{0} & \mathbf{0} & \mathbf{0} & \mathbf{0}\end{bmatrix},\quad \mathbf{D}_{\Omega}^{\alpha_4}=\begin{bmatrix}\mathbf{0} & \mathbf{0} & \mathbf{0} & \mathbf{0}\\ \mathbf{0} & \mathbf{0} & \mathbf{0} & \overline{\mathbf{D}}_{\Omega}^{\alpha_4}\\ \mathbf{0} & \mathbf{0} & \mathbf{0} & \widetilde{\mathbf{D}}_{\Omega}^{\alpha_4}\end{bmatrix} \tag{26}$$

Once the definition equations are introduced for a three-dimensional solid, they are embedded within the ELW model by substituting Eqn. (10) in Eqn. (17), as extensively shown in Ref. [22]:

$$\boldsymbol{\pi}^{(k)}=\mathbf{D}\boldsymbol{\Delta}^{(k)}=\mathbf{D}_{\zeta}\mathbf{D}_{\Omega}\boldsymbol{\Delta}^{(k)}=\mathbf{D}_{\zeta}\sum_{i=1}^{4}\mathbf{D}_{\Omega}^{\alpha_i}\boldsymbol{\Delta}^{(k)}=$$
$$=\sum_{\tau=0}^{N+1}\sum_{i=1}^{4}\mathbf{D}_{\zeta}\mathbf{D}_{\Omega}^{\alpha_i}\mathbf{F}_{\tau}^{(k)}\boldsymbol{\delta}^{(\tau)}=\sum_{\tau=0}^{N+1}\sum_{i=1}^{4}\mathbf{D}_{\zeta}F_{\tau}^{(k)\alpha_i}\mathbf{D}_{\Omega}^{\alpha_i}\boldsymbol{\delta}^{(\tau)}=\sum_{\tau=0}^{N+1}\sum_{i=1}^{4}\mathbf{Z}^{(k\tau)\alpha_i}\mathbf{D}_{\Omega}^{\alpha_i}\boldsymbol{\delta}^{(\tau)}=\sum_{\tau=0}^{N+1}\sum_{i=1}^{4}\mathbf{Z}^{(k\tau)\alpha_i}\boldsymbol{\pi}^{(\tau)\alpha_i} \tag{27}$$

As can be seen, the vector $\boldsymbol{\pi}^{(k)}$ of the three-dimensional primary variables, introduced in Eqn. (17), is expanded up to the $N+1$-th order. In this way, the vector of the generalized primary variables, denoted by $\boldsymbol{\pi}^{(\tau)\alpha_i}$, is introduced for each $\tau=0,\ldots,N+1$ and $i=1,\ldots,4$. Employing a matrix notation, the previous relation can be expressed as follows [22]:

$$\begin{bmatrix}\sigma_1^{(k)}\\ \sigma_2^{(k)}\\ \tau_{12}^{(k)}\\ \tau_{13}^{(k)}\\ \tau_{23}^{(k)}\\ \sigma_3^{(k)}\\ \hline \eta^{(k)}\\ \hline h_1^{(k)}\\ h_2^{(k)}\\ h_3^{(k)}\end{bmatrix}=\left[\begin{array}{cccccc|c|ccc}\overline{C}_{11}^{(k)} & \overline{C}_{12}^{(k)} & \overline{C}_{16}^{(k)} & \overline{C}_{14}^{(k)} & \overline{C}_{15}^{(k)} & \overline{C}_{13}^{(k)} & -\overline{z}_{11}^{(k)} & 0 & 0 & 0\\ \overline{C}_{12}^{(k)} & \overline{C}_{22}^{(k)} & \overline{C}_{26}^{(k)} & \overline{C}_{24}^{(k)} & \overline{C}_{25}^{(k)} & \overline{C}_{23}^{(k)} & -\overline{z}_{22}^{(k)} & 0 & 0 & 0\\ \overline{C}_{16}^{(k)} & \overline{C}_{26}^{(k)} & \overline{C}_{66}^{(k)} & \overline{C}_{46}^{(k)} & \overline{C}_{56}^{(k)} & \overline{C}_{36}^{(k)} & -\overline{z}_{12}^{(k)} & 0 & 0 & 0\\ \overline{C}_{14}^{(k)} & \overline{C}_{24}^{(k)} & \overline{C}_{46}^{(k)} & \overline{C}_{44}^{(k)} & \overline{C}_{45}^{(k)} & \overline{C}_{34}^{(k)} & -\overline{z}_{13}^{(k)} & 0 & 0 & 0\\ \overline{C}_{15}^{(k)} & \overline{C}_{25}^{(k)} & \overline{C}_{56}^{(k)} & \overline{C}_{45}^{(k)} & \overline{C}_{55}^{(k)} & \overline{C}_{35}^{(k)} & -\overline{z}_{23}^{(k)} & 0 & 0 & 0\\ \overline{C}_{13}^{(k)} & \overline{C}_{23}^{(k)} & \overline{C}_{36}^{(k)} & \overline{C}_{34}^{(k)} & \overline{C}_{35}^{(k)} & \overline{C}_{33}^{(k)} & -\overline{z}_{33}^{(k)} & 0 & 0 & 0\\ \hline \overline{z}_{11}^{(k)} & \overline{z}_{22}^{(k)} & \overline{z}_{12}^{(k)} & \overline{z}_{13}^{(k)} & \overline{z}_{23}^{(k)} & \overline{z}_{33}^{(k)} & \overline{\xi}_{11}^{(k)} & 0 & 0 & 0\\ \hline 0 & 0 & 0 & 0 & 0 & 0 & 0 & \overline{k}_{11}^{(k)} & \overline{k}_{12}^{(k)} & \overline{k}_{13}^{(k)}\\ 0 & 0 & 0 & 0 & 0 & 0 & 0 & \overline{k}_{21}^{(k)} & \overline{k}_{22}^{(k)} & \overline{k}_{23}^{(k)}\\ 0 & 0 & 0 & 0 & 0 & 0 & 0 & \overline{k}_{31}^{(k)} & \overline{k}_{32}^{(k)} & \overline{k}_{33}^{(k)}\end{array}\right]\begin{bmatrix}\varepsilon_1^{(k)}\\ \varepsilon_2^{(k)}\\ \gamma_{12}^{(k)}\\ \gamma_{13}^{(k)}\\ \gamma_{23}^{(k)}\\ \varepsilon_3^{(k)}\\ \hline \widehat{\Delta\mathrm{T}}^{(k)}\\ \hline \theta_1^{(k)}\\ \theta_2^{(k)}\\ \theta_3^{(k)}\end{bmatrix} \tag{31}$$

$$\boldsymbol{\pi}^{(k)}=\sum_{\tau=0}^{N+1}\sum_{i=1}^{4}\mathbf{Z}^{(k\tau)\alpha_i}\boldsymbol{\pi}^{(\tau)\alpha_i}\quad\Leftrightarrow\quad\begin{bmatrix}\boldsymbol{\varepsilon}^{(k)}\\ \widehat{\Delta\mathrm{T}}^{(k)}\\ \boldsymbol{\theta}^{(k)}\end{bmatrix}$$
$$=\sum_{\tau=0}^{N+1}\sum_{i=1}^{4}\begin{bmatrix}\mathbf{Z}_1^{(k\tau)\alpha_i} & \mathbf{0} & \mathbf{0}\\ \mathbf{0} & \mathbf{Z}_3^{(k\tau)\alpha_i} & \mathbf{0}\\ \mathbf{0} & \mathbf{0} & \mathbf{Z}_2^{(k\tau)\alpha_i}\end{bmatrix}\begin{bmatrix}\boldsymbol{\varepsilon}^{(\tau)\alpha_i}\\ \widehat{\Delta\mathrm{T}}^{(\tau)\alpha_i}\\ \boldsymbol{\theta}^{(\tau)\alpha_i}\end{bmatrix} \tag{28}$$

where the vectors $\boldsymbol{\varepsilon}^{(\tau)\alpha_i}$, $\widehat{\Delta\mathrm{T}}^{(\tau)\alpha_i}$ and $\boldsymbol{\theta}^{(\tau)\alpha_i}$ collect the generalized primary variables of the thermo-mechanical problem:

$$\widehat{\Delta\mathrm{T}}^{(\tau)\alpha_i}(\alpha_1,\alpha_2)=\widehat{\Delta\mathrm{T}}^{(\tau)\alpha_i},\quad\boldsymbol{\theta}^{(\tau)\alpha_i}(\alpha_1,\alpha_2)=\begin{bmatrix}\theta_1^{(\tau)\alpha_i} & \theta_2^{(\tau)\alpha_i} & \theta_3^{(\tau)\alpha_i}\end{bmatrix}^T$$
$$\boldsymbol{\varepsilon}^{(\tau)\alpha_i}(\alpha_1,\alpha_2)=\begin{bmatrix}\varepsilon_1^{(\tau)\alpha_i} & \varepsilon_2^{(\tau)\alpha_i} & \gamma_1^{(\tau)\alpha_i} & \gamma_2^{(\tau)\alpha_i} & \gamma_{13}^{(\tau)\alpha_i} & \gamma_{23}^{(\tau)\alpha_i} & \omega_{13}^{(\tau)\alpha_i} & \omega_{23}^{(\tau)\alpha_i} & \varepsilon_3^{(\tau)\alpha_i}\end{bmatrix}^T \tag{29}$$

The matrices $\mathbf{Z}_1^{(k\tau)\alpha_i}$, $\mathbf{Z}_2^{(k\tau)\alpha_i}$ and $\mathbf{Z}_3^{(k\tau)\alpha_i}$ introduced in Eqn. (28) are written in terms of the corresponding thickness function $F_{\tau}^{(k)\alpha_i}$ according to the following expression:

$$\mathbf{Z}_m^{(k\tau)\alpha_i}=\mathbf{D}_{\zeta(m)}F_{\tau}^{(k)\alpha_i}\quad m=1,2,3 \tag{30}$$

4. Constitutive equations

In the present work, an arbitrary k-th layer of the doubly-curved shell solid is modelled as a linear elastic generally anisotropic material [22], accounting for both the mechanical and the heat conduction problem. To this end, the following constitutive relation is considered in each point of the solid, written with respect to the curvilinear reference system of the shell:

In a more compact form, the previous equation takes the following form:

$$\boldsymbol{\chi}^{(k)}=\overline{\boldsymbol{\Gamma}}^{(k)}\boldsymbol{\pi}^{(k)}\quad\Leftrightarrow\quad\begin{bmatrix}\boldsymbol{\sigma}^{(k)}\\ \eta^{(k)}\\ \mathbf{h}^{(k)}\end{bmatrix}=\begin{bmatrix}\overline{\boldsymbol{\Gamma}}_{\mathrm{C}}^{(k)} & -\overline{\boldsymbol{\Gamma}}_{z}^{(k)T} & \mathbf{0}\\ \overline{\boldsymbol{\Gamma}}_{z}^{(k)} & \overline{\boldsymbol{\Gamma}}_{\mathrm{TT}}^{(k)} & \mathbf{0}\\ \mathbf{0} & \mathbf{0} & \overline{\boldsymbol{\Gamma}}_{\mathrm{K}}^{(k)}\end{bmatrix}\begin{bmatrix}\boldsymbol{\varepsilon}^{(k)}\\ \widehat{\Delta\mathrm{T}}^{(k)}\\ \boldsymbol{\theta}^{(k)}\end{bmatrix} \tag{32}$$

where the vectors $\boldsymbol{\sigma}^{(k)}=\begin{bmatrix}\sigma_1^{(k)} & \sigma_2^{(k)} & \tau_{12}^{(k)} & \tau_{13}^{(k)} & \tau_{23}^{(k)} & \sigma_3^{(k)}\end{bmatrix}^T$ and $\mathbf{h}^{(k)}=\begin{bmatrix}h_1^{(k)} & h_2^{(k)} & h_3^{(k)}\end{bmatrix}^T$ collect the three-dimensional stress components and the heat flux components, respectively, while the scalar quantity $\eta^{(k)}$ denotes the specific entropy of the system. The multifield stiffness matrix $\overline{\boldsymbol{\Gamma}}^{(k)}$ contains the sub-matrices $\overline{\boldsymbol{\Gamma}}_{\mathrm{C}}^{(k)}$ and $\overline{\boldsymbol{\Gamma}}_{\mathrm{K}}^{(k)}$, which are the three-dimensional stiffness matrix and the conductivity matrix, respectively. The matrix $\overline{\boldsymbol{\Gamma}}_{\mathrm{TT}}^{(k)}=\overline{\xi}_{11}^{(k)}=\rho^{(k)}c^{(k)}/\mathrm{T}_0$ is a 1×1 matrix that allows expressing the specific entropy $\eta^{(k)}$ in terms of the temperature variation $\widehat{\Delta\mathrm{T}}^{(k)}=\Delta\mathrm{T}^{(k)}$, being $\rho^{(k)}$ and $c^{(k)}$ the density and the specific heat of the constituent material, respectively. Finally, $\overline{\boldsymbol{\Gamma}}_{z}^{(k)}$ accounts for the coupling

between the heat conduction problem and the mechanical elasticity equations. The thermo-mechanical constitutive matrix $\overline{\mathbf{\Gamma}}^{(k)}$ occurring in Eqn. (32), written in the geometric reference system, is obtained from the rotation of the matrix $\mathbf{\Gamma}^{(k)}$ written for each point of the three-dimensional solid in the material reference system of the k-th layer, denoted by $O'\widehat{\alpha}_1^{(k)}\widehat{\alpha}_2^{(k)}\widehat{\zeta}^{(k)}$. In this way, the constitutive relation (32) can be expressed in terms of the vectors of the primary and secondary variables $\widehat{\boldsymbol{\pi}}^{(k)}$ and $\widehat{\boldsymbol{\chi}}^{(k)}$, respectively, referred to $O'\widehat{\alpha}_1^{(k)}\widehat{\alpha}_2^{(k)}\widehat{\zeta}^{(k)}$:

$$\widehat{\boldsymbol{\chi}}^{(k)} = \mathbf{\Gamma}^{(k)}\widehat{\boldsymbol{\pi}}^{(k)} \;\Leftrightarrow\; \begin{bmatrix} \widehat{\boldsymbol{\sigma}}^{(k)} \\ \eta^{(k)} \\ \widehat{\mathbf{h}}^{(k)} \end{bmatrix} = \begin{bmatrix} \mathbf{\Gamma}_{\mathrm{C}}^{(k)} & -\mathbf{\Gamma}_{\mathrm{z}}^{(k)T} & \mathbf{0} \\ \mathbf{\Gamma}_{\mathrm{z}}^{(k)} & \mathbf{\Gamma}_{\mathrm{TT}}^{(k)} & \mathbf{0} \\ \mathbf{0} & \mathbf{0} & \mathbf{\Gamma}_{\mathrm{K}}^{(k)} \end{bmatrix} \begin{bmatrix} \widehat{\boldsymbol{\varepsilon}}^{(k)} \\ \widehat{\Delta \mathrm{T}}^{(k)} \\ \widehat{\boldsymbol{\theta}}^{(k)} \end{bmatrix} \tag{33}$$

In the present study, it is assumed that the material and geometric reference systems have the same origin. Furthermore, the planes $\widehat{\alpha}_1^{(k)} - \widehat{\alpha}_2^{(k)}$ and $\alpha_1 - \alpha_2$ are parallel, therefore the identity $\widehat{\zeta}^{(k)} = \zeta$ can be considered. In other words, the material axis $\widehat{\alpha}_1^{(k)}$ is rotated by an angle $\vartheta^{(k)}$ with respect to α_1. As a consequence, the following rotation matrices $\mathbf{H}^{(k)}$ and $\mathbf{T}^{(k)}$ are conveniently introduced [22]:

$$\mathbf{H}^{(k)} = \begin{bmatrix} \cos\vartheta^{(k)} & \sin\vartheta^{(k)} & 0 \\ -\sin\vartheta^{(k)} & \cos\vartheta^{(k)} & 0 \\ 0 & 0 & 1 \end{bmatrix} \tag{34}$$

$$\mathbf{T}^{(k)} = \begin{bmatrix} \cos^2\vartheta^{(k)} & \sin^2\vartheta^{(k)} & -2\sin\vartheta^{(k)}\cos\vartheta^{(k)} & 0 & 0 & 0 \\ \sin^2\vartheta^{(k)} & \cos^2\vartheta^{(k)} & 2\sin\vartheta^{(k)}\cos\vartheta^{(k)} & 0 & 0 & 0 \\ \sin\vartheta^{(k)}\cos\vartheta^{(k)} & -\sin\vartheta^{(k)}\cos\vartheta^{(k)} & \cos^2\vartheta^{(k)} - \sin^2\vartheta^{(k)} & 0 & 0 & 0 \\ 0 & 0 & 0 & \cos\vartheta^{(k)} & -\sin\vartheta^{(k)} & 0 \\ 0 & 0 & 0 & \sin\vartheta^{(k)} & \cos\vartheta^{(k)} & 0 \\ 0 & 0 & 0 & 0 & 0 & 1 \end{bmatrix} \tag{35}$$

$$\overline{\mathbf{\Gamma}}_{\mathrm{z}}^{(k)T} = \overline{\mathbf{\Gamma}}_{\mathrm{C}}^{(k)}\overline{\mathbf{\Gamma}}_{\mathrm{a}}^{(k)} \tag{37}$$

where $\overline{\mathbf{\Gamma}}_{\mathrm{a}}^{(k)}$ is the vector of the rotated quantities $\overline{a}_{ij}^{(k)}$ with $i,j = 1,2,3$, conveniently arranged in the matrix $\overline{\mathbf{A}}^{(k)}$ defined as:

$$\overline{\mathbf{A}}^{(k)} = \mathbf{Y}_{\varepsilon} \odot \left(\mathbf{H}^{(k)T} \widehat{\mathbf{A}}^{(k)} \mathbf{H}^{(k)} \right) \tag{38}$$

setting $\odot$ as the well-known Hadamard product. In the previous relation, $\mathbf{Y}_{\varepsilon}$ is the matrix that allows for the conversion between the engineering strain components and the strain components. If the thermal expansion coefficients $\widehat{a}_{ij}^{(k)}$ of the constitutive material are collected in the matrix $\widehat{\mathbf{A}}^{(k)}$, one gets:

$$\mathbf{A}^{(k)} = \begin{bmatrix} a_{11}^{(k)} & a_{12}^{(k)} & a_{13}^{(k)} \\ a_{12}^{(k)} & a_{22}^{(k)} & a_{23}^{(k)} \\ a_{13}^{(k)} & a_{23}^{(k)} & a_{33}^{(k)} \end{bmatrix} = \begin{bmatrix} 1 & 2 & 2 \\ 2 & 1 & 2 \\ 2 & 2 & 1 \end{bmatrix} \odot \begin{bmatrix} \widehat{a}_{11}^{(k)} & \widehat{a}_{12}^{(k)} & \widehat{a}_{13}^{(k)} \\ \widehat{a}_{12}^{(k)} & \widehat{a}_{22}^{(k)} & \widehat{a}_{23}^{(k)} \\ \widehat{a}_{13}^{(k)} & \widehat{a}_{23}^{(k)} & \widehat{a}_{33}^{(k)} \end{bmatrix} = \mathbf{Y}_{\varepsilon} \odot \widehat{\mathbf{A}}^{(k)} \tag{39}$$

The three-dimensional thermo-mechanical constitutive relation (32) is embedded in the generalized ELW model through the evaluation of the virtual variation of the total free energy of the system Y [22], remembering the kinematic assumptions of Eqn. (10):

$$\begin{aligned} \delta Y &= \sum_{k=1}^{l} \int_{\alpha_1} \int_{\alpha_2} \int_{\zeta_k}^{\zeta_{k+1}} \left(\delta\overline{\boldsymbol{\pi}}^{(k)T} \overline{\boldsymbol{\chi}}^{(k)} \right) A_1 A_2 H_1 H_2 d\alpha_1 d\alpha_2 d\zeta = \\ &= \sum_{k=1}^{l} \int_{\alpha_1} \int_{\alpha_2} \int_{\zeta_k}^{\zeta_{k+1}} \left(\delta\boldsymbol{\varepsilon}^{(k)T} \boldsymbol{\sigma}^{(k)} - \eta^{(k)} \delta\widehat{\Delta \mathrm{T}}^{(k)} - \delta\boldsymbol{\theta}^{(k)T} \left(\frac{\mathbf{h}^{(k)}}{\mathrm{T}_0} + \frac{\mu_{\infty} \mathbf{c}^{(k)}}{\mathrm{T}_0} \right) \right) A_1 A_2 H_1 H_2 d\alpha_1 d\alpha_2 d\zeta \end{aligned} \tag{40}$$

After some proper substitutions, the multifield constitutive matrix $\overline{\mathbf{\Gamma}}^{(k)}$, written in the geometric reference system, is thus derived from the constitutive relation (33) of the material reference system as follows:

$$\overline{\mathbf{\Gamma}}^{(k)} = \begin{bmatrix} \mathbf{T}^{(k)} \mathbf{\Gamma}_{\mathrm{C}}^{(k)} \mathbf{T}^{(k)T} & -\mathbf{T}^{(k)} \mathbf{\Gamma}_{\mathrm{C}}^{(k)} \mathbf{T}^{(k)T} \overline{\mathbf{\Gamma}}_{\mathrm{a}}^{(k)} & \mathbf{0} \\ \overline{\mathbf{\Gamma}}_{\mathrm{a}}^{(k)T} \mathbf{T}^{(k)T} \mathbf{\Gamma}_{\mathrm{C}}^{(k)} \mathbf{T}^{(k)} & \mathbf{\Gamma}_{\mathrm{TT}}^{(k)} & \mathbf{0} \\ \mathbf{0} & \mathbf{0} & \mathbf{H}^{(k)T} \mathbf{\Gamma}_{\mathrm{K}}^{(k)} \mathbf{H}^{(k)} \end{bmatrix} \tag{36}$$

The matrix $\overline{\mathbf{\Gamma}}_{\mathrm{z}}^{(k)}$ is derived from the three-dimensional stiffness matrix $\overline{\mathbf{\Gamma}}_{\mathrm{C}}^{(k)}$ according to the relation reported below [22]:

where $\delta\overline{\boldsymbol{\pi}}^{(k)}$ denotes the virtual variation of the vector of the thermo-mechanical primary variables, while $\overline{\boldsymbol{\chi}}^{(k)}$ is the modified vector of the secondary variables, derived from the vector $\boldsymbol{\chi}^{(k)}$ introduced previously as follows, setting $\widehat{\mathbf{I}}$ and $\mathbf{I}$ the identity matrices of size 6×6 and 3×3, respectively:

$$\overline{\boldsymbol{\chi}}^{(k)} = \mathbf{B}\,\boldsymbol{\chi}^{(k)} \;\Leftrightarrow\; \begin{bmatrix} \boldsymbol{\sigma}^{(k)} \\ \eta^{(k)} \\ \overline{\mathbf{h}}^{(k)} \end{bmatrix} = \begin{bmatrix} \widehat{\mathbf{I}} & 0 & \mathbf{0} \\ \mathbf{0} & 1 & \mathbf{0} \\ \mathbf{0} & 0 & \dfrac{1}{\mathrm{T}_0}\mathbf{I} \end{bmatrix} \begin{bmatrix} \boldsymbol{\sigma}^{(k)} \\ \eta^{(k)} \\ \mathbf{h}^{(k)} \end{bmatrix} \tag{41}$$

Introducing the ELW definition equations (28) in Eqn. (40), as well as the definition of Eqn. (41), one gets the following relation:

$$\begin{aligned} \delta \mathrm{Y} &= \sum_{k=1}^{l} \int_{\alpha_1} \int_{\alpha_2} \int_{\zeta_k}^{\zeta_{k+1}} \left(\sum_{\tau=0}^{N+1} \sum_{i=1}^{4} \mathbf{Z}^{(k\tau)\alpha_i} \delta\overline{\boldsymbol{\pi}}^{(\tau)\alpha_i} \right)^T \mathbf{B}\,\boldsymbol{\chi}^{(k)} A_1 A_2 H_1 H_2 d\zeta d\alpha_1 d\alpha_2 = \\ &= \sum_{\tau=0}^{N+1} \sum_{i=1}^{4} \int_{\alpha_1} \int_{\alpha_2} \left(\delta\overline{\boldsymbol{\pi}}^{(\tau)\alpha_i} \right)^T \overline{\mathbf{B}} \left(\sum_{k=1}^{l} \int_{\zeta_k}^{\zeta_{k+1}} \left(\mathbf{Z}^{(k\tau)\alpha_i} \right)^T \boldsymbol{\chi}^{(k)} H_1 H_2 d\zeta \right) A_1 A_2 d\alpha_1 d\alpha_2 = \\ &= \sum_{\tau=0}^{N+1} \sum_{i=1}^{4} \int_{\alpha_1} \int_{\alpha_2} \left(\delta\overline{\boldsymbol{\pi}}^{(\tau)\alpha_i} \right)^T \overline{\mathbf{B}}\,\overline{\boldsymbol{\Sigma}}^{(\tau)\alpha_i} A_1 A_2 d\alpha_1 d\alpha_2 = \sum_{\tau=0}^{N+1} \sum_{i=1}^{4} \int_{\alpha_1} \int_{\alpha_2} \left(\delta\overline{\boldsymbol{\pi}}^{(\tau)\alpha_i} \right)^T \overline{\boldsymbol{\Sigma}}^{(\tau)\alpha_i} A_1 A_2 d\alpha_1 d\alpha_2 \end{aligned} \tag{42}$$

The vector $\mathbf{\Sigma}^{(\tau)\alpha_i} = \left[\mathbf{S}^{(\tau)\alpha_i T} \quad E^{(\tau)\alpha_i} \quad \mathbf{H}^{(\tau)\alpha_i T}\right]^T$ of the generalized secondary variables resultants is introduced previously for each $i = 1, ..., 4$, defined as follows [22]:

$$\mathbf{\Sigma}^{(\tau)\alpha_i} = \sum_{k=1}^{l} \int_{\zeta_k}^{\zeta_{k+1}} \left(\mathbf{Z}^{(k\tau)\alpha_i}\right)^T \boldsymbol{\chi}^{(k)} H_1 H_2 d\zeta \tag{43}$$

The sub-vectors $\mathbf{S}^{(\tau)\alpha_i}, \mathbf{H}^{(\tau)\alpha_i}$ belonging to the vector $\mathbf{\Sigma}^{(\tau)\alpha_i}$ take the following aspect:

$$\begin{gathered}\mathbf{S}^{(\tau)\alpha_i} = \left[N_1^{(\tau)\alpha_i} \quad N_2^{(\tau)\alpha_i} \quad N_{12}^{(\tau)\alpha_i} \quad N_{21}^{(\tau)\alpha_i} \quad T_1^{(\tau)\alpha_i} \quad T_2^{(\tau)\alpha_i} \quad P_1^{(\tau)\alpha_i} \quad P_2^{(\tau)\alpha_i} \quad S_3^{(\tau)\alpha_i}\right]^T \\ \mathbf{H}^{(\tau)\alpha_i} = \left[H_1^{(\tau)\alpha_i} \quad H_2^{(\tau)\alpha_i} \quad H_3^{(\tau)\alpha_i}\right]^T\end{gathered} \tag{44}$$

Performing the matrix multiplications of Eqn. (42), one gets the definitions reported below:

$$\begin{gathered}N_1^{(\tau)\alpha_i} = \sum_{k=1}^{l} \int_{\zeta_k}^{\zeta_{k+1}} \sigma_1^{(k)} F_\tau^{(k)\alpha_i} H_2 d\zeta, \quad N_2^{(\tau)\alpha_i} = \sum_{k=1}^{l} \int_{\zeta_k}^{\zeta_{k+1}} \sigma_2^{(k)} F_\tau^{(k)\alpha_i} H_1 d\zeta, \quad N_{12}^{(\tau)\alpha_i} = \sum_{k=1}^{l} \int_{\zeta_k}^{\zeta_{k+1}} \tau_{12}^{(k)} F_\tau^{(k)\alpha_i} H_2 d\zeta, \\ N_{21}^{(\tau)\alpha_i} = \sum_{k=1}^{l} \int_{\zeta_k}^{\zeta_{k+1}} \tau_{12}^{(k)} F_\tau^{(k)\alpha_i} H_1 d\zeta, \quad T_1^{(\tau)\alpha_i} = \sum_{k=1}^{l} \int_{\zeta_k}^{\zeta_{k+1}} \tau_{13}^{(k)} F_\tau^{(k)\alpha_i} H_2 d\zeta, \quad T_2^{(\tau)\alpha_i} = \sum_{k=1}^{l} \int_{\zeta_k}^{\zeta_{k+1}} \tau_{23}^{(k)} F_\tau^{(k)\alpha_i} H_1 d\zeta, \\ P_1^{(\tau)\alpha_i} = \sum_{k=1}^{l} \int_{\zeta_k}^{\zeta_{k+1}} \tau_{13}^{(k)} \frac{\partial F_\tau^{(k)\alpha_i}}{\partial \zeta} H_1 H_2 d\zeta, \quad P_2^{(\tau)\alpha_i} = \sum_{k=1}^{l} \int_{\zeta_k}^{\zeta_{k+1}} \tau_{23}^{(k)} \frac{\partial F_\tau^{(k)\alpha_i}}{\partial \zeta} H_1 H_2 d\zeta, \quad S_3^{(\tau)\alpha_i} = \sum_{k=1}^{l} \int_{\zeta_k}^{\zeta_{k+1}} \sigma_3^{(k)} \frac{\partial F_\tau^{(k)\alpha_i}}{\partial \zeta} H_1 H_2 d\zeta, \\ H_1^{(\tau)\alpha_i} = \sum_{k=1}^{l} \int_{\zeta_k}^{\zeta_{k+1}} h_1^{(k)} F_\tau^{(k)\alpha_i} H_2 d\zeta, \quad H_2^{(\tau)\alpha_i} = \sum_{k=1}^{l} \int_{\zeta_k}^{\zeta_{k+1}} h_2^{(k)} F_\tau^{(k)\alpha_i} H_1 d\zeta, \quad H_3^{(\tau)\alpha_i} = \sum_{k=1}^{l} \int_{\zeta_k}^{\zeta_{k+1}} h_3^{(k)} \frac{\partial F_\tau^{(k)\alpha_i}}{\partial \zeta} H_1 H_2 d\zeta, \\ E^{(\tau)\alpha_i} = \sum_{k=1}^{l} \int_{\zeta_k}^{\zeta_{k+1}} \eta^{(k)} F_\tau^{(k)\alpha_i} H_1 H_2 d\zeta\end{gathered} \tag{45}$$

The generalized vector $\overline{\mathbf{\Sigma}}^{(\tau)\alpha_i}$ introduced in Eqn. (42) is linked to the vector $\mathbf{\Sigma}^{(\tau)\alpha_i}$ through the matrix $\overline{\mathbf{B}}$ defined in terms of identity matrices of proper size, according to the following condensed relation:

$$\overline{\mathbf{\Sigma}}^{(\tau)\alpha_i} = \overline{\mathbf{B}}\,\mathbf{\Sigma}^{(\tau)\alpha_i} \quad \Leftrightarrow \quad \begin{bmatrix} \mathbf{S}^{(\tau)\alpha_i} \\ E^{(\tau)\alpha_i} \\ \overline{\mathbf{H}}^{(\tau)\alpha_i} \end{bmatrix} = \begin{bmatrix} \breve{\mathbf{I}} & 0 & \mathbf{0} \\ \mathbf{0} & 1 & \mathbf{0} \\ \mathbf{0} & 0 & \dfrac{1}{\mathrm{T}_0}\mathbf{I} \end{bmatrix} \begin{bmatrix} \mathbf{S}^{(\tau)\alpha_i} \\ E^{(\tau)\alpha_i} \\ \mathbf{H}^{(\tau)\alpha_i} \end{bmatrix} \tag{46}$$

Moving from Eqn. (43), a novel expression of the generalized actions is provided introducing the constitutive relation (32) and the ELW definition equations outlined in Eqn. (28). In this way, the vector $\mathbf{\Sigma}^{(\tau)\alpha_i}$ is directly linked to the vectors $\boldsymbol{\pi}^{(\eta)\alpha_j}$ of the generalized strain resultants with $\eta = 0, ..., N+1$ as follows [22]:

$$\begin{aligned}\mathbf{\Sigma}^{(\tau)\alpha_i} &= \sum_{\eta=0}^{N+1} \sum_{j=1}^{4} \left(\sum_{k=1}^{l} \int_{\zeta_k}^{\zeta_{k+1}} \left(\mathbf{Z}^{(k\tau)\alpha_i}\right)^T \overline{\mathbf{\Gamma}}^{(k)} \mathbf{Z}^{(k\eta)\alpha_j} H_1 H_2 d\zeta \right) \boldsymbol{\pi}^{(\eta)\alpha_j} \\ &= \sum_{\eta=0}^{N+1} \sum_{j=1}^{4} \mathbf{A}^{(\tau\eta)\alpha_i\alpha_j} \boldsymbol{\pi}^{(\eta)\alpha_j}\end{aligned} \tag{47}$$

where $\mathbf{A}^{(\tau\eta)\alpha_i\alpha_j}$ is the generalized multifield stiffness matrix, defined for each $i,j = 1, ..., 4$ and $\tau, \eta = 0, ..., N+1$, whose arbitrary element $A_{rsnm\,(pq)}^{(\tau\eta)[fg]\,\alpha_i\alpha_j}$ with $r,s = \varepsilon, \mathrm{T}, \theta$ is calculated from the relation reported below [22]:

$$A_{rsnm\,(pq)}^{(\tau\eta)[fg]\,\alpha_i\alpha_j} = \sum\nolimits_{k=1}^{l} \int_{\zeta_k}^{\zeta_{k+1}} \overline{\mathrm{Y}}_{nm}^{(k)} \frac{\partial^f F_\tau^{(k)\alpha_i}}{\partial \zeta^f} \frac{\partial^g F_\eta^{(k)\alpha_j}}{\partial \zeta^g} \frac{H_1 H_2}{H_1^p H_2^q} d\zeta \quad \begin{array}{r} \text{for } \tau,\eta = 0, ..., N+1 \\ \text{for } n,m = 1, ..., 6 \\ \text{for } p,q = 0, 1, 2 \\ \text{for } i,j = 1, ..., 4 \end{array} \tag{48}$$

Here, $\overline{\mathrm{Y}}_{nm}^{(k)}$ denotes the arbitrary element of the three-dimensional constitutive matrix (31), which is corrected by means of the shear correction factor $\kappa(\zeta) = 5/6$ that allows one to compute the effects of shear stresses even in those structural theories with a uniform through-the-thickness distribution of the out-of-plane variable:

$$\overline{\mathrm{Y}}_{nm}^{(k)} = \kappa(\zeta)\overline{\Gamma}_{nm}^{(k)} \tag{49}$$

When lower order theories are considered, it can be useful to adopt the reduced elastic constants $\overline{\mathrm{Y}}_{\mathrm{R}nm}^{(k)} = \overline{C}_{\mathrm{R}nm}^{(k)}, \pm\overline{z}_{\mathrm{R}nm}^{(k)}$, which can be computed from the following relation from Ref. [22]:

$$\overline{C}_{\mathrm{R}nm}^{(k)} = \overline{C}_{nm}^{(k)} - \frac{\overline{C}_{m3}^{(k)}\overline{C}_{n3}^{(k)}}{\overline{C}_{33}^{(k)}}, \quad \overline{z}_{\mathrm{R}nm}^{(k)} = \overline{z}_{nm}^{(k)} - \frac{\overline{C}_{m3}^{(k)}\overline{z}_{33}^{(k)}}{\overline{C}_{33}^{(k)}} \tag{50}$$

Moving from Eqn. (32), the generalized matrix $\mathbf{A}^{(\tau\eta)\alpha_i\alpha_j}$ takes the following form:

$$\mathbf{A}^{(\tau\eta)\alpha_i\alpha_j} = \begin{bmatrix} \mathbf{A}_{\varepsilon\varepsilon}^{(\tau\eta)\alpha_i\alpha_j} & \mathbf{A}_{\varepsilon\mathrm{T}}^{(\tau\eta)\alpha_i\alpha_j} & \mathbf{0} \\ \mathbf{A}_{T\varepsilon}^{(\tau\eta)\alpha_i\alpha_j} & \mathbf{A}_{\mathrm{TT}}^{(\tau\eta)\alpha_i\alpha_j} & \mathbf{0} \\ \mathbf{0} & \mathbf{0} & \mathbf{A}_{\theta\theta}^{(\tau\eta)\alpha_i\alpha_j} \end{bmatrix} \tag{51}$$

where the sub-matrices $\mathbf{A}_{\varepsilon\varepsilon}^{(\tau\eta)\alpha_i\alpha_j}, \mathbf{A}_{\varepsilon\mathrm{T}}^{(\tau\eta)\alpha_i\alpha_j}, \mathbf{A}_{T\varepsilon}^{(\tau\eta)\alpha_i\alpha_j}, \mathbf{A}_{\mathrm{TT}}^{(\tau\eta)\alpha_i\alpha_j}$ and $\mathbf{A}_{\theta\theta}^{(\tau\eta)\alpha_i\alpha_j}$ are reported in the following in an extended form [22]:

$$
\mathbf{A}_{\varepsilon\varepsilon}^{(\tau\eta)\alpha_i\alpha_j} = \left[\begin{array}{ccccccc|ccc}
A_{11(20)}^{(\tau\eta)[00]\alpha_i\alpha_j} & A_{12(11)}^{(\tau\eta)[00]\alpha_i\alpha_j} & A_{16(20)}^{(\tau\eta)[00]\alpha_i\alpha_j} & A_{16(11)}^{(\tau\eta)[00]\alpha_i\alpha_j} & A_{14(20)}^{(\tau\eta)[00]\alpha_i\alpha_j} & A_{15(11)}^{(\tau\eta)[00]\alpha_i\alpha_j} & A_{14(10)}^{(\tau\eta)[01]\alpha_i\alpha_j} & A_{15(10)}^{(\tau\eta)[01]\alpha_i\alpha_j} & A_{13(10)}^{(\tau\eta)[01]\alpha_i\alpha_j} \\
A_{12(11)}^{(\tau\eta)[00]\alpha_i\alpha_j} & A_{22(02)}^{(\tau\eta)[00]\alpha_i\alpha_j} & A_{26(11)}^{(\tau\eta)[00]\alpha_i\alpha_j} & A_{26(02)}^{(\tau\eta)[00]\alpha_i\alpha_j} & A_{24(11)}^{(\tau\eta)[00]\alpha_i\alpha_j} & A_{25(02)}^{(\tau\eta)[00]\alpha_i\alpha_j} & A_{24(01)}^{(\tau\eta)[01]\alpha_i\alpha_j} & A_{25(01)}^{(\tau\eta)[01]\alpha_i\alpha_j} & A_{23(01)}^{(\tau\eta)[01]\alpha_i\alpha_j} \\
A_{16(20)}^{(\tau\eta)[00]\alpha_i\alpha_j} & A_{26(11)}^{(\tau\eta)[00]\alpha_i\alpha_j} & A_{66(20)}^{(\tau\eta)[00]\alpha_i\alpha_j} & A_{66(11)}^{(\tau\eta)[00]\alpha_i\alpha_j} & A_{46(20)}^{(\tau\eta)[00]\alpha_i\alpha_j} & A_{56(11)}^{(\tau\eta)[00]\alpha_i\alpha_j} & A_{46(10)}^{(\tau\eta)[01]\alpha_i\alpha_j} & A_{56(10)}^{(\tau\eta)[01]\alpha_i\alpha_j} & A_{36(10)}^{(\tau\eta)[01]\alpha_i\alpha_j} \\
A_{16(11)}^{(\tau\eta)[00]\alpha_i\alpha_j} & A_{26(02)}^{(\tau\eta)[00]\alpha_i\alpha_j} & A_{66(11)}^{(\tau\eta)[00]\alpha_i\alpha_j} & A_{66(02)}^{(\tau\eta)[00]\alpha_i\alpha_j} & A_{46(11)}^{(\tau\eta)[00]\alpha_i\alpha_j} & A_{56(02)}^{(\tau\eta)[00]\alpha_i\alpha_j} & A_{46(01)}^{(\tau\eta)[01]\alpha_i\alpha_j} & A_{56(01)}^{(\tau\eta)[01]\alpha_i\alpha_j} & A_{36(01)}^{(\tau\eta)[01]\alpha_i\alpha_j} \\
A_{14(20)}^{(\tau\eta)[00]\alpha_i\alpha_j} & A_{24(11)}^{(\tau\eta)[00]\alpha_i\alpha_j} & A_{46(20)}^{(\tau\eta)[00]\alpha_i\alpha_j} & A_{46(11)}^{(\tau\eta)[00]\alpha_i\alpha_j} & A_{44(20)}^{(\tau\eta)[00]\alpha_i\alpha_j} & A_{45(11)}^{(\tau\eta)[00]\alpha_i\alpha_j} & A_{44(10)}^{(\tau\eta)[01]\alpha_i\alpha_j} & A_{45(10)}^{(\tau\eta)[01]\alpha_i\alpha_j} & A_{34(10)}^{(\tau\eta)[01]\alpha_i\alpha_j} \\
A_{15(11)}^{(\tau\eta)[00]\alpha_i\alpha_j} & A_{25(02)}^{(\tau\eta)[00]\alpha_i\alpha_j} & A_{56(11)}^{(\tau\eta)[00]\alpha_i\alpha_j} & A_{56(02)}^{(\tau\eta)[00]\alpha_i\alpha_j} & A_{45(11)}^{(\tau\eta)[00]\alpha_i\alpha_j} & A_{55(02)}^{(\tau\eta)[00]\alpha_i\alpha_j} & A_{45(01)}^{(\tau\eta)[01]\alpha_i\alpha_j} & A_{55(01)}^{(\tau\eta)[01]\alpha_i\alpha_j} & A_{35(01)}^{(\tau\eta)[01]\alpha_i\alpha_j} \\
\hline
A_{14(10)}^{(\tau\eta)[10]\alpha_i\alpha_j} & A_{24(01)}^{(\tau\eta)[10]\alpha_i\alpha_j} & A_{46(10)}^{(\tau\eta)[10]\alpha_i\alpha_j} & A_{46(01)}^{(\tau\eta)[10]\alpha_i\alpha_j} & A_{44(10)}^{(\tau\eta)[10]\alpha_i\alpha_j} & A_{45(01)}^{(\tau\eta)[10]\alpha_i\alpha_j} & A_{44(00)}^{(\tau\eta)[11]\alpha_i\alpha_j} & A_{45(00)}^{(\tau\eta)[11]\alpha_i\alpha_j} & A_{34(00)}^{(\tau\eta)[11]\alpha_i\alpha_j} \\
A_{15(10)}^{(\tau\eta)[10]\alpha_i\alpha_j} & A_{25(01)}^{(\tau\eta)[10]\alpha_i\alpha_j} & A_{56(10)}^{(\tau\eta)[10]\alpha_i\alpha_j} & A_{56(01)}^{(\tau\eta)[10]\alpha_i\alpha_j} & A_{45(10)}^{(\tau\eta)[10]\alpha_i\alpha_j} & A_{55(01)}^{(\tau\eta)[10]\alpha_i\alpha_j} & A_{45(00)}^{(\tau\eta)[11]\alpha_i\alpha_j} & A_{55(00)}^{(\tau\eta)[11]\alpha_i\alpha_j} & A_{35(00)}^{(\tau\eta)[11]\alpha_i\alpha_j} \\
A_{13(10)}^{(\tau\eta)[10]\alpha_i\alpha_j} & A_{23(01)}^{(\tau\eta)[10]\alpha_i\alpha_j} & A_{36(10)}^{(\tau\eta)[10]\alpha_i\alpha_j} & A_{36(01)}^{(\tau\eta)[10]\alpha_i\alpha_j} & A_{34(10)}^{(\tau\eta)[10]\alpha_i\alpha_j} & A_{35(01)}^{(\tau\eta)[10]\alpha_i\alpha_j} & A_{34(00)}^{(\tau\eta)[11]\alpha_i\alpha_j} & A_{35(00)}^{(\tau\eta)[11]\alpha_i\alpha_j} & A_{33(00)}^{(\tau\eta)[11]\alpha_i\alpha_j}
\end{array}\right]
$$

$$
\mathbf{A}_{\varepsilon\mathrm{T}}^{(\tau\eta)\alpha_i\alpha_j} = -\left[\begin{array}{cccccccccc}
Z_{11(10)}^{(\tau\eta)[00]\alpha_i\alpha_j} & Z_{22(01)}^{(\tau\eta)[00]\alpha_i\alpha_j} & Z_{12(10)}^{(\tau\eta)[00]\alpha_i\alpha_j} & Z_{12(01)}^{(\tau\eta)[00]\alpha_i\alpha_j} & Z_{13(10)}^{(\tau\eta)[00]\alpha_i\alpha_j} & Z_{23(01)}^{(\tau\eta)[00]\alpha_i\alpha_j} & Z_{13(00)}^{(\tau\eta)[10]\alpha_i\alpha_j} & Z_{23(00)}^{(\tau\eta)[10]\alpha_i\alpha_j} & Z_{33(00)}^{(\tau\eta)[10]\alpha_i\alpha_j}
\end{array}\right]^T
$$

$$
\mathbf{A}_{\mathrm{T}\varepsilon}^{(\tau\eta)\alpha_i\alpha_j} = \left[\begin{array}{cccccccccc}
Z_{11(10)}^{(\tau\eta)[00]\alpha_i\alpha_j} & Z_{22(01)}^{(\tau\eta)[00]\alpha_i\alpha_j} & Z_{12(10)}^{(\tau\eta)[00]\alpha_i\alpha_j} & Z_{12(01)}^{(\tau\eta)[00]\alpha_i\alpha_j} & Z_{13(10)}^{(\tau\eta)[00]\alpha_i\alpha_j} & Z_{23(01)}^{(\tau\eta)[00]\alpha_i\alpha_j} & Z_{13(00)}^{(\tau\eta)[01]\alpha_i\alpha_j} & Z_{23(00)}^{(\tau\eta)[01]\alpha_i\alpha_j} & Z_{33(00)}^{(\tau\eta)[01]\alpha_i\alpha_j}
\end{array}\right]
$$

$$
\mathbf{A}_{\mathrm{TT}}^{(\tau\eta)\alpha_i\alpha_j} = C_{11(00)}^{(\tau\eta)[00]\alpha_i\alpha_j}
$$

$$
\mathbf{A}_{\theta\theta}^{(\tau\eta)\alpha_i\alpha_j} = \left[\begin{array}{cc|c}
K_{11(20)}^{(\tau\eta)[00]\alpha_i\alpha_j} & K_{12(11)}^{(\tau\eta)[00]\alpha_i\alpha_j} & K_{13(10)}^{(\tau\eta)[01]\alpha_i\alpha_j} \\
K_{12(11)}^{(\tau\eta)[00]\alpha_i\alpha_j} & K_{22(02)}^{(\tau\eta)[00]\alpha_i\alpha_j} & K_{23(01)}^{(\tau\eta)[01]\alpha_i\alpha_j} \\
\hline
K_{13(10)}^{(\tau\eta)[10]\alpha_i\alpha_j} & K_{23(01)}^{(\tau\eta)[10]\alpha_i\alpha_j} & K_{33(00)}^{(\tau\eta)[11]\alpha_i\alpha_j}
\end{array}\right]
$$

(52)

Introducing in Eqn. (47) the definition of the generalized strains $\boldsymbol{\pi}^{(\eta)\alpha_j}$ in terms of the vector $\boldsymbol{\delta}^{(\eta)}$ of the unknown variables of the formulation, the following useful relation is obtained:

$$
\boldsymbol{\Sigma}^{(\tau)\alpha_i} = \sum_{\eta=0}^{N+1}\sum_{j=1}^{4}\mathbf{A}^{(\tau\eta)\alpha_i\alpha_j}\mathbf{D}_{\Omega}^{\alpha_j}\boldsymbol{\delta}^{(\eta)} = \sum_{\eta=0}^{N+1}\mathbf{O}^{(\tau\eta)\alpha_i}\boldsymbol{\delta}^{(\eta)} \tag{53}
$$

In Appendix I, the interested reader can find the extended expression of the elements of the vector $\boldsymbol{\Sigma}^{(\tau)\alpha_i}$ in terms of the generalized configuration variables, as already outlined in compact form in Eqn. (53).

5. Thermo-mechanical governing equations

In the present section, the governing equations are derived for the present generalized thermo-mechanical formulation. To this end, the Master Balance principle is adopted under thermodynamic equilibrium conditions, thus neglecting all the irreversible processes. In this context, the time integral of the virtual variation of the total energy of the system E, restricted to an arbitrary time interval $[t_1, t_2]$, assumes a null value [22]:

$$
\int_{t_1}^{t_2}\delta\mathrm{E}\,dt = \int_{t_1}^{t_2}(\delta\mathrm{Y} - \delta L)dt = 0 \tag{54}
$$

where Y is the total free energy of the doubly-curved shell solid, and $\delta L = \delta L_{\mathrm{T}} + \delta L_s$ denotes the generalized virtual work of the thermo-mechanical external actions. This virtual work is made up of two contributions. The first one, denoted by δL_{T}, is the virtual work associated with the reference entropy of the system, while the quantity δL_s is the virtual work of the generalized external actions that are applied at the top (+) and bottom (−) surfaces of the shell, located at $\zeta = h/2$ and $\zeta = -h/2$, respectively. It consists of the external surface loads $q_{1s}^{(+)}, q_{2s}^{(+)}$, $q_{3s}^{(+)}$ and $q_{1s}^{(-)}, q_{2s}^{(-)}, q_{3s}^{(-)}$, along with the virtual work of the thermal loads $q_{\mathrm{T}}^{(+)}$ and $q_{\mathrm{T}}^{(-)}$:

$$
\begin{aligned}
\delta L_s = \delta L_{es} + \delta L_{fs} + \delta \mathrm{Q}_{\mathrm{T}s} = \int_{\alpha_1}\int_{\alpha_2}\Bigg(\Bigg(\widetilde{q}_{1s}^{(-)}\delta U_1^{(-)} + \widetilde{q}_{2s}^{(-)}\delta U_2^{(-)} + \widetilde{q}_{3s}^{(-)}\delta U_3^{(-)} + \frac{q_{\mathrm{T}}^{(-)}}{\mathrm{T}_0}\delta\Delta\mathrm{T}^{(-)}\Bigg)H_1^{(-)}H_2^{(-)} + \\
+ \Bigg(\widetilde{q}_{1s}^{(+)}\delta U_1^{(+)} + \widetilde{q}_{2s}^{(+)}\delta U_2^{(+)} + \widetilde{q}_{3s}^{(+)}\delta U_3^{(+)} + \frac{q_{\mathrm{T}}^{(+)}}{\mathrm{T}_0}\delta\Delta\mathrm{T}^{(+)}\Bigg)H_1^{(+)}H_2^{(+)}\Bigg)A_1A_2\,d\alpha_1 d\alpha_2
\end{aligned} \tag{55}
$$

being $\delta U_1^{(+)}, \delta U_2^{(+)}, \delta U_3^{(+)}$ and $\delta U_1^{(-)}, \delta U_2^{(-)}, \delta U_3^{(-)}$ the virtual variations of the three-dimensional displacement field variables, whereas $\widetilde{q}_{is}^{(-)} = q_{is}^{(-)} + q_{iefk}^{(-)}$ and $\widetilde{q}_{is}^{(+)} = q_{is}^{(+)} + q_{iefk}^{(+)}$ for $i = 1,2,3$. On the other hand, δL_{fs} denotes the virtual work of the elastic foundation located at the top and bottom shell surfaces It should be noted that Eqn. (55) is based on the definition of virtual work also for the case of thermal loads since the quantities $q_{\mathrm{T}}^{(+)}, q_{\mathrm{T}}^{(-)}$, defining the secondary variables of the heat transfer problem, are multiplied by $\delta\Delta\mathrm{T}^{(\pm)}$, which is the virtual variation of the corresponding configuration variable. On the other hand, the integral (55) accounts for the geometric scale factors $H_1^{(+)}, H_2^{(+)}$ and $H_1^{(-)}, H_2^{(-)}$, which are calculated according to Eqn. (6) setting $\zeta = h/2$ and $\zeta = -h/2$, respectively:

$$
H_i^{(-)} = 1 - \frac{h}{2R_i}, \quad H_i^{(+)} = 1 + \frac{h}{2R_i} \tag{56}
$$

The virtual work δL_{fs} of Eqn. (55) is associated with the actions $q_{1fk}^{(-)}, q_{2fk}^{(-)}$, $q_{3fk}^{(-)}$ and $q_{1fk}^{(+)}, q_{2fk}^{(+)}, q_{3fk}^{(+)}$ induced by the elastic foundation at the top and

bottom surfaces of the shell. The Winkler-Pasternak two-parameters foundation model [22] is employed in the present study to derive these external actions:

$$\begin{aligned} q_{1efk}^{(\pm)} &= -k_{1f}^{(\pm)} U_1^{(\pm)} \\ q_{2efk}^{(\pm)} &= -k_{2f}^{(\pm)} U_2^{(\pm)} \\ q_{3efk}^{(\pm)} &= -k_{3f}^{(\pm)} U_3^{(\pm)} + G_f^{(\pm)} \nabla_{(\pm)}^2 U_3^{(\pm)} \end{aligned} \tag{57}$$

where $k_{if}^{(\pm)}$ with $i = 1, 2, 3$ are the spring stiffnesses, whereas $G_f^{(\pm)}$ is the shear modulus of the foundation. The Laplacian operator $\nabla_{(\pm)}^2$ in Eqn. (57) is expressed in the curvilinear coordinate system of the solid as follows [22]:

$$\begin{aligned} \nabla_{(\pm)}^2 = &\left(\frac{1}{A_1^2 \left(H_1^{(\pm)}\right)^2} \frac{\partial^2}{\partial \alpha_1^2} + \frac{1}{A_2^2 \left(H_2^{(\pm)}\right)^2} \frac{\partial^2}{\partial \alpha_2^2} + \left(\frac{1}{A_1^2 A_2 \left(H_1^{(\pm)}\right)^2} \frac{\partial A_2}{\partial \alpha_1} - \frac{h}{2A_1^2 R_2^2 \left(H_1^{(\pm)}\right)^2 H_2^{(\pm)}} \frac{\partial R_2}{\partial \alpha_1} + \right.\right. \\ &- \frac{1}{A_1^3 \left(H_1^{(\pm)}\right)^2} \frac{\partial A_1}{\partial \alpha_1} - \left.\left. \frac{h}{2A_1^2 R_1^2 \left(H_1^{(\pm)}\right)^3} \frac{\partial R_1}{\partial \alpha_1} \right) \frac{\partial}{\partial \alpha_1} + \left(\frac{1}{A_1 A_2^2 \left(H_2^{(\pm)}\right)^2} \frac{\partial A_1}{\partial \alpha_2} + \frac{h}{2A_2^2 R_1^2 \left(H_2^{(\pm)}\right)^2 H_1^{(\pm)}} \frac{\partial R_1}{\partial \alpha_2} + \right. \\ &\left. \left. - \frac{1}{A_2^3 \left(H_2^{(\pm)}\right)^2} \frac{\partial A_2}{\partial \alpha_2} - \frac{h}{2A_2^2 R_2^2 \left(H_2^{(\pm)}\right)^3} \frac{\partial R_2}{\partial \alpha_2} \right) \frac{\partial}{\partial \alpha_2} \right) \end{aligned} \tag{58}$$

being $H_1^{(\pm)}$ and $H_2^{(\pm)}$ the scaling operators calculated for the top ($\zeta = h/2$) and bottom ($\zeta = -h/2$) surfaces according to Eqn. (56). Moving from Eqn. (55), generalized surface actions are defined for each τ-th kinematic expansion order, denoted by $\widetilde{q}_{is}^{(\tau)} = q_{is}^{(\tau)} + q_{iefk}^{(\tau)}$ with $i = 1, 2, 3$, which correspond to the mechanical pressures oriented along α_i principal directions, along with the external thermal flux $q_{\mathrm{T}s}^{(\tau)}$ oriented along ζ axis. Introducing the kinematic model (10) in Eqn. (55), one gets after some mathematical substitutions:

$$\begin{aligned} \delta L_s &= \delta L_{is} \\ &= \int_{\alpha_1} \int_{\alpha_2} \sum_{\tau=0}^{N+1} \left(\widetilde{q}_{1s}^{(\tau)} \delta u_1^{(\tau)} + \widetilde{q}_{2s}^{(\tau)} \delta u_2^{(\tau)} + \widetilde{q}_{3s}^{(\tau)} \delta u_3^{(\tau)} + \frac{q_{\mathrm{T}s}^{(\tau)}}{\mathrm{T}_0} \delta \xi^{(\tau)} \right) A_1 A_2 d\alpha_1 d\alpha_2 \end{aligned} \tag{59}$$

setting $\delta u_1^{(\tau)}, \delta u_2^{(\tau)}, \delta u_3^{(\tau)}$ and $\delta \xi^{(\tau)}$ the virtual variation of the generalized configuration variables defined in Eqn. (10). The generalized surface actions are thus computed from the following expressions [22]:

$$\begin{aligned} \widetilde{q}_{1s}^{(\tau)} &= \widetilde{q}_{1s}^{(-)} F_\tau^{(1)\alpha_1(-)} H_1^{(-)} H_2^{(-)} + \widetilde{q}_{1s}^{(+)} F_\tau^{(l)\alpha_1(+)} H_1^{(+)} H_2^{(+)} \\ \widetilde{q}_{2s}^{(\tau)} &= \widetilde{q}_{2s}^{(-)} F_\tau^{(1)\alpha_2(-)} H_1^{(-)} H_2^{(-)} + \widetilde{q}_{2s}^{(+)} F_\tau^{(l)\alpha_2(+)} H_1^{(+)} H_2^{(+)} \\ \widetilde{q}_{3s}^{(\tau)} &= \widetilde{q}_{3s}^{(-)} F_\tau^{(1)\alpha_3(-)} H_1^{(-)} H_2^{(-)} + \widetilde{q}_{3s}^{(+)} F_\tau^{(l)\alpha_3(+)} H_1^{(+)} H_2^{(+)} \\ q_{\mathrm{T}s}^{(\tau)} &= q_{\mathrm{T}}^{(-)} F_\tau^{(1)\alpha_4(-)} H_1^{(-)} H_2^{(-)} + q_{\mathrm{T}}^{(+)} F_\tau^{(l)\alpha_4(+)} H_1^{(+)} H_2^{(+)} \end{aligned} \tag{60}$$

being $F_\tau^{(1)\alpha_1(-)}, F_\tau^{(1)\alpha_2(-)}, F_\tau^{(1)\alpha_3(-)}, F_\tau^{(1)\alpha_4(-)}$ and $F_\tau^{(1)\alpha_1(+)}, F_\tau^{(1)\alpha_2(+)}, F_\tau^{(1)\alpha_3(+)}, F_\tau^{(1)\alpha_4(+)}$ the values assumed by the thickness functions at $\zeta = h/2$ and $\zeta = -h/2$, respectively. These quantities are conveniently arranged in the algebraic vector $\mathbf{q}^{(\tau)} = \mathbf{q}_s^{(\tau)} + \mathbf{q}_{efk}^{(\tau)}$ with $\mathbf{q}_s^{(\tau)} = \left[q_{1s}^{(\tau)} \quad q_{2s}^{(\tau)} \quad q_{3s}^{(\tau)} \quad q_{\mathrm{T}s}^{(\tau)} \right]^T$ and $\mathbf{q}_{efk}^{(\tau)} = \left[q_{1efk}^{(\tau)} \quad q_{2efk}^{(\tau)} \quad q_{3efk}^{(\tau)} \quad 0 \right]^T$, defined for each $\tau = 0, \ldots, N+1$. The nonzero elements vector $\mathbf{q}_{efk}^{(\tau)}$ can be evaluated as follows:

$$\begin{aligned} q_{1efk}^{(\tau)} &= -L_{fm1}^{(\tau\eta)\alpha_1} u_1^{(\tau)} = -\left(k_{1f}^{(-)} F_\eta^{(1)\alpha_1(-)} F_\tau^{(1)\alpha_1(-)} H_1^{(-)} H_2^{(-)} + k_{1f}^{(+)} F_\eta^{(l)\alpha_1(+)} F_\tau^{(l)\alpha_1(+)} H_1^{(+)} H_2^{(+)} \right) u_1^{(\tau)} \\ q_{2efk}^{(\tau)} &= -L_{fm2}^{(\tau\eta)\alpha_2\alpha_2} u_2^{(\tau)} = -\left(k_{2f}^{(-)} F_\eta^{(1)\alpha_2(-)} F_\tau^{(1)\alpha_2(-)} H_1^{(-)} H_2^{(-)} + k_{2f}^{(+)} F_\eta^{(l)\alpha_2(+)} F_\tau^{(l)\alpha_2(+)} H_1^{(+)} H_2^{(+)} \right) u_2^{(\tau)} \\ q_{3efk}^{(\tau)} &= -L_{fm3}^{(\tau\eta)\alpha_3\alpha_3} u_3^{(\tau)} = -\left(\left(k_{3f}^{(-)} - G_f^{(-)} \nabla_{(-)}^2 \right) F_\eta^{(1)\alpha_3(-)} F_\tau^{(1)\alpha_3(-)} H_1^{(-)} H_2^{(-)} + \left(k_{3f}^{(+)} - G_f^{(+)} \nabla_{(+)}^2 \right) F_\eta^{(l)\alpha_3(+)} F_\tau^{(l)\alpha_3(+)} H_1^{(+)} H_2^{(+)} \right) u_3^{(\tau)} \end{aligned} \tag{61}$$

Finally, the virtual work δL_{T} associated with the reference entropy density $\overline{\eta}^{(k)}$ of each point of the three-dimensional solid is computed as follows [22]:

$$\delta L_{\mathrm{T}} = -\sum_{k=1}^{l} \int_{\zeta_k}^{\zeta_{k+1}} \int_{\alpha_1} \int_{\alpha_2} \overline{\eta}^{(k)} \delta \Delta \mathrm{T}^{(k)} H_1 H_2 A_1 A_2 d\alpha_1 d\alpha_2 d\zeta \tag{62}$$

In this paper, since irreversible processes are neglected, the virtual work δL_{T} is set equal to zero. This simplification results in the virtual variation of the total free energy of the shell taking the following form:

$$\begin{aligned} \delta Y = &\sum_{k=1}^{l} \int_{\alpha_1} \int_{\alpha_2} \int_{\zeta_k}^{\zeta_{k+1}} \delta \overline{\boldsymbol{\pi}}^{(k)T} \overline{\boldsymbol{\chi}}^{(k)} A_1 A_2 H_1 H_2 d\zeta d\alpha_1 d\alpha_2 = \sum_{\tau=0}^{N+1} \sum_{i=1}^{4} \int_{\alpha_1} \int_{\alpha_2} \left(\delta \boldsymbol{\pi}^{(\tau)\alpha_i} \right)^T \widetilde{\boldsymbol{\Sigma}}^{(\tau)\alpha_i} A_1 A_2 d\alpha_1 d\alpha_2 = \\ &= \sum_{\tau=0}^{N+1} \sum_{i=1}^{4} \int_{\alpha_1} \int_{\alpha_2} \left(\delta \boldsymbol{\varepsilon}^{(\tau)\alpha_i} \right)^T \mathbf{S}^{(\tau)\alpha_i} A_1 A_2 d\alpha_1 d\alpha_2 + \\ &- \sum_{\tau=0}^{N+1} \sum_{i=1}^{4} \int_{\alpha_1} \int_{\alpha_2} \left(\delta \boldsymbol{\theta}^{(\tau)\alpha_i} \right)^T \frac{1}{\mathrm{T}_0} \mathbf{H}^{(\tau)\alpha_i} A_1 A_2 d\alpha_1 d\alpha_2 - \sum_{\tau=0}^{N+1} \sum_{i=1}^{4} \int_{\alpha_1} \int_{\alpha_2} E^{(\tau)\alpha_i} \delta \widehat{\Delta \mathrm{T}}^{(\tau)\alpha_i} A_1 A_2 d\alpha_1 d\alpha_2 \end{aligned} \tag{63}$$

Finally, the higher order thermo-mechanical balance equations are obtained for an arbitrary $\tau = 0, ..., N+1$, remembering that the time integral assumes a null value according to Eqn. (54):

$$\frac{1}{A_1}\frac{\partial N_1^{(\tau)\alpha_1}}{\partial\alpha_1}+\frac{N_1^{(\tau)\alpha_1}}{A_1A_2}\frac{\partial A_2}{\partial\alpha_1}+\frac{1}{A_2}\frac{\partial N_{21}^{(\tau)\alpha_1}}{\partial\alpha_2}+\frac{N_{21}^{(\tau)\alpha_1}}{A_1A_2}\frac{\partial A_1}{\partial\alpha_2}+\frac{N_{12}^{(\tau)\alpha_1}}{A_1A_2}\frac{\partial A_1}{\partial\alpha_2}$$
$$-\frac{N_2^{(\tau)\alpha_1}}{A_1A_2}\frac{\partial A_2}{\partial\alpha_1}+\frac{T_1^{(\tau)\alpha_1}}{R_1}-P_1^{(\tau)\alpha_1}+\widetilde{q}_{1s}^{(\tau)}=0$$

$$\frac{1}{A_2}\frac{\partial N_2^{(\tau)\alpha_2}}{\partial\alpha_2}+\frac{N_2^{(\tau)\alpha_2}}{A_1A_2}\frac{\partial A_1}{\partial\alpha_2}+\frac{1}{A_1}\frac{\partial N_{12}^{(\tau)\alpha_2}}{\partial\alpha_1}+\frac{N_{12}^{(\tau)\alpha_2}}{A_1A_2}\frac{\partial A_2}{\partial\alpha_1}+\frac{N_{21}^{(\tau)\alpha_2}}{A_1A_2}\frac{\partial A_2}{\partial\alpha_1}$$
$$-\frac{N_1^{(\tau)\alpha_2}}{A_1A_2}\frac{\partial A_1}{\partial\alpha_2}+\frac{T_2^{(\tau)\alpha_2}}{R_2}-P_2^{(\tau)\alpha_2}+\widetilde{q}_{2s}^{(\tau)}=0$$

$$\frac{1}{A_1}\frac{\partial T_1^{(\tau)\alpha_3}}{\partial\alpha_1}+\frac{T_1^{(\tau)\alpha_3}}{A_1A_2}\frac{\partial A_2}{\partial\alpha_1}+\frac{1}{A_2}\frac{\partial T_2^{(\tau)\alpha_3}}{\partial\alpha_2}+\frac{T_2^{(\tau)\alpha_3}}{A_1A_2}\frac{\partial A_1}{\partial\alpha_2}-\frac{N_1^{(\tau)\alpha_3}}{R_1}-\frac{N_2^{(\tau)\alpha_3}}{R_2}$$
$$-S_3^{(\tau)\alpha_3}+\widetilde{q}_{3s}^{(\tau)}=0$$

$$\frac{1}{A_1}\frac{\partial H_1^{(\tau)\alpha_4}}{\partial\alpha_1}+\frac{H_1^{(\tau)\alpha_4}}{A_1A_2}\frac{\partial A_2}{\partial\alpha_1}+\frac{1}{A_2}\frac{\partial H_2^{(\tau)\alpha_4}}{\partial\alpha_2}+\frac{H_2^{(\tau)\alpha_4}}{A_1A_2}\frac{\partial A_1}{\partial\alpha_2}-H_3^{(\tau)\alpha_4}+q_{Ts}^{(\tau)}=0 \tag{64}$$

In the same way, the application of the integration-by-parts rule allows one to derive the following relations:

$$\begin{aligned}
&\left(\overline{N}_1^{(\tau)\alpha_1}-N_1^{(\tau)\alpha_1}\right)\delta u_1^{(\tau)}=0 \quad \left(\overline{N}_{21}^{(\tau)\alpha_1}-N_{21}^{(\tau)\alpha_1}\right)\delta u_1^{(\tau)}=0\\
&\left(\overline{N}_{12}^{(\tau)\alpha_2}-N_{12}^{(\tau)\alpha_2}\right)\delta u_2^{(\tau)}=0 \quad \left(\overline{N}_2^{(\tau)\alpha_2}-N_2^{(\tau)\alpha_2}\right)\delta u_2^{(\tau)}=0\\
&\left(\overline{T}_1^{(\tau)\alpha_3}-T_1^{(\tau)\alpha_3}\right)\delta u_3^{(\tau)}=0 \quad \left(\overline{T}_2^{(\tau)\alpha_3}-T_2^{(\tau)\alpha_3}\right)\delta u_3^{(\tau)}=0\\
&\left(\overline{H}_1^{(\tau)\alpha_6}-H_1^{(\tau)\alpha_6}\right)\delta\xi^{(\tau)}=0 \quad \left(\overline{H}_2^{(\tau)\alpha_6}-H_2^{(\tau)\alpha_6}\right)\delta\xi^{(\tau)}=0
\end{aligned} \tag{65}$$

As will be seen later, Eqn. (65) will be employed later for the assessment of the boundary conditions along the four edges of the rectangular physical domain. Using a compact notation, the balance relations from Eqn. (64) can be expressed as [22]:

$$\sum_{i=1}^{4}\mathbf{D}_{\Omega}^{*\alpha_i}\boldsymbol{\Sigma}^{(\tau)\alpha_i}+\mathbf{q}^{(\tau)}=\sum_{i=1}^{4}\mathbf{D}_{\Omega}^{*\alpha_i}\boldsymbol{\Sigma}^{(\tau)\alpha_i}+\mathbf{q}_s^{(\tau)}+\mathbf{q}_{efk}^{(\tau)}=\mathbf{0} \tag{66}$$

where $\mathbf{D}_{\Omega}^{*\alpha_i}$ with $i=1,...,4$ are the equilibrium operators, whose extended form is reported below:

$$\begin{aligned}
\mathbf{D}_{\Omega}^{*\alpha_1}&=\begin{bmatrix}\overline{\mathbf{D}}_{\Omega}^{*\alpha_1} & \mathbf{0} & \mathbf{0}\\ \mathbf{0} & \mathbf{0} & \mathbf{0}\\ \mathbf{0} & \mathbf{0} & \mathbf{0}\\ \mathbf{0} & \mathbf{0} & \mathbf{0}\end{bmatrix},\quad \mathbf{D}_{\Omega}^{*\alpha_2}=\begin{bmatrix}\mathbf{0} & \mathbf{0} & \mathbf{0}\\ \overline{\mathbf{D}}_{\Omega}^{*\alpha_2} & \mathbf{0} & \mathbf{0}\\ \mathbf{0} & \mathbf{0} & \mathbf{0}\\ \mathbf{0} & \mathbf{0} & \mathbf{0}\end{bmatrix},\quad \mathbf{D}_{\Omega}^{*\alpha_3}\\
&=\begin{bmatrix}\mathbf{0} & \mathbf{0} & \mathbf{0}\\ \mathbf{0} & \mathbf{0} & \mathbf{0}\\ \overline{\mathbf{D}}_{\Omega}^{*\alpha_3} & \mathbf{0} & \mathbf{0}\\ \mathbf{0} & \mathbf{0} & \mathbf{0}\end{bmatrix},\quad \mathbf{D}_{\Omega}^{*\alpha_4}=\begin{bmatrix}\mathbf{0} & \mathbf{0} & \mathbf{0}\\ \mathbf{0} & \mathbf{0} & \mathbf{0}\\ \mathbf{0} & \mathbf{0} & \mathbf{0}\\ \mathbf{0} & \mathbf{1} & \overline{\mathbf{D}}_{\Omega}^{*\alpha_4}\end{bmatrix}
\end{aligned} \tag{67}$$

The extended version of matrices $\overline{\mathbf{D}}_{\Omega}^{*\alpha_i}$ with $i=1,...,4$ can be found in the following equation:

$$\begin{aligned}
\overline{\mathbf{D}}_{\Omega}^{*\alpha_1}&=\left[\frac{1}{A_1}\frac{\partial}{\partial\alpha_1}+\frac{1}{A_1A_2}\frac{\partial A_2}{\partial\alpha_1} \quad -\frac{1}{A_1A_2}\frac{\partial A_2}{\partial\alpha_1} \quad \frac{1}{A_1A_2}\frac{\partial A_1}{\partial\alpha_2} \quad \frac{1}{A_2}\frac{\partial}{\partial\alpha_2}+\frac{1}{A_1A_2}\frac{\partial A_1}{\partial\alpha_2} \quad \frac{1}{R_1} \quad 0 \quad -1 \quad 0 \quad 0\right]\\
\overline{\mathbf{D}}_{\Omega}^{*\alpha_2}&=\left[-\frac{1}{A_1A_2}\frac{\partial A_1}{\partial\alpha_2} \quad \frac{1}{A_2}\frac{\partial}{\partial\alpha_2}+\frac{1}{A_1A_2}\frac{\partial A_1}{\partial\alpha_2} \quad \frac{1}{A_1}\frac{\partial}{\partial\alpha_1}+\frac{1}{A_1A_2}\frac{\partial A_2}{\partial\alpha_1} \quad \frac{1}{A_1A_2}\frac{\partial A_2}{\partial\alpha_1} \quad 0 \quad \frac{1}{R_2} \quad 0 \quad -1 \quad 0\right]\\
\overline{\mathbf{D}}_{\Omega}^{*\alpha_3}&=\left[-\frac{1}{R_1} \quad -\frac{1}{R_2} \quad 0 \quad 0 \quad \frac{1}{A_1}\frac{\partial}{\partial\alpha_1}+\frac{1}{A_1A_2}\frac{\partial A_2}{\partial\alpha_1} \quad \frac{1}{A_2}\frac{\partial}{\partial\alpha_2}+\frac{1}{A_1A_2}\frac{\partial A_1}{\partial\alpha_2} \quad 0 \quad 0 \quad -1\right]\\
\overline{\mathbf{D}}_{\Omega}^{*\alpha_4}&=\left[\frac{1}{A_1}\frac{\partial}{\partial\alpha_1}+\frac{1}{A_1A_2}\frac{\partial A_2}{\partial\alpha_1} \quad \frac{1}{A_2}\frac{\partial}{\partial\alpha_2}+\frac{1}{A_1A_2}\frac{\partial A_1}{\partial\alpha_2} \quad -1\right]
\end{aligned} \tag{68}$$

By substituting the definition of the generalized secondary variables given in Eqn. (53) into Eqn. (66), the fundamental governing equations are derived for each $\tau = 0, ..., N+1$. These equations are expressed in terms of the elements of the vector $\boldsymbol{\delta}^{(\eta)}$, with $\eta = 0, ..., N+1$, collecting the unknown field variables of the present formulation:

$$\sum_{\eta=0}^{N+1}\mathbf{L}^{(\tau\eta)}\boldsymbol{\delta}^{(\eta)}+\mathbf{q}_{efk}^{(\tau)}+\mathbf{q}_s^{(\tau)}=\sum_{\eta=0}^{N+1}\left(\mathbf{L}^{(\tau\eta)}-\mathbf{L}_{fm}^{(\tau\eta)}\right)\boldsymbol{\delta}^{(\eta)}+\mathbf{q}_s^{(\tau)}=\mathbf{0} \tag{69}$$

being $\mathbf{L}^{(\tau\eta)}$ the fundamental matrix, written for each $\tau, \eta = 0, ..., N+1$, while $\mathbf{L}_{fm}^{(\tau\eta)}$ denotes the fundamental matrix of the elastic foundation. In a more expanded form, Eqn. (69) can be expressed as:

$$\begin{aligned}
&\sum_{\eta=0}^{N+1}\left(\left[\begin{array}{ccc|c}L_{11}^{(\tau\eta)\alpha_1\alpha_1} & L_{12}^{(\tau\eta)\alpha_1\alpha_2} & L_{13}^{(\tau\eta)\alpha_1\alpha_3} & L_{14}^{(\tau\eta)\alpha_1\alpha_4}\\ L_{21}^{(\tau\eta)\alpha_2\alpha_1} & L_{22}^{(\tau\eta)\alpha_2\alpha_2} & L_{23}^{(\tau\eta)\alpha_2\alpha_3} & L_{24}^{(\tau\eta)\alpha_2\alpha_4}\\ L_{31}^{(\tau\eta)\alpha_3\alpha_1} & L_{32}^{(\tau\eta)\alpha_3\alpha_2} & L_{33}^{(\tau\eta)\alpha_3\alpha_3} & L_{34}^{(\tau\eta)\alpha_3\alpha_4}\\ L_{41}^{(\tau\eta)\alpha_4\alpha_1} & L_{42}^{(\tau\eta)\alpha_4\alpha_2} & L_{43}^{(\tau\eta)\alpha_4\alpha_3} & L_{44}^{(\tau\eta)\alpha_4\alpha_4}\end{array}\right]\right.\\
&\left.-\left[\begin{array}{ccc|c}L_{fm1}^{(\tau\eta)\alpha_1\alpha_1} & 0 & 0 & 0\\ 0 & L_{fm2}^{(\tau\eta)\alpha_2\alpha_2} & 0 & 0\\ 0 & 0 & L_{fm3}^{(\tau\eta)\alpha_3\alpha_3} & 0\\ 0 & 0 & 0 & 0\end{array}\right]\right)\begin{bmatrix}u_1^{(\tau)}\\ u_2^{(\tau)}\\ u_3^{(\tau)}\\ \xi^{(\tau)}\end{bmatrix}+\begin{bmatrix}q_{1s}^{(\tau)}\\ q_{2s}^{(\tau)}\\ q_{3s}^{(\tau)}\\ q_{Ts}^{(\tau)}\end{bmatrix}\\
&=\begin{bmatrix}0\\0\\0\\0\end{bmatrix}
\end{aligned} \tag{70}$$

setting $L_{ij}^{(\tau\eta)\alpha_i\alpha_j}$ with $i,j=1,...,4$ the arbitrary element of the matrix $\mathbf{L}^{(\tau\eta)}$, which can be evaluated from the following relation:

$$\mathbf{L}^{(\tau\eta)} = \begin{bmatrix} \overline{\mathbf{D}}_{\Omega}^{*\alpha_1}\mathbf{A}_{\varepsilon\varepsilon}^{(\tau\eta)\alpha_1\alpha_1}\overline{\mathbf{D}}_{\Omega}^{\alpha_1} & \overline{\mathbf{D}}_{\Omega}^{*\alpha_1}\mathbf{A}_{\varepsilon\varepsilon}^{(\tau\eta)\alpha_1\alpha_2}\overline{\mathbf{D}}_{\Omega}^{\alpha_2} & \overline{\mathbf{D}}_{\Omega}^{*\alpha_1}\mathbf{A}_{\varepsilon\varepsilon}^{(\tau\eta)\alpha_1\alpha_3}\overline{\mathbf{D}}_{\Omega}^{\alpha_3} & | & \overline{\mathbf{D}}_{\Omega}^{*\alpha_1}\mathbf{A}_{\varepsilon\mathrm{T}}^{(\tau\eta)\alpha_1\alpha_4}\overline{\mathbf{D}}_{\Omega}^{\alpha_4} \\ \overline{\mathbf{D}}_{\Omega}^{*\alpha_2}\mathbf{A}_{\varepsilon\varepsilon}^{(\tau\eta)\alpha_2\alpha_1}\overline{\mathbf{D}}_{\Omega}^{\alpha_1} & \overline{\mathbf{D}}_{\Omega}^{*\alpha_2}\mathbf{A}_{\varepsilon\varepsilon}^{(\tau\eta)\alpha_2\alpha_2}\overline{\mathbf{D}}_{\Omega}^{\alpha_2} & \overline{\mathbf{D}}_{\Omega}^{*\alpha_2}\mathbf{A}_{\varepsilon\varepsilon}^{(\tau\eta)\alpha_2\alpha_3}\overline{\mathbf{D}}_{\Omega}^{\alpha_3} & | & \overline{\mathbf{D}}_{\Omega}^{*\alpha_2}\mathbf{A}_{\varepsilon\mathrm{T}}^{(\tau\eta)\alpha_2\alpha_4}\overline{\mathbf{D}}_{\Omega}^{\alpha_4} \\ \overline{\mathbf{D}}_{\Omega}^{*\alpha_3}\mathbf{A}_{\varepsilon\varepsilon}^{(\tau\eta)\alpha_3\alpha_1}\overline{\mathbf{D}}_{\Omega}^{\alpha_1} & \overline{\mathbf{D}}_{\Omega}^{*\alpha_3}\mathbf{A}_{\varepsilon\varepsilon}^{(\tau\eta)\alpha_3\alpha_2}\overline{\mathbf{D}}_{\Omega}^{\alpha_2} & \overline{\mathbf{D}}_{\Omega}^{*\alpha_3}\mathbf{A}_{\varepsilon\varepsilon}^{(\tau\eta)\alpha_3\alpha_3}\overline{\mathbf{D}}_{\Omega}^{\alpha_3} & | & \overline{\mathbf{D}}_{\Omega}^{*\alpha_3}\mathbf{A}_{\varepsilon\mathrm{T}}^{(\tau\eta)\alpha_3\alpha_4}\overline{\mathbf{D}}_{\Omega}^{\alpha_4} \\ 0 & 0 & 0 & | & \overline{\mathbf{D}}_{\Omega}^{*\alpha_4}\mathbf{A}_{\theta\theta}^{(\tau\eta)\alpha_4\alpha_4}\overline{\mathbf{D}}_{\Omega}^{\alpha_4} \end{bmatrix} \tag{71}$$

Finally, the boundary conditions of the two-dimensional formulations are derived from Eqn. (65), by setting either a null value of the virtual variation of the thermo-mechanical field variable or a null value of the generalized actions along the boundaries of the physical domain. As a consequence, the Simply-supported (S) boundary condition [22], considered in the simulations, can be defined as follows:

$$\begin{aligned} &N_1^{(\tau)\alpha_1} = 0, \quad u_2^{(\tau)} = u_3^{(\tau)} = \xi^{(\tau)} = 0 \quad \text{at} \quad \alpha_1 = \alpha_1^0 \ \text{ or } \ \alpha_1 = \alpha_1^1 \\ &N_2^{(\tau)\alpha_2} = 0, \quad u_1^{(\tau)} = u_3^{(\tau)} = \xi^{(\tau)} = 0 \quad \text{at} \quad \alpha_2 = \alpha_2^0 \ \text{ or } \ \alpha_2 = \alpha_2^1 \end{aligned} \tag{72}$$

At this point, a semi-analytical solution of the fundamental system of equations (70) is obtained. Each element of the vector $\boldsymbol{\delta}^{(\tau)}$ of the generalized configuration variables is expanded for each $\tau = 0, \ldots, N+1$ along α_1, α_2 directions with a harmonic expression, where $L_i = s_i^1 - s_i^0$ for $i = 1, 2$ denotes the total length of the parametric line along $\alpha_i = \alpha_1$, α_2 [22]:

$$\begin{aligned} u_1^{(\tau)}(s_1, s_2) &= \sum_{n=1}^{\bar{N}}\sum_{m=1}^{\bar{M}} \mathrm{U}_{1nm}^{(\tau)} \cos\left(\frac{n\pi}{L_1}s_1\right) sin\left(\frac{m\pi}{L_2}s_2\right) \\ u_2^{(\tau)}(s_1, s_2) &= \sum_{n=1}^{\bar{N}}\sum_{m=1}^{\bar{M}} \mathrm{U}_{2nm}^{(\tau)} \sin\left(\frac{n\pi}{L_1}s_1\right) \cos\left(\frac{m\pi}{L_2}s_2\right) \\ u_3^{(\tau)}(s_1, s_2) &= \sum_{n=1}^{\bar{N}}\sum_{m=1}^{\bar{M}} \mathrm{U}_{3nm}^{(\tau)} \sin\left(\frac{n\pi}{L_1}s_1\right) sin\left(\frac{m\pi}{L_2}s_2\right) \\ \xi^{(\tau)}(s_1, s_2) &= \sum_{n=1}^{\bar{N}}\sum_{m=1}^{\bar{M}} \Xi_{nm}^{(\tau)} \sin\left(\frac{n\pi}{L_1}s_1\right) sin\left(\frac{m\pi}{L_2}s_2\right) \end{aligned} \tag{73}$$

setting $\mathrm{U}_{1nm}^{(\tau)}, \mathrm{U}_{2nm}^{(\tau)}, \mathrm{U}_{3nm}^{(\tau)}$ and $\Xi_{nm}^{(\tau)}$ the wave amplitudes, defined for each n, $m \in \mathbb{N}$, of the unknown variables of the problem $u_1^{(\tau)}, u_2^{(\tau)}, u_3^{(\tau)}$ and $\xi^{(\tau)}$, respectively. In the same way, an harmonic expansion through trigonometric functions is assumed for the external surface loads $q_{1s}^{(\tau)}, q_{2s}^{(\tau)}, q_{3s}^{(\tau)}$ and $q_{\mathrm{Ts}}^{(\tau)}$ is assumed with wave amplitudes $Q_{1snm}^{(\tau)}, Q_{2snm}^{(\tau)}, Q_{3snm}^{(\tau)}$ and $Q_{\mathrm{T}snm}^{(\tau)}$, all arranged within the vector $\mathbf{Q}_{snm}^{(\tau)} = \begin{bmatrix} Q_{1snm}^{(\tau)} & Q_{2snm}^{(\tau)} & Q_{3snm}^{(\tau)} & Q_{\mathrm{T}snm}^{(\tau)} \end{bmatrix}^T$:

$$\begin{aligned} q_{1s}^{(\tau)}(s_1, s_2) &= \sum_{n=1}^{\bar{N}}\sum_{m=1}^{\bar{M}} Q_{1snm}^{(\tau)} \cos\left(\frac{n\pi}{L_1}s_1\right) sin\left(\frac{m\pi}{L_2}s_2\right) \\ q_{2s}^{(\tau)}(s_1, s_2) &= \sum_{n=1}^{\bar{N}}\sum_{m=1}^{\bar{M}} Q_{2snm}^{(\tau)} \sin\left(\frac{n\pi}{L_1}s_1\right) \cos\left(\frac{m\pi}{L_2}s_2\right) \\ q_{3s}^{(\tau)}(s_1, s_2) &= \sum_{n=1}^{\bar{N}}\sum_{m=1}^{\bar{M}} Q_{3snm}^{(\tau)} \sin\left(\frac{n\pi}{L_1}s_1\right) sin\left(\frac{m\pi}{L_2}s_2\right) \\ q_{\mathrm{Ts}}^{(\tau)}(s_1, s_2) &= \sum_{n=1}^{\bar{N}}\sum_{m=1}^{\bar{M}} Q_{\mathrm{T}snm}^{(\tau)} \sin\left(\frac{n\pi}{L_1}s_1\right) sin\left(\frac{m\pi}{L_2}s_2\right) \end{aligned} \tag{74}$$

The comparison of Eqn. (74) to the ELW definition (60) of thermo-mechanical external surface loads leads to the following relations for the previously introduced wave amplitudes [22]:

$$\begin{aligned} Q_{1snm}^{(\tau)} &= Q_{1snm}^{(-)} F_{\tau}^{(1)\alpha_1(-)} H_1^{(-)} H_2^{(-)} + Q_{1snm}^{(+)} F_{\tau}^{(l)\alpha_1(+)} H_1^{(+)} H_2^{(+)} \\ Q_{2snm}^{(\tau)} &= Q_{2snm}^{(-)} F_{\tau}^{(1)\alpha_2(-)} H_1^{(-)} H_2^{(-)} + Q_{2snm}^{(+)} F_{\tau}^{(l)\alpha_2(+)} H_1^{(+)} H_2^{(+)} \\ Q_{3snm}^{(\tau)} &= Q_{3snm}^{(-)} F_{\tau}^{(1)\alpha_3(-)} H_1^{(-)} H_2^{(-)} + Q_{3snm}^{(+)} F_{\tau}^{(l)\alpha_3(+)} H_1^{(+)} H_2^{(+)} \\ Q_{\mathrm{T}snm}^{(\tau)} &= Q_{\mathrm{T}snm}^{(-)} F_{\tau}^{(1)\alpha_4(-)} H_1^{(-)} H_2^{(-)} + Q_{\mathrm{T}snm}^{(+)} F_{\tau}^{(l)\alpha_4(+)} H_1^{(+)} H_2^{(+)} \end{aligned} \tag{75}$$

Here, $Q_{1snm}^{(+)}, Q_{2snm}^{(+)}, Q_{3snm}^{(+)}, Q_{\mathrm{T}snm}^{(+)}$ and $Q_{1snm}^{(-)}, Q_{2snm}^{(-)}, Q_{3snm}^{(-)}, Q_{\mathrm{T}snm}^{(-)}$ represent the wave amplitudes of the harmonic expansion of the external surface loads applied at the top and bottom surfaces of the shell, respectively. The semi-analytical solution proposed here is valid under the assumption of uniform Lamè parameters $A_i = A_1, A_2$ and principal radii of curvature $R_i = R_1, R_2$ throughout the physical domain:

$$\begin{aligned} A_i = \text{cost} &\Rightarrow \frac{\partial^{n+m} A_i}{\partial s_1^n \partial s_2^m} = 0 \\ R_i = \text{cost} &\Rightarrow \frac{\partial^{n+m} R_i}{\partial s_1^n \partial s_2^m} = 0 \end{aligned} \tag{76}$$

As a consequence, the expression of the Laplacian operator $\nabla_{(\pm)}^2$ of Eqn. (58) is simplified as follows:

$$\nabla_{(\pm)}^2 = \frac{1}{\left(H_1^{(\pm)}\right)^2}\frac{\partial^2}{\partial s_1^2} + \frac{1}{\left(H_2^{(\pm)}\right)^2}\frac{\partial^2}{\partial s_2^2} \tag{77}$$

The integration of the geometric relation in Eqn. (7) enables the computation of the lengths L_1, L_2 of the physical domain $\left[\alpha_1^0, \alpha_1^1\right] \times \left[\alpha_2^0, \alpha_2^1\right]$ along α_1, α_2, respectively, as follows:

$$\begin{aligned} s_1 = R(\varphi - \varphi_0) \ &\rightarrow L_1 = s_1^1 - s_1^0 = R(\varphi_1 - \varphi_0) \\ s_2 = R(\vartheta - \vartheta_0) \ &\rightarrow L_2 = s_2^1 - s_2^0 = R(\vartheta_1 - \vartheta_0) \end{aligned} \tag{78}$$

In case of cylindrical surface with $R_1 = R$ and $k_{n2} = 0$, Eqn. (78) reduces as follows:

$$\begin{aligned} s_1 = R(\varphi - \varphi_0) \ &\rightarrow L_1 = s_1^1 - s_1^0 = R(\varphi_1 - \varphi_0) \\ s_2 = y \ &\rightarrow L_2 = s_2^1 - s_2^0 \end{aligned} \tag{79}$$

In this case, the generalized constitutive coefficients $A_{rsnm\ (pq)}^{(\tau\eta)[fg]\,\alpha_i\alpha_j}$ in Eqn. (48) are calculated using the relation provided below:

$$A_{rsnm\ (pq)}^{(\tau\eta)[fg]\alpha_i\alpha_j} = \sum_{k=1}^{l}\int_{\zeta_k}^{\zeta_{k+1}} \overline{\Upsilon}_{nm}^{(k)} \frac{\partial^f F^{(k\eta)\alpha_j}}{\partial\zeta^f}\frac{\partial^g F^{(k\tau)\alpha_i}}{\partial\zeta^g}\frac{H_2}{H_2^q}d\zeta \tag{80}$$

Similarly, for a rectangular plate characterized by $k_{n1} = k_{n2} = 0$ the expression of $A_{rsnm\ (pq)}^{(\tau\eta)[fg]\,\alpha_i\alpha_j}$ is assumed as follows:

$$A_{rsnm\ (pq)}^{(\tau\eta)[fg]\alpha_i\alpha_j} = \sum_{k=1}^{l}\int_{\zeta_k}^{\zeta_{k+1}} \overline{\Upsilon}_{nm}^{(k)} \frac{\partial^f F^{(k\eta)\alpha_j}}{\partial\zeta^f}\frac{\partial^g F^{(k\tau)\alpha_i}}{\partial\zeta^g}d\zeta \tag{81}$$

The semi-analytical solution of the thermo-mechanical formulation is derived for cross-ply lamination schemes [22]. Therefore, for each k-th layer, the following three-dimensional constitutive relationship, written in the geometric reference system, is considered instead of Eqn. (31):

$$\begin{bmatrix} \sigma_1^{(k)} \\ \sigma_2^{(k)} \\ \tau_{12}^{(k)} \\ \tau_{13}^{(k)} \\ \tau_{23}^{(k)} \\ \sigma_3^{(k)} \\ \hline \eta^{(k)} \\ \hline h_1^{(k)} \\ h_2^{(k)} \\ h_3^{(k)} \end{bmatrix} = \left[\begin{array}{ccccc|c|ccc} \overline{C}_{11}^{(k)} & \overline{C}_{12}^{(k)} & 0 & 0 & 0 & \overline{C}_{13}^{(k)} & -\overline{z}_{11}^{(k)} & 0 & 0 & 0 \\ \overline{C}_{12}^{(k)} & \overline{C}_{22}^{(k)} & 0 & 0 & 0 & \overline{C}_{23}^{(k)} & -\overline{z}_{22}^{(k)} & 0 & 0 & 0 \\ 0 & 0 & \overline{C}_{66}^{(k)} & 0 & 0 & 0 & 0 & 0 & 0 & 0 \\ 0 & 0 & 0 & \overline{C}_{44}^{(k)} & 0 & 0 & 0 & 0 & 0 & 0 \\ 0 & 0 & 0 & 0 & \overline{C}_{55}^{(k)} & 0 & 0 & 0 & 0 & 0 \\ \overline{C}_{13}^{(k)} & \overline{C}_{23}^{(k)} & 0 & 0 & 0 & \overline{C}_{33}^{(k)} & -\overline{z}_{33}^{(k)} & 0 & 0 & 0 \\ \hline \overline{z}_{11}^{(k)} & \overline{z}_{22}^{(k)} & 0 & 0 & 0 & \overline{z}_{33}^{(k)} & \overline{\xi}_{11}^{(k)} & 0 & 0 & 0 \\ \hline 0 & 0 & 0 & 0 & 0 & 0 & 0 & \overline{k}_{11}^{(k)} & 0 & 0 \\ 0 & 0 & 0 & 0 & 0 & 0 & 0 & 0 & \overline{k}_{22}^{(k)} & 0 \\ 0 & 0 & 0 & 0 & 0 & 0 & 0 & 0 & 0 & \overline{k}_{33}^{(k)} \end{array}\right] \begin{bmatrix} \varepsilon_1^{(k)} \\ \varepsilon_2^{(k)} \\ \gamma_{12}^{(k)} \\ \gamma_{13}^{(k)} \\ \gamma_{23}^{(k)} \\ \varepsilon_3^{(k)} \\ \hline \widehat{\Delta \mathrm{T}}^{(k)} \\ \hline \theta_1^{(k)} \\ \theta_2^{(k)} \\ \theta_3^{(k)} \end{bmatrix} \tag{82}$$

Eqn. (82) is obtained if the laminae of the shell solid are made of orthotropic materials and are oriented with either $\vartheta^{(k)} = 0$ or $\vartheta^{(k)} = \pm\pi/2$. Under these kinematic (73), geometric (76) and mechanical (82) assumptions, the fundamental equations (69) are expressed as an algebraic linear system, as shown below:

$$\sum_{n=1}^{\tilde{N}} \sum_{m=1}^{\tilde{M}} \left(\sum_{\eta=0}^{N+1} \left(\widetilde{\mathbf{L}}_{nm}^{(\tau\eta)} - \widetilde{\mathbf{L}}_{fnm}^{(\tau\eta)} \right) \mathbf{U}_{nm}^{(\eta)} + \mathbf{Q}_{snm}^{(\tau)} \right) = \mathbf{0} \tag{83}$$

where the vector $\mathbf{U}_{nm}^{(\eta)} = \left[\mathrm{U}_{1nm}^{(\tau)} \quad \mathrm{U}_{2nm}^{(\tau)} \quad \mathrm{U}_{3nm}^{(\tau)} \quad \Xi_{nm}^{(\tau)} \right]^T$ gathers the amplitudes of the unknown field variables introduced in Eqn. (73), written for each n,m, while $\widetilde{N} = \widetilde{M} = +\infty$. In a more expanded form, Eqn. (83) takes the following expression:

$$\sum_{n=1}^{\tilde{N}} \sum_{m=1}^{\tilde{M}} \left(\sum_{\eta=0}^{N+1} \left(\left[\begin{array}{ccc|c} \widetilde{L}_{11nm}^{(\tau\eta)\alpha_1\alpha_1} & \widetilde{L}_{12nm}^{(\tau\eta)\alpha_1\alpha_2} & \widetilde{L}_{13nm}^{(\tau\eta)\alpha_1\alpha_3} & \widetilde{L}_{14nm}^{(\tau\eta)\alpha_1\alpha_4} \\ \widetilde{L}_{21nm}^{(\tau\eta)\alpha_2\alpha_1} & \widetilde{L}_{22nm}^{(\tau\eta)\alpha_2\alpha_2} & \widetilde{L}_{23nm}^{(\tau\eta)\alpha_2\alpha_3} & \widetilde{L}_{24nm}^{(\tau\eta)\alpha_2\alpha_4} \\ \widetilde{L}_{31nm}^{(\tau\eta)\alpha_3\alpha_1} & \widetilde{L}_{32nm}^{(\tau\eta)\alpha_3\alpha_2} & \widetilde{L}_{33nm}^{(\tau\eta)\alpha_3\alpha_3} & \widetilde{L}_{34nm}^{(\tau\eta)\alpha_3\alpha_4} \\ \hline \widetilde{L}_{41nm}^{(\tau\eta)\alpha_4\alpha_1} & \widetilde{L}_{42nm}^{(\tau\eta)\alpha_4\alpha_2} & \widetilde{L}_{43nm}^{(\tau\eta)\alpha_4\alpha_3} & \widetilde{L}_{44nm}^{(\tau\eta)\alpha_4\alpha_4} \end{array}\right] - \left[\begin{array}{ccc|c} \widetilde{L}_{fm1nm}^{(\tau\eta)\alpha_1\alpha_1} & 0 & 0 & 0 \\ 0 & \widetilde{L}_{fm2nm}^{(\tau\eta)\alpha_2\alpha_2} & 0 & 0 \\ 0 & 0 & \widetilde{L}_{fm3nm}^{(\tau\eta)\alpha_3\alpha_3} & 0 \\ \hline 0 & 0 & 0 & 0 \end{array}\right] \right) \begin{bmatrix} \mathrm{U}_{1nm}^{(\eta)} \\ \mathrm{U}_{2nm}^{(\eta)} \\ \mathrm{U}_{3nm}^{(\eta)} \\ \Xi_{nm}^{(\eta)} \end{bmatrix} + \begin{bmatrix} Q_{1snm}^{(\tau)} \\ Q_{2snm}^{(\tau)} \\ Q_{3snm}^{(\tau)} \\ Q_{\mathrm{T}snm}^{(\tau)} \end{bmatrix} \right) = \begin{bmatrix} 0 \\ 0 \\ 0 \\ 0 \end{bmatrix} \tag{84}$$

The expressions for the coefficients $\widetilde{L}_{fm1nm}^{(\tau\eta)\alpha_1\alpha_1}$, $\widetilde{L}_{fm2nm}^{(\tau\eta)\alpha_2\alpha_2}$ and $\widetilde{L}_{fm3nm}^{(\tau\eta)\alpha_3\alpha_3}$, accounting for the presence of the Winkler-Pasternak elastic foundation, take the following form:

$$\begin{aligned} L_{fm1nm}^{(\tau\eta)\alpha_1} &= k_{1f}^{(-)} F_{\eta}^{(1)\alpha_1(-)} F_{\tau}^{(1)\alpha_1(-)} H_1^{(-)} H_2^{(-)} + k_{1f}^{(+)} F_{\eta}^{(l)\alpha_1(+)} F_{\tau}^{(l)\alpha_1(+)} H_1^{(+)} H_2^{(+)} \\ L_{fm2nm}^{(\tau\eta)\alpha_2} &= k_{2f}^{(-)} F_{\eta}^{(1)\alpha_2(-)} F_{\tau}^{(1)\alpha_2(-)} H_1^{(-)} H_2^{(-)} + k_{2f}^{(+)} F_{\eta}^{(l)\alpha_2(+)} F_{\tau}^{(l)\alpha_2(+)} H_1^{(+)} H_2^{(+)} \\ L_{fm3nm}^{(\tau\eta)\alpha_3} &= \left(k_{3f}^{(-)} + G_f^{(-)} \left(\frac{1}{\left(H_1^{(-)} \right)^2} \left(\frac{n\pi}{L_1} \right)^2 + \frac{1}{\left(H_2^{(-)} \right)^2} \left(\frac{m\pi}{L_2} \right)^2 \right) \right) F_{\eta}^{(1)\alpha_3(-)} F_{\tau}^{(1)\alpha_3(-)} H_1^{(-)} H_2^{(-)} + \\ &+ \left(k_{3f}^{(+)} + G_f^{(+)} \left(\frac{1}{\left(H_1^{(+)} \right)^2} \left(\frac{n\pi}{L_1} \right)^2 + \frac{1}{\left(H_2^{(+)} \right)^2} \left(\frac{m\pi}{L_2} \right)^2 \right) \right) F_{\eta}^{(l)\alpha_3(+)} F_{\tau}^{(l)\alpha_3(+)} H_1^{(+)} H_2^{(+)} \end{aligned} \tag{85}$$

The complete expression of the coefficients $\widetilde{L}_{ijnm}^{(\tau\eta)\alpha_i\alpha_j}$ with $i,j = 1,\ldots,4$ of the semi-analytical fundamental matrix $\widetilde{\mathbf{L}}_{nm}^{(\tau\eta)}$ can be found in Appendix II. Finally, it should be noted that Eqn. (83), which accounts for an harmonic expansion of the solution with an infinite number of terms, is usually truncated up to a real value of $\widetilde{N}, \widetilde{M}$ when the convergence of results is seen with a sufficient level of accuracy.

6. Numerical implementation

The present formulation is based on a semi-analytical approach for the derivation of the solution of the fundamental equations. On the other hand, a numerical technique is adopted for the computation of derivatives in the post-processing recovery procedure. In the same way, the generalized constitutive coefficients $A_{rsnm}^{(\tau\eta)[fg]\,\alpha_i\alpha_j\,(pq)}$ are calculated according to Eqn. (48) with an integral, which is computed numerically. To this end, the F-GDQ and the GTIQ method are adopted, respectively, and they are presented hereafter for the one-dimensional case.

Generally speaking, the n-th order derivative of an arbitrary smooth function $f = f(x)$ with $x \in [a,b]$ is calculated in matrix form as follows, where $\mathbf{D}^{(n)}$ represents the n-th order differentiation matrix [56]:

$$\mathbf{f}^{(n)} = \mathbf{D}^{(n)} \mathbf{f} \tag{86}$$

In the previous relation, $\mathbf{f}$ denotes the vector of the values assumed by the function f on a discrete grid of I_Q sample points, while $\mathbf{f}^{(n)}$ collects the

Rectangular plate

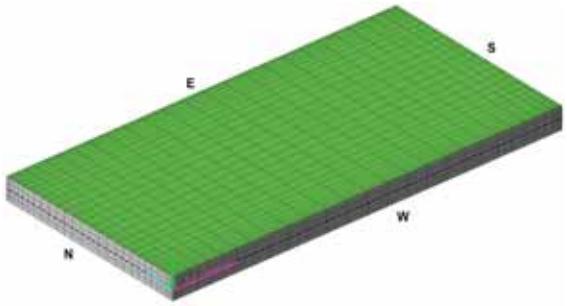

$$\mathbf{r}(s_1,s_2)=\mathbf{r}(x,y)=-x\,\mathbf{e}_2+y\,\mathbf{e}_3$$
$$(x,y)\in[0,L_x]\times[0,L_y]$$
$$L_x=2\text{ m},\ L_y=1\text{ m}$$
$$[s_1^0,s_1^1]=[0,L_x],\ [s_2^0,s_2^1]=[0,L_y]$$

Lamination scheme: $(0/90/0/90)$, $h_1=h_2=h_3=h_4=0.025$ m

Material properties: 1st to 4th layer - Graphite-epoxy

Cylindrical panel

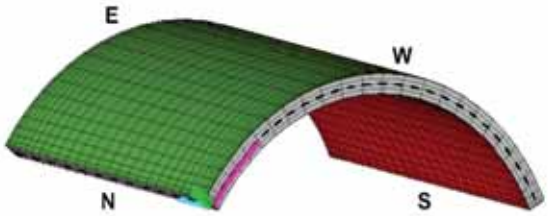

$$\mathbf{r}(s_1,s_2)=\mathbf{r}(\varphi,y)=R\cos\varphi\,\mathbf{e}_1-y\,\mathbf{e}_2+R\sin\varphi\,\mathbf{e}_3,\quad R=3\text{ m}$$
$$s_1=R(\varphi-\varphi_0),\quad s_2=y$$
$$(\varphi,y)\in[\varphi_0,\varphi_1]\times[0,L_y]$$
$$[\varphi_0,\varphi_1]=[-60°,60°],\quad L_y=2\text{ m}$$
$$[s_1^0,s_1^1]=[0,R(\varphi_1-\varphi_0)],\quad [s_2^0,s_2^1]=[0,L_y]$$

Lamination scheme: $(0/90/0/90)$, $h_1=h_2=h_3=h_4=0.025$ m

Material properties: 1st to 4th layer - Graphite-epoxy

Shallow spherical panel

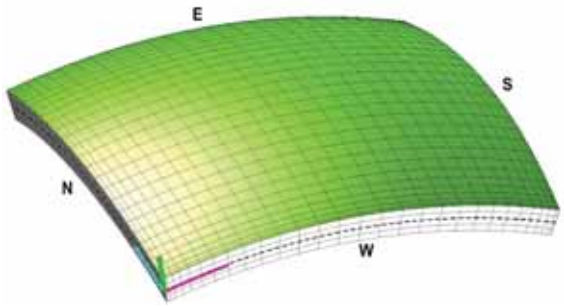

$$\mathbf{r}(s_1,s_2)=\mathbf{r}(\varphi,\vartheta)=R_0(\varphi)\cos\vartheta\,\mathbf{e}_1-R_0(\varphi)\sin\vartheta\,\mathbf{e}_2+$$
$$+\left(R-\sqrt{R^2-\left(R_0(\varphi)\right)^2}\right)\mathbf{e}_3$$
$$s_1=R(\varphi-\varphi_0),\quad s_2=R(\vartheta-\vartheta_0)$$
$$R_0(\varphi)=R\sin\varphi,\quad (\varphi,\vartheta)\in[\varphi_0,\varphi_1]\times[\vartheta_0,\vartheta_1]$$
$$[\varphi_0,\varphi_1]=[75°,105°],\ [\vartheta_0,\vartheta_1]=[-15°,15°],\ R=3\text{ m}$$
$$[s_1^0,s_1^1]=[0,R(\varphi_1-\varphi_0)],\quad [s_2^0,s_2^1]=[0,R(\vartheta_1-\vartheta_0)]$$

Lamination scheme: $(90/0/0/90)$, $h_1=h_2=h_3=h_4=0.025$ m

Material properties: Gr-Ep = Graphite-epoxy

1st and 4th layer - Gr-Ep, 2nd layer - Gr-Ep-s5, 3rd layer - Gr-Ep-s10

Fig. 1. Two-dimensional models developed for the thermo-mechanical analysis of a rectangular plate, a cylindrical panel and a spherical surface under various thermal and mechanical loading conditions.

Table 1
Vertical deflection of the central point of a SSSS rectangular plate made of three layers made of Gr-Ep. Convergence of GDQ and F-GDQ numerical techniques for different sizes of the computational grid for various higher order theories. Comparison to ELW analytical solutions and a 3D FEM model. All the quantities reported in the table are expressed in 10^{-4} m.

3D FEM (1298247 DOFs)	5.74625											
	ELD2		ELDZL2		ELD3		ELDZL3		ELD4		ELDZL4	
Exact	5.69873		5.73171		5.74178		5.74386		5.74174		5.74383	
	GDQ	F-GDQ	GDQ	F-GDQ	GDQ	F-GDQ	GDQ	F-GDQ	GDQ	F-GDQ	GDQ	F-GDQ
$I_N=I_M=5$	5.87898	5.73576	5.73919	5.73916	5.73916	5.73916	5.73916	5.73916	5.73916	5.73916	5.73916	5.73916
$I_N=I_M=7$	4.58233	5.74075	5.73864	5.73915	5.73916	5.73916	5.73916	5.73916	5.73916	5.73916	5.73916	5.73916
$I_N=I_M=9$	5.91973	5.77654	5.77997	5.77994	5.77994	5.77994	5.77994	5.77994	5.77994	5.77994	5.77994	5.77994
$I_N=I_M=11$	4.60795	5.78182	5.77941	5.77993	5.77994	5.77994	5.77994	5.77994	5.77994	5.77994	5.77994	5.77994
$I_N=I_M=13$	5.88143	5.73837	5.74181	5.74178	5.74178	5.74178	5.74178	5.74178	5.74178	5.74178	5.74178	5.74178
$I_N=I_M=15$	4.40082	5.74386	5.74115	5.74176	5.74177	5.74178	5.74178	5.74178	5.74178	5.74178	5.74178	5.74178
$I_N=I_M=17$	5.88349	5.74046	5.74389	5.74386	5.74386	5.74386	5.74386	5.74386	5.74386	5.74386	5.74386	5.74386
$I_N=I_M=19$	4.40202	5.74598	5.74323	5.74385	5.74386	5.74386	5.74386	5.74386	5.74386	5.74386	5.74386	5.74386
$I_N=I_M=21$	5.88140	5.73834	5.74177	5.74174	5.74174	5.74174	5.74174	5.74174	5.74174	5.74174	5.74174	5.74174
$I_N=I_M=23$	4.40076	5.74382	5.74111	5.74173	5.74174	5.74174	5.74174	5.74174	5.74174	5.74174	5.74174	5.74174
$I_N=I_M=25$	5.88347	5.74043	5.74386	5.74383	5.74383	5.74383	5.74383	5.74383	5.74383	5.74383	5.74383	5.74383
$I_N=I_M=27$	4.40197	5.74595	5.74320	5.74382	5.74383	5.74383	5.74383	5.74383	5.74383	5.74383	5.74383	5.74383
$I_N=I_M=29$	5.87898	5.73576	5.73919	5.73916	5.73916	5.73916	5.73916	5.73916	5.73916	5.73916	5.73916	5.73916
$I_N=I_M=31$	4.58233	5.74075	5.73864	5.73915	5.73916	5.73916	5.73916	5.73916	5.73916	5.73916	5.73916	5.73916
$I_N=I_M=33$	5.91973	5.77654	5.77997	5.77994	5.77994	5.77994	5.77994	5.77994	5.77994	5.77994	5.77994	5.77994

Table 2
Vertical deflection of the central point of a SSSS rectangular plate made of two external layers of Gr-Ep and a central Gr-Ep-s5 core. Convergence of GDQ and F-GDQ numerical techniques for different sizes of the computational grid for various higher order theories. Comparison to ELW analytical solutions and a 3D FEM model. All the quantities reported in the table are expressed in 10^{-4} m.

3D FEM (1298247 DOFs)	7.63086											
	ELD2		ELDZL2		ELD3		ELDZL3		ELD4		ELDZL4	
Exact	6.9621		7.6157		7.2560		7.6313		7.2559		7.6315	
	GDQ	F-GDQ	GDQ	F-GDQ	GDQ	F-GDQ	GDQ	F-GDQ	GDQ	F-GDQ	GDQ	F-GDQ
$I_N = I_M = 5$	7.47634	6.03116	8.19939	6.50823	7.69509	5.95638	8.02557	6.15858	7.69498	5.95627	8.02565	6.15852
$I_N = I_M = 7$	7.30514	7.31250	8.02727	8.03712	7.52393	7.53288	7.85391	7.86423	7.52381	7.53276	7.85398	7.86430
$I_N = I_M = 9$	7.30916	7.30855	8.03129	8.03051	7.52795	7.52716	7.85705	7.85793	7.52783	7.52704	7.85800	7.85712
$I_N = I_M = 11$	7.30913	7.30912	8.03125	8.03125	7.52791	7.52790	7.85790	7.85789	7.52780	7.52779	7.85797	7.85796
$I_N = I_M = 13$	7.30913	7.30913	8.03125	8.03125	7.52791	7.52791	7.85790	7.85790	7.52780	7.52780	7.85797	7.85797
$I_N = I_M = 15$	7.30913	7.30913	8.03125	8.03125	7.52791	7.52791	7.85790	7.85790	7.52780	7.52780	7.85797	7.85797
$I_N = I_M = 17$	7.30913	7.30913	8.03125	8.03125	7.52791	7.52791	7.85790	7.85790	7.52780	7.52780	7.85797	7.85797
$I_N = I_M = 19$	7.30913	7.30913	8.03125	8.03125	7.52791	7.52791	7.85790	7.85790	7.52780	7.52780	7.85797	7.85797
$I_N = I_M = 21$	7.30913	7.30913	8.03125	8.03125	7.52791	7.52791	7.85790	7.85790	7.52780	7.52780	7.85797	7.85797
$I_N = I_M = 23$	7.30913	7.30913	8.03125	8.03125	7.52791	7.52791	7.85790	7.85790	7.52780	7.52780	7.85797	7.85797
$I_N = I_M = 25$	7.30913	7.30913	8.03125	8.03125	7.52791	7.52791	7.85790	7.85790	7.52780	7.52780	7.85797	7.85797
$I_N = I_M = 27$	7.30913	7.30913	8.03125	8.03125	7.52791	7.52791	7.85790	7.85790	7.52780	7.52780	7.85797	7.85797
$I_N = I_M = 29$	7.30913	7.30913	8.03125	8.03125	7.52791	7.52791	7.85790	7.85790	7.52780	7.52780	7.85797	7.85797
$I_N = I_M = 31$	7.30913	7.30913	8.03125	8.03125	7.52791	7.52791	7.85790	7.85790	7.52780	7.52780	7.85797	7.85797
$I_N = I_M = 33$	7.30913	7.30913	8.03125	8.03125	7.52791	7.52791	7.85790	7.85790	7.52780	7.52780	7.85797	7.85797

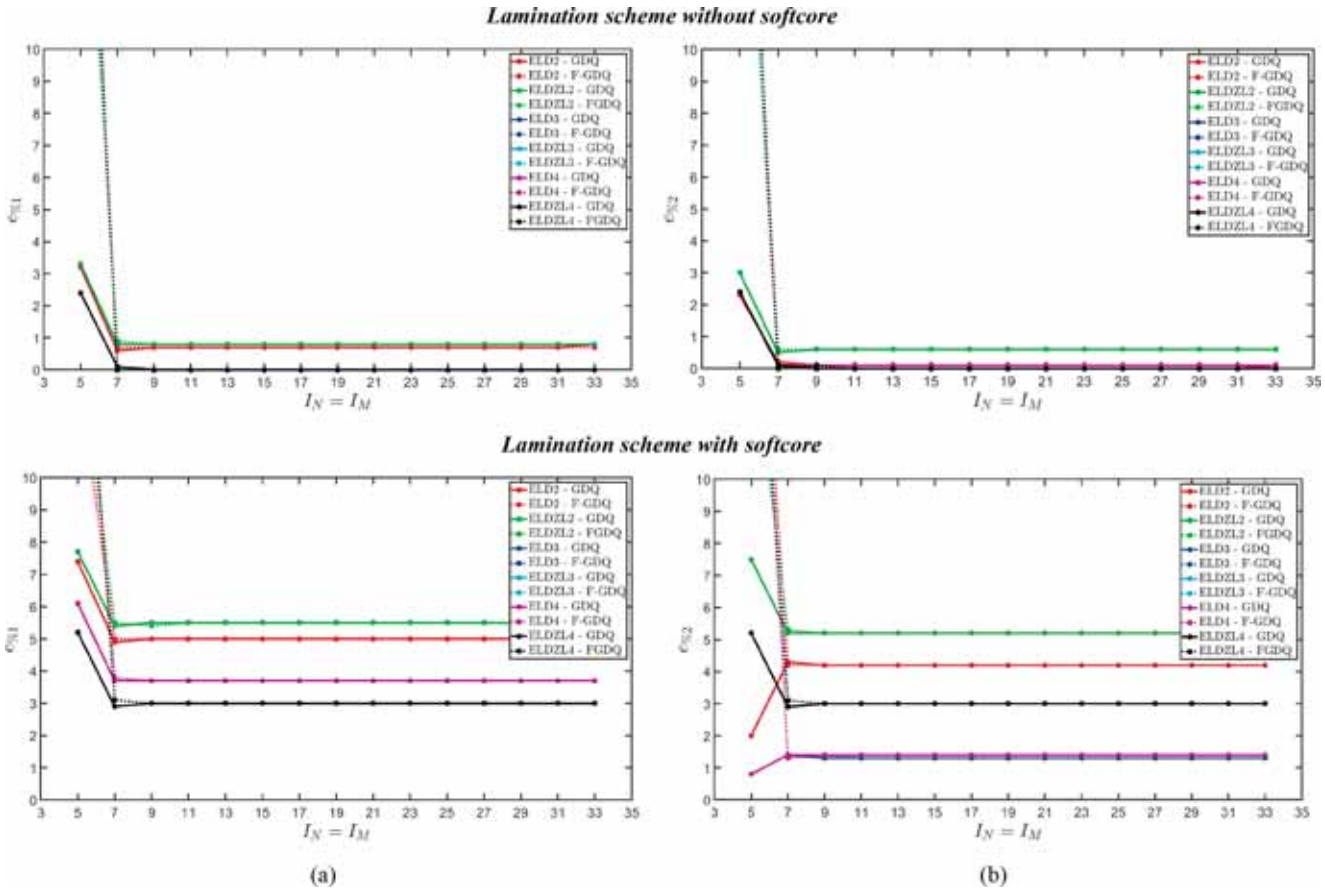

Fig. 2. Maximum vertical deflection of a SSSS laminated rectangular plate subjected to a sinusoidal load with $n = m = 1$ of magnitude $Q^{(+)}_{3snm} = -1 \times 10^5$ N/m^2. Convergence of the results derived from a numerical GDQ-based model and a F-GDQ-based model with respect to those coming from an analytical higher order simulation (a) and a refined 3D FEM model (b).

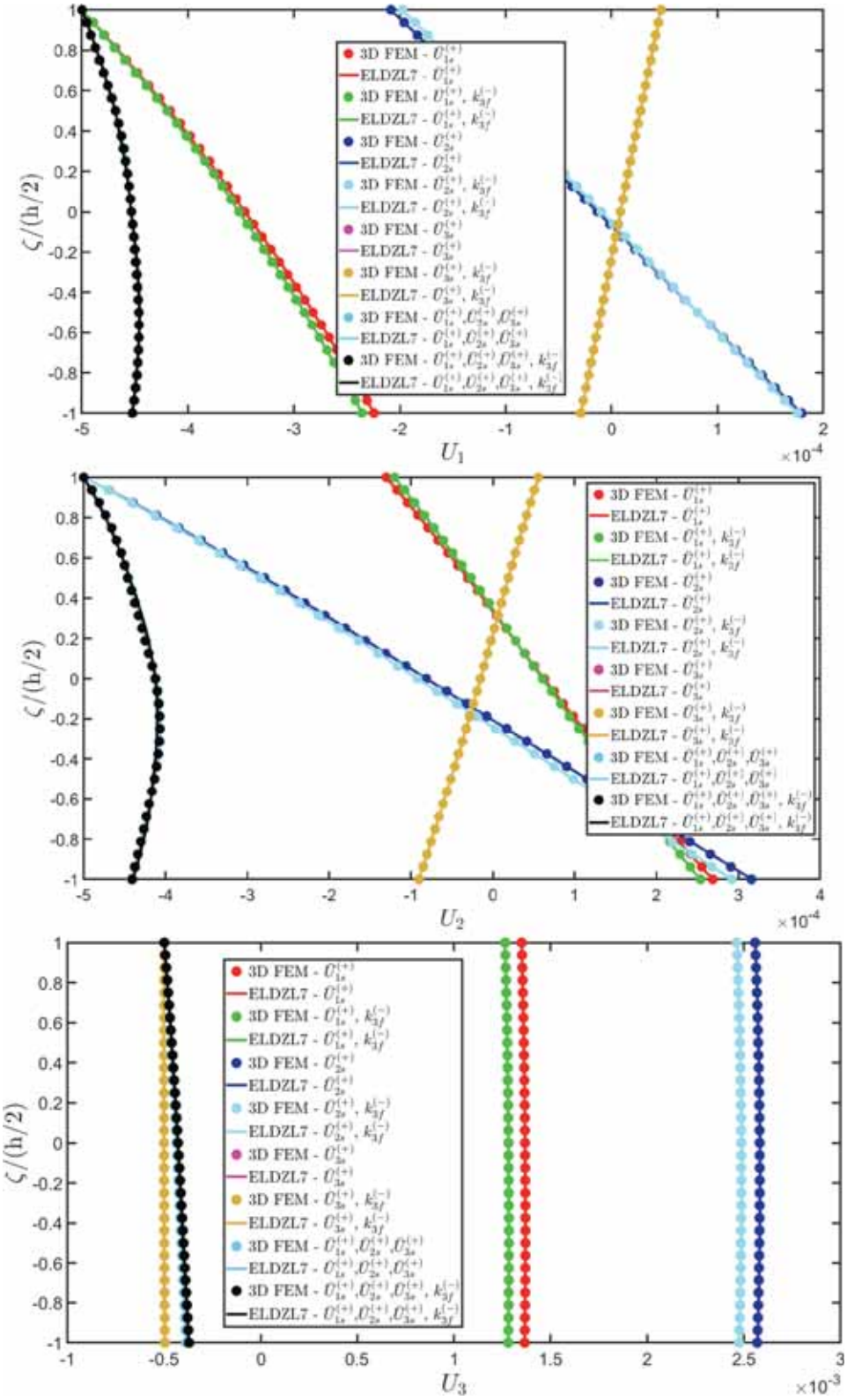

Fig. 3. Through-the-thickness distribution of the three-dimensional displacement field components [m] along the thickness direction of a simply-supported laminated rectangular plate with a prescribed sinusoidal dispersion of each configuration variable with $\tilde{N} = \tilde{M} = 1$, whose amplitudes are set equal to $\overline{U}_{1s}^{(+)} = \overline{U}_{2s}^{(+)} = \overline{U}_{3s}^{(+)} = -1 \times 10^{-3}$ m. Effect of a uniformly-distributed Winkler foundation of various stiffnesses. Visualization of thickness plots at the point $(0.25\,L_1, 0.25\,L_2)$ of the physical domain.

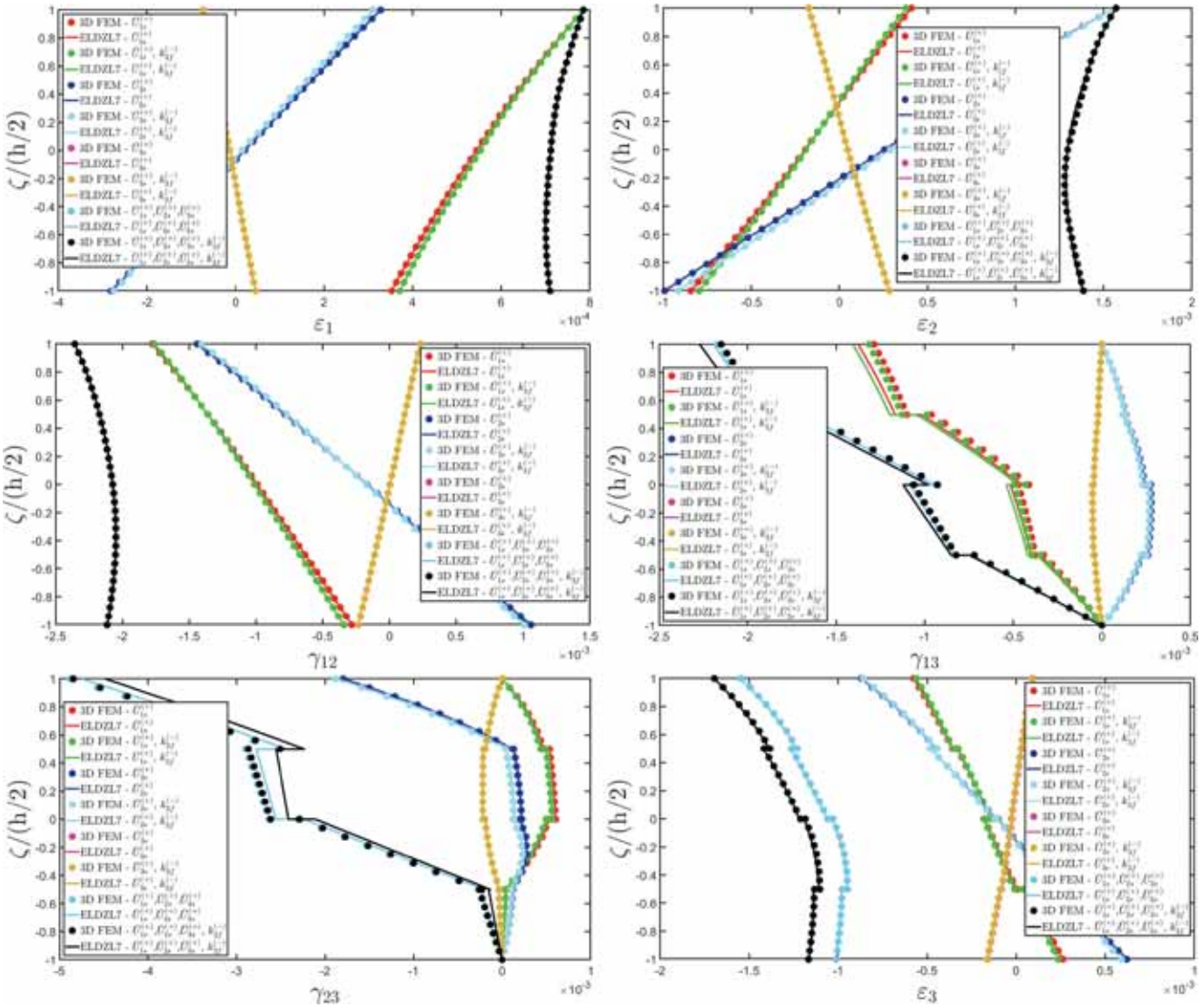

Fig. 4. Through-the-thickness distribution of the three-dimensional strain components along the thickness direction of a simply-supported laminated rectangular plate with a prescribed sinusoidal dispersion of each configuration variable with $\widetilde{N} = \widetilde{M} = 1$, whose amplitudes are set equal to $\overline{U}_{1s}^{(+)} = \overline{U}_{2s}^{(+)} = \overline{U}_{3s}^{(+)} = -1 \times 10^{-3}$ m. Effect of a uniformly-distributed Winkler foundation of various stiffness. Visualization of thickness plots at the point $(0.25L_1, 0.25L_2)$ of the physical domain.

values of the n-th order derivative of f at the same grid:

$$\mathbf{f} = \begin{bmatrix} f(x_1) & f(x_2) & \cdots & f(x_{I_Q}) \end{bmatrix}^T$$
$$\mathbf{f}^{(n)} = \left[\left.\frac{\partial^n f}{\partial x^n}\right|_{x_1} \quad \left.\frac{\partial^n f}{\partial x^n}\right|_{x_2} \quad \cdots \quad \left.\frac{\partial^n f}{\partial x^n}\right|_{x_{I_Q}} \right]^T \tag{87}$$

The value assumed by unknown function f at the discrete point x_i can be approximated through a linear combination of I_Q basis functions, denoted by $\psi_{ij} = \psi_j(x_i)$ for $i, j = 1, \ldots, I_Q$, according to the following relation from Ref. [56]:

$$f(x_i) \cong \sum_{j=1}^{I_Q} \lambda_{ij} \psi_j(x_i) \tag{88}$$

where λ_{ij} with $i, j = 1, \ldots, I_Q$ are proper weighting coefficients. Employing a matrix notation, Eqn. (88) can be written as:

$$\mathbf{f} = \mathbf{A}\boldsymbol{\lambda} \tag{89}$$

The arbitrary element of the matrix $\mathbf{A}$ is denoted as $A_{ij} = \psi_j(x_i)$. In this way, the n-th order derivative of f, evaluated at $x = x_i$, can be computed as follows:

$$\left.\frac{\partial^n f}{\partial x^n}\right|_{x_i} = \sum_{j=1}^{I_Q} \lambda_{ij} \left.\frac{\partial^n \psi_j}{\partial x^n}\right|_{x_i} \tag{90}$$

or equivalently in matrix form:

$$\mathbf{f}^{(n)} = \mathbf{A}^{(n)}\boldsymbol{\lambda} \quad \text{with} \quad A_{ij}^{(n)} = \left.\frac{\partial^n \psi_j}{\partial x^n}\right|_{x_i} \tag{91}$$

If the matrix $\mathbf{A}$ is invertible, from Eqn. (89) one gets $\boldsymbol{\lambda} = \mathbf{A}^{-1}\mathbf{f}$. As a consequence, Eqn. (91) can be written as follows:

$$\mathbf{f}^{(n)} = \mathbf{A}^{(n)}\boldsymbol{\lambda} = \mathbf{A}^{(n)}\mathbf{A}^{-1}\mathbf{f} = \mathbf{D}^{(n)}\mathbf{f} \tag{92}$$

Finally, from Eqn. (92) it can be stated that the n-th order derivative of the function $f = f(x)$ can be numerically approximated as a weighted sum of the values assumed by the function itself in a discrete computational grid of I_Q elements [56]:

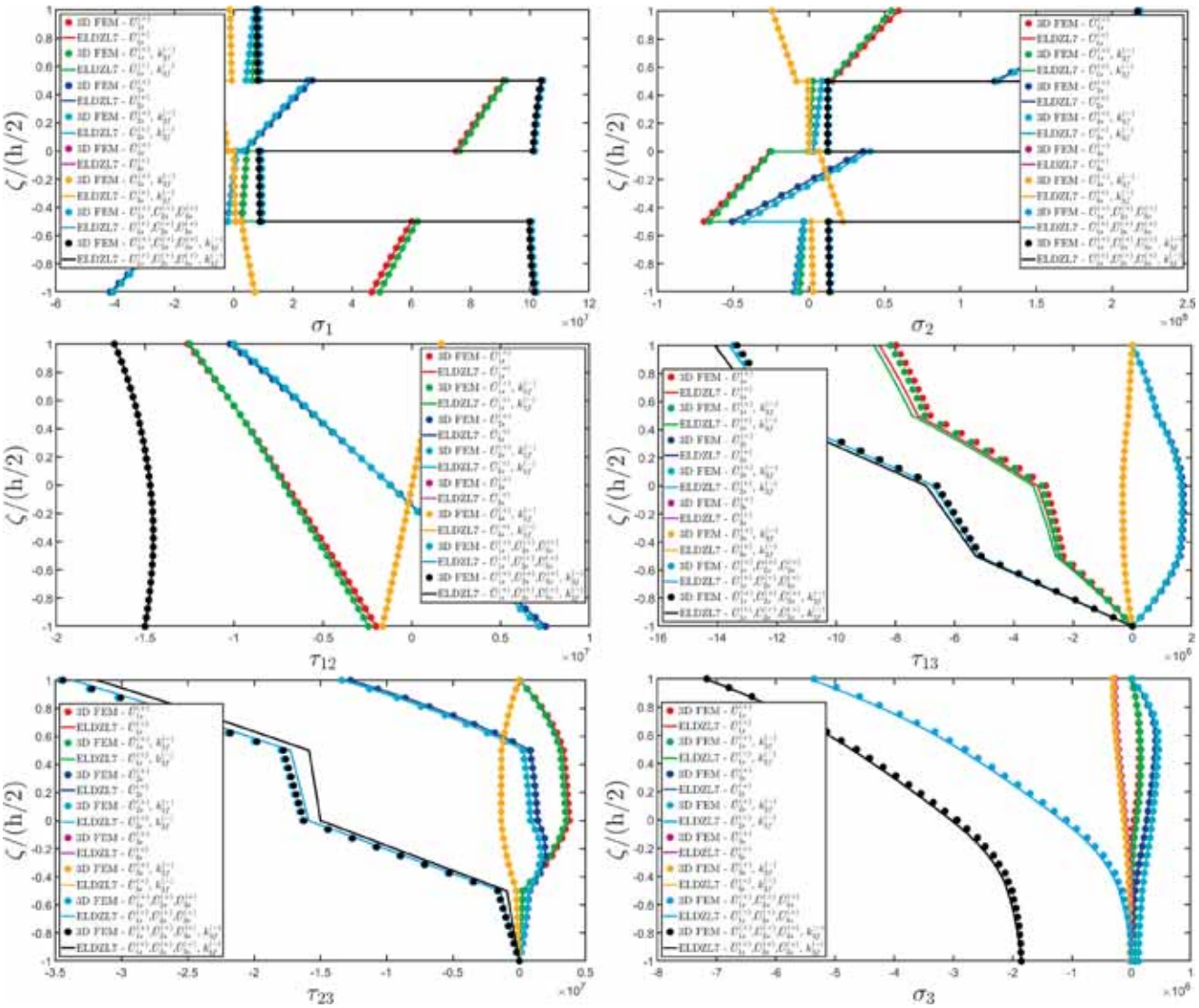

Fig. 5. Through-the-thickness distribution of the three-dimensional stress components [Pa] along the thickness direction of a simply-supported laminated rectangular plate with a prescribed sinusoidal dispersion of each configuration variable with $\widetilde{N} = \widetilde{M} = 1$, whose amplitudes are set equal to $\overline{U}_{1s}^{(+)} = \overline{U}_{2s}^{(+)} = \overline{U}_{3s}^{(+)} = -1 \times 10^{-3}$ m. Effect of a uniformly-distributed Winkler foundation of various stiffnesses. Visualization of thickness plots at the point $(0.25L_1, 0.25L_2)$ of the physical domain.

$$f^{(n)}(x_i) = \left.\frac{\partial^n f(x)}{\partial x^n}\right|_{x=x_i} \cong \sum_{j=1}^{I_Q} D_{ij}^{(n)} f(x_j) \tag{93}$$

for $i = 1, 2, ..., I_Q$. In this relation, $D_{ij}^{(n)} = \left(\mathbf{A}^{(n)}\mathbf{A}^{-1}\right)_{ij}$ denotes the GDQ weighting coefficients. The selection of discrete points x_i from the definition domain is made according to the Chebyshev-Gauss-Lobatto (CGL) harmonic distribution [56], which has demonstrated in previous papers to provide computational efficiency and stability to the present numerical method. Referring to the interval $[-1, 1]$, an arbitrary element denoted by r_i with $i = 1, ..., I_Q$ of the CGL grid is computed as follows:

$$r_i = -\cos\left(\frac{i-1}{I_Q - 1}\pi\right) \tag{94}$$

In the present study, Fourier functions are used as basis functions ψ_{ij} defined in the closed interval $[-1, 1]$:

$$\psi_{ij} = \psi_j(r_i) = \cos\left((-1)^{j-1}\frac{j-1}{2}r_i + \frac{\pi}{4}\left(1 + (-1)^j\right)\right) \tag{95}$$

It should be noted that Eqn. (95) allows one to derive the GDQ coefficients for the n-th order derivative, denoted by $\widetilde{D}_{ij}^{(n)}$, defined for the interval $[-1, 1]$. As a consequence, a coordinate transformation is performed to express the GDQ coefficients $D_{ij}^{(n)}$ of Eqn. (93) referred to the interval $[a, b]$. The following relation [56] is adopted to derive the discrete points $x_i \in [a, b]$ with $i = 1, ..., I_Q$ starting from those r_i belonging to $[-1, 1]$ defined in Eqn. (94):

$$x_i = \frac{x_{I_Q} - x_1}{r_{I_Q} - r_1}(r_i - r_1) + x_1 \tag{96}$$

for $i = 1, ..., I_Q$. Employing this coordinate transformation, the derivative of an arbitrary n-th order of the function f at a discrete point x_i is expressed by means of the chain rule:

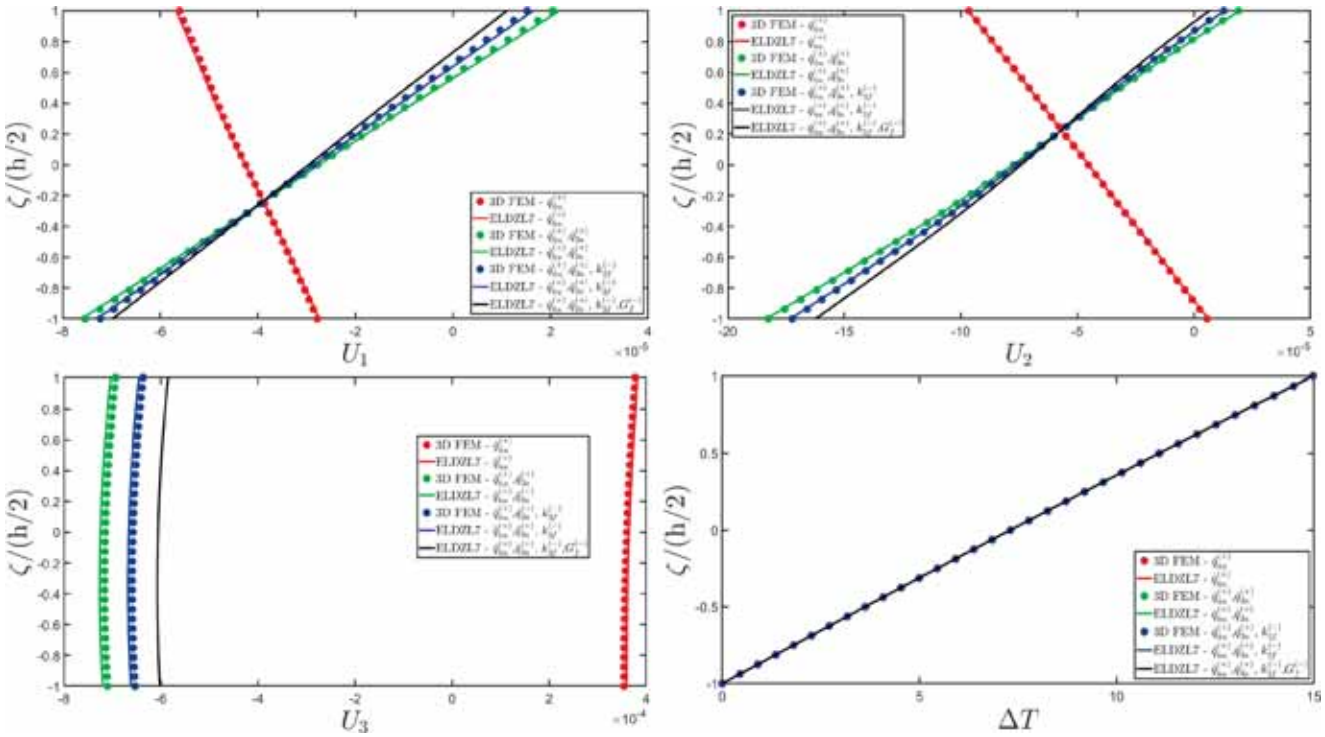

Fig. 6. Three-dimensional displacement field components [m] and temperature distribution [K] of a rectangular plate with a uniformly-distributed heat flux at the top surface of magnitude $\overline{q}_{hu}^{(+)} = -80$ J/m^2 subjected to a uniform mechanical pressure of magnitude $\overline{q}_{3u}^{(+)} = -7 \times 10^5$ N/m^2. The temperature variation configuration variable is enforced to assume a null value at the bottom surface, namely $\overline{\Delta T}^{(-)} = 0$ K. Effect of a Winkler-Pasternak elastic foundation of stiffness $k_{3f}^{(-)} = 5 \times 10^7$ Pa/m and shear modulus equal to $G_f^{(-)} = 5 \times 10^6$ Pa. Visualization of thickness plots at the point $(0.25\,L_1, 0.25\,L_2)$ of the physical domain, setting $\widetilde{N} = \widetilde{M} = 300$.

$$\left.\frac{\partial^n f}{\partial x^n}\right|_{x_i} = \left(\frac{r_{I_Q} - r_1}{x_{I_Q} - x_1}\right)^n \left.\frac{\partial^n f}{\partial r^n}\right|_{r_i} \tag{97}$$

Finally, from Eqn. (97), it can be shown that the F-GDQ coefficients $D_{ij}^{(n)}$ are calculated as follows [56]:

$$D_{ij}^{(n)} = \left(\frac{r_{I_Q} - r_1}{x_{I_Q} - x_1}\right)^n \widetilde{D}_{ij}^{(n)} \tag{98}$$

where $\widetilde{D}_{ij}^{(n)}$ for $i,j = 1, ..., I_Q$ are the GDQ coefficients referred to the interval $[-1, 1]$.

Moving from the GDQ rule of Eqn. (93), the GTIQ method [56] provides an efficient numerical computation of the integral, restricted to the interval $[x_i, x_j]$ with $i, j = 1, ..., I_Q$, of a given function $f = f(x)$ defined in the closed interval $[a, b]$, being $x_i, x_j \in [a, b]$ the extremes of integration. If the integrand function f is expanded through Taylor's series near the sample point x_i, the integral of f can be expressed as:

$$\int_{x_i}^{x_j} f(x)dx = \sum_{r=0}^{m-1} \frac{(x_j - x_i)^{r+1}}{(r+1)!} \left.\frac{d^r f}{dx^r}\right|_{x_i} \tag{99}$$

being $m \leqslant I_Q$. Following the same approach, a more accurate evaluation of the integral in hand can be performed by means of the following relation:

$$\int_{x_i}^{x_j} f(x)dx = \int_{x_i}^{\frac{x_j+x_i}{2}} f(x)dx - \int_{x_j}^{\frac{x_j+x_i}{2}} f(x)dx \tag{100}$$

If the two integrals occurring in the previous relation are expanded through Taylor's series near the discrete points x_i and x_j, and if the r-th order derivatives are numerically calculated using the GDQ method of Eqn. (93), one obtains the following relation:

$$\begin{aligned}\int_{x_i}^{x_j} f(x)dx &= \sum_{r=0}^{m-1} \frac{(x_j - x_i)^{r+1}}{2^{r+1}(r+1)!} \sum_{k=1}^{N} \varsigma_{ik}^{(r)} f(x_k) - \sum_{r=0}^{m-1} \frac{(x_i - x_j)^{r+1}}{2^{r+1}(r+1)!} \sum_{k=1}^{N} \varsigma_{jk}^{(r)} f(x_k) = \\ &= \sum_{k=1}^{N} \left(\sum_{r=0}^{m-1} \left(\frac{(x_j - x_i)^{r+1}}{2^{r+1}(r+1)!} \varsigma_{ik}^{(r)} - \frac{(x_i - x_j)^{r+1}}{2^{r+1}(r+1)!} \varsigma_{jk}^{(r)} \right) \right) f(x_k) = \\ &= \sum_{k=1}^{N} \left(\sum_{r=0}^{m-1} \frac{(x_j - x_i)^{r+1}}{2^{r+1}(r+1)!} \left(\varsigma_{ik}^{(r)} + (-1)^{r+2} \varsigma_{jk}^{(r)} \right) \right) f(x_k) = \sum_{k=1}^{N} w_k^{ij} f(x_k)\end{aligned} \tag{101}$$

Finally, Eqn. (101) is used to compute the integral of f restricted to $[a = x_1, b = x_N]$ as the sum of the integrals of the same functions evaluated in the intervals $[x_i, x_{i+1}]$, leading to the following equation:

$$\begin{aligned}\int_a^b f(x)dx &= \sum_{i=1}^{N-1} \int_{x_i}^{x_{i+1}} f(x)dx = \sum_{i=1}^{N-1} \left(\sum_{k=1}^{N} w_k^{i(i+1)} f(x_k) \right) \\ &= \sum_{k=1}^{N} \left(\sum_{i=1}^{N-1} w_k^{i(i+1)} \right) f(x_k) = \sum_{k=1}^{N} w_k^{1N} f(x_k)\end{aligned} \tag{102}$$

The GTIQ weighting coefficients introduced in Eqn. (102) are thus calculated from the following recursive relation [56]:

$$w_k^{1N} = \sum_{i=1}^{N-1} w_k^{i(i+1)} = \sum_{i=1}^{N-1} \sum_{r=0}^{m-1} \frac{(x_{i+1} - x_i)^{r+1}}{2^{r+1}(r+1)!} \left(\varsigma_{ik}^{(r)} + (-1)^{r+2} \varsigma_{(i+1)k}^{(r)} \right) \tag{103}$$

7. Post-processing reconstruction of secondary variables

In the previous sections, a semi-analytical solution was provided for the higher order two-dimensional thermo-mechanical ELW model. The

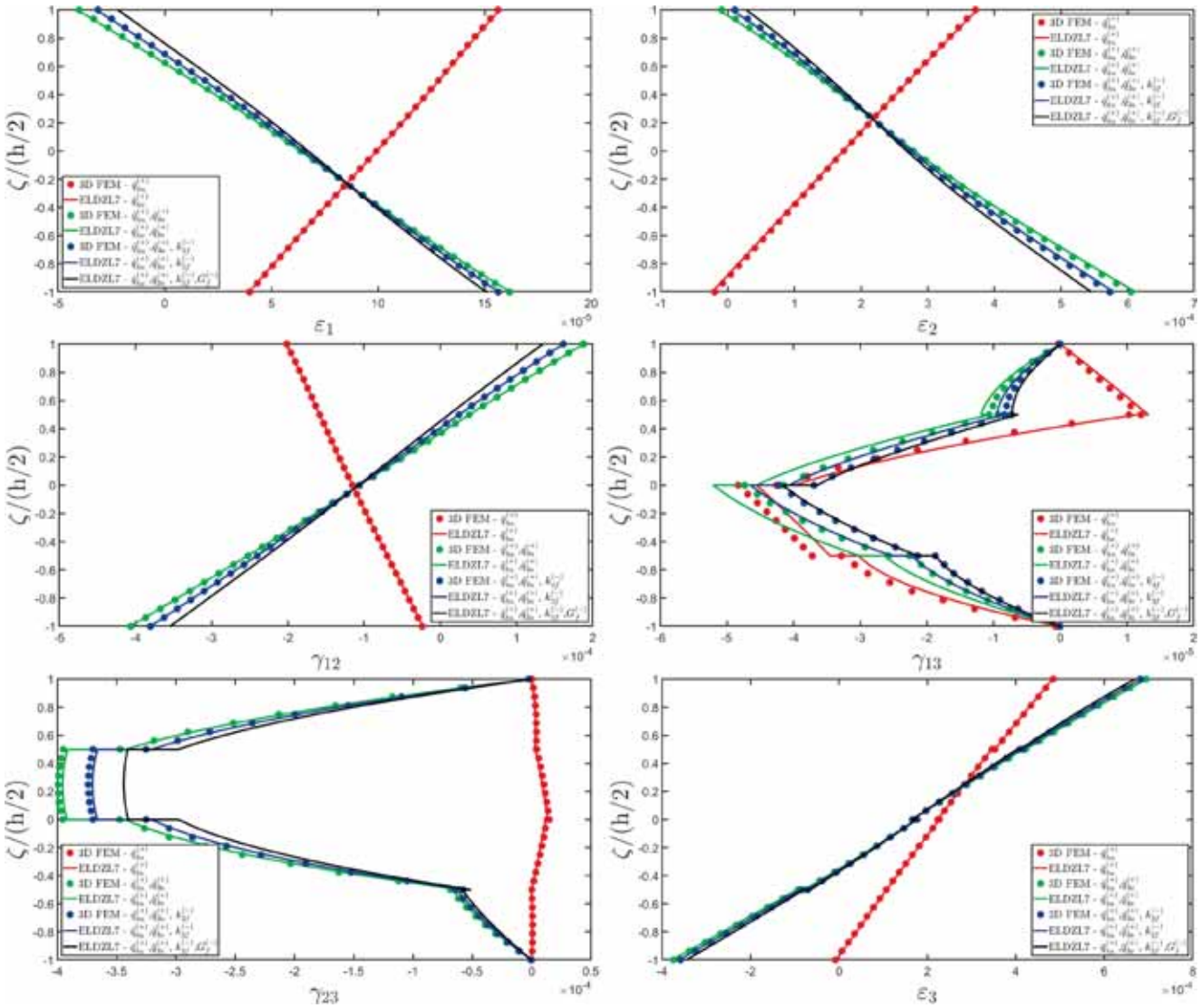

Fig. 7. Three-dimensional strain components of a rectangular plate with a uniformly-distributed heat flux at the top surface of magnitude $\overline{q}_{hu}^{(+)} = -80$ J/m^2 subjected to a uniform mechanical pressure of magnitude $\overline{q}_{3u}^{(+)} = -7 \times 10^5$ N/m^2. The temperature variation configuration variable is enforced to assume a null value at the bottom surface, namely $\overline{\Delta T}^{(-)} = 0$ K. Effect of a Winkler-Pasternak elastic foundation of stiffness $k_{3f}^{(-)} = 5 \times 10^7$ Pa/m and shear modulus equal to $G_f^{(-)} = 5 \times 10^6$ Pa. Visualization of thickness plots at the point $(0.25L_1, 0.25L_2)$ of the physical domain, setting $\widetilde{N} = \widetilde{M} = 300$.

solution of the two-dimensional formulation is used to derive the actual distribution of primary and secondary variables within the laminated three-dimensional solid, composed of l laminae. The starting point is the definition of discrete grid consisting of I_Q sample points, denoted by $\zeta_{\tilde{m}}^{(k)}$ with $\tilde{m} = 1, ..., I_Q$, in each k-th layer of the solid. Each sample point is located in the interval $[\zeta_k, \zeta_{k+1}]$, where ζ_k and ζ_{k+1} are the locations of the lower and upper skins of the k-th lamina:

$$\zeta_{\tilde{m}}^{(k)} = \frac{\zeta_{k+1} - \zeta_k}{2}\overline{x}_{\tilde{m}} + \frac{\zeta_{k+1} + \zeta_k}{2} = \frac{h_k}{2}\overline{x}_{\tilde{m}} + \frac{\zeta_{k+1} + \zeta_k}{2} \tag{104}$$

The discrete points (104) are collected in the vector $\boldsymbol{\zeta}^{(k)} = \left[\zeta_1^{(k)} \quad \cdots \quad \zeta_{\tilde{m}}^{(k)} \quad \cdots \quad \zeta_{I_Q}^{(k)}\right]^T$ of size $I_Q \times 1$, defined for each $k = 1, ..., I_Q$. The quantity $\overline{x}_{\tilde{m}} \in [-1, 1]$ is computed according to the CGL grid distribution:

$$\overline{x}_{\tilde{m}} = -\cos\left(\frac{\tilde{m} - 1}{I_Q - 1}\pi\right) \tag{105}$$

The vector $\boldsymbol{\zeta}^{(k)}$ is, thus, assembled into a vector of size $lI_Q \times 1$, where l denotes the number of layers within the solid, and its arbitrary element is denoted as ζ_m with $m = (k-1)I_Q + \tilde{m}$:

$$[\zeta_1 \ \cdots \ \zeta_m \ \cdots \ \zeta_{lI_T}]^T = [\boldsymbol{\zeta}^{(1)T} \ \cdots \ \boldsymbol{\zeta}^{(k)T} \ \cdots \ \boldsymbol{\zeta}^{(l)T}] \tag{106}$$

As can be seen, Eqn. (106) provides a set of lI_Q discrete sampling points throughout the interval $[-h/2, h/2]$. Following a similar procedure, a two-dimensional grid of size $I_N \times I_M$ can be defined within the rectangular physical domain employing the CGL grid distribution, setting $s_{1i} \in [0, L_1]$ and $s_{2j} \in [0, L_2]$:

$$s_{1i} = \frac{L_1}{2}\left(1 - \cos\left(\frac{i-1}{I_N - 1}\pi\right)\right), \quad s_{2j} = \frac{L_2}{2}\left(1 - \cos\left(\frac{j-1}{I_M - 1}\pi\right)\right) \tag{107}$$

In this way, the three-dimensional configuration variables, collected in the vector $\boldsymbol{\Delta}_{(ijm)}^{(k)}$ with $i = 1, ..., I_N$, $j = 1, ..., I_M$ and $m = 1, ..., lI_Q$, are computed at each point of the three-dimensional solid from the discrete form of Eqn. (10) reported below:

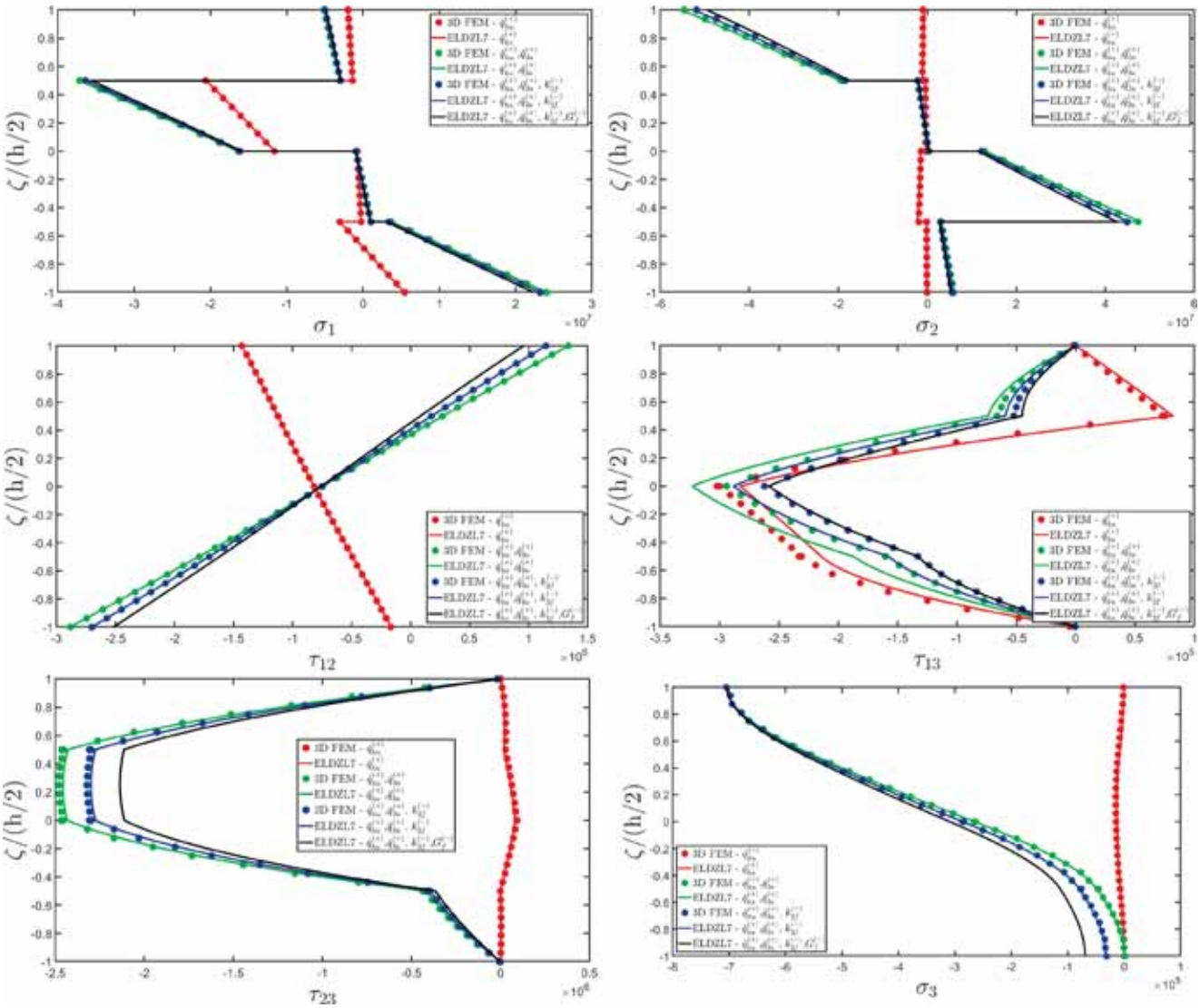

Fig. 8. Three-dimensional stress components [Pa] of a rectangular plate with a uniformly-distributed heat flux at the top surface of magnitude $\overline{q}_{hu}^{(+)} = -80$ J/m^2 subjected to a uniform mechanical pressure of magnitude $\overline{q}_{3u}^{(+)} = -7 \times 10^5$ N/m^2. The temperature variation configuration variable is enforced to assume a null value at the bottom surface, namely $\overline{\Delta \mathrm{T}}^{(-)} = 0$ K. Effect of a Winkler-Pasternak elastic foundation of stiffness $k_{3f}^{(-)} = 5 \times 10^7$ Pa/m and shear modulus equal to $G_f^{(-)} = 5 \times 10^6$ Pa. Visualization of thickness plots at the point $(0.25\,L_1, 0.25\,L_2)$ of the physical domain, setting $\widetilde{N} = \widetilde{M} = 300$.

$$\mathbf{\Delta}_{(ijm)}^{(k)} = \sum_{\tau=0}^{N+1} \mathbf{F}_{\tau(ijm)}^{(k)} \boldsymbol{\delta}_{(ij)}^{(\tau)} \tag{108}$$

where $\boldsymbol{\delta}_{(ij)}^{(\tau)}$ is the vector of the generalized configuration variables, solution of the fundamental equations (69) for the point (s_{1i}, s_{2j}), while $\mathbf{F}_{\tau(ijm)}^{(k)}$ represents the matrix of the thickness functions. Once the vector $\mathbf{\Delta}_{(ijm)}^{(k)}$ is derived from Eqn. (108), the vector $\boldsymbol{\pi}_{(ijm)}^{(k)}$ of the primary variables is calculated from the discrete form of Eqn. (27):

$$\boldsymbol{\pi}_{(ijm)}^{(k)} = \sum_{\tau=0}^{N+1} \sum_{i=1}^{4} \mathbf{Z}_{(ij)}^{(k\tau)\alpha_i} \boldsymbol{\pi}_{(ij)}^{(\tau)\alpha_i} \tag{109}$$

In-plane secondary variables of the thermo-mechanical problem are derived from the three-dimensional constitutive relationship (31), under the assumptions of Eqn. (82):

$$\begin{aligned}
\sigma_{1(ijm)}^{(k)} &= \overline{C}_{11}^{(k)} \varepsilon_{1(ijm)}^{(k)} + \overline{C}_{12}^{(k)} \varepsilon_{2(ijm)}^{(k)} + \overline{C}_{13}^{(k)} \varepsilon_{3(ijm)}^{(k)} - \overline{z}_{11}^{(k)} \widehat{\Delta \mathrm{T}}_{(ijm)}^{(k)} \\
\sigma_{2(ijm)}^{(k)} &= \overline{C}_{12}^{(k)} \varepsilon_{1(ijm)}^{(k)} + \overline{C}_{22}^{(k)} \varepsilon_{2(ijm)}^{(k)} + \overline{C}_{23}^{(k)} \varepsilon_{3(ijm)}^{(k)} - \overline{z}_{22}^{(k)} \widehat{\Delta \mathrm{T}}_{(ijm)}^{(k)} \\
\tau_{12(ijm)}^{(k)} &= \overline{C}_{66}^{(k)} \gamma_{12(ijm)}^{(k)} \\
h_{1(ijm)}^{(k)} &= \overline{k}_{11}^{(k)} \theta_{1(ijm)}^{(k)} \\
h_{2(ijm)}^{(k)} &= \overline{k}_{22}^{(k)} \theta_{2(ijm)}^{(k)}
\end{aligned} \tag{110}$$

The out-of-plane secondary variables $\tau_{13}^{(k)}$ and $\tau_{23}^{(k)}$ are derived from the three-dimensional equilibrium equations, which are reported in the following [22]:

$$\begin{aligned}
&\frac{\partial \tau_{13}^{(k)}}{\partial \zeta} + \tau_{13}^{(k)} \left(\frac{2}{R_1 + \zeta} + \frac{1}{R_2 + \zeta} \right) = -\frac{1}{A_1 (1 + \zeta / R_1)} \frac{\partial \sigma_1^{(k)}}{\partial \alpha_1} + \\
&+ \frac{\sigma_2^{(k)} - \sigma_1^{(k)}}{A_1 A_2 (1 + \zeta / R_2)} \frac{\partial A_2}{\partial \alpha_1} - \frac{1}{A_2 (1 + \zeta / R_2)} \frac{\partial \tau_{12}^{(k)}}{\partial \alpha_2} - \frac{2 \tau_{12}^{(k)}}{A_1 A_2 (1 + \zeta / R_1)} \frac{\partial A_1}{\partial \alpha_2}
\end{aligned}$$

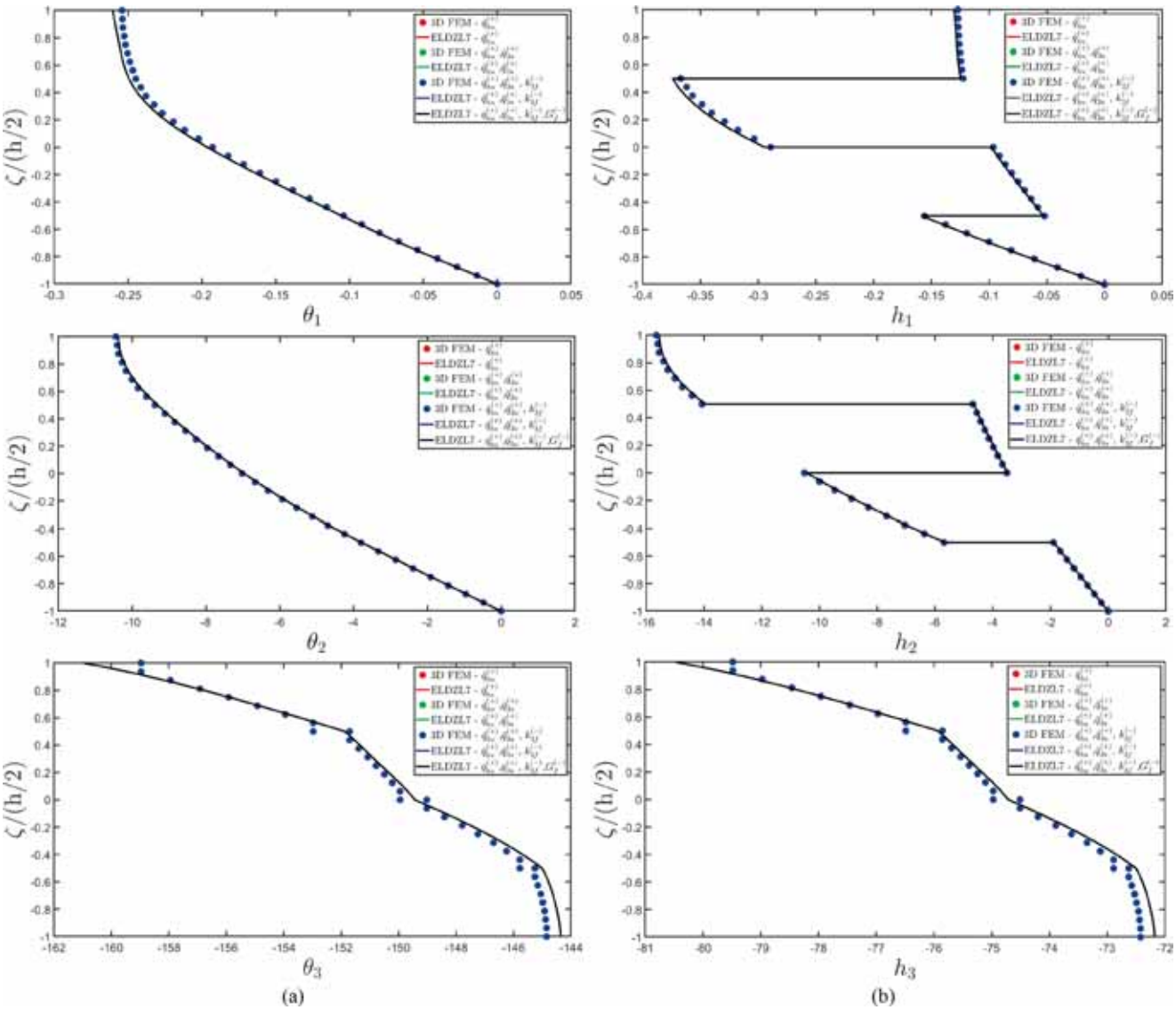

Fig. 9. Three-dimensional thermal gradient components (a) and heat flux components (b), expressed in [J/m^2], of a rectangular plate with a uniformly-distributed heat flux at the top surface of magnitude $\overline{q}_{hu}^{(+)} = -80$ J/m^2 subjected to a uniform mechanical pressure of magnitude $\overline{q}_{3u}^{(+)} = -7 \times 10^5$ N/m^2. The temperature variation configuration variable is enforced to assume a null value at the bottom surface, namely $\overline{\Delta T}^{(-)} = 0$ K. Effect of a Winkler-Pasternak elastic foundation of stiffness $k_{3f}^{(-)} = 5 \times 10^7$ Pa/m and shear modulus equal to $G_f^{(-)} = 5 \times 10^6$ Pa. Visualization of thickness plots at the point $(0.25 L_1, 0.25 L_2)$ of the physical domain, setting $\widetilde{N} = \widetilde{M} = 300$.

$$\frac{\partial \tau_{23}^{(k)}}{\partial \zeta} + \tau_{23}^{(k)} \left(\frac{1}{R_1 + \zeta} + \frac{2}{R_2 + \zeta} \right) = -\frac{1}{A_2(1+\zeta/R_2)} \frac{\partial \sigma_2^{(k)}}{\partial \alpha_2} + \\ + \frac{\sigma_1^{(k)} - \sigma_2^{(k)}}{A_1 A_2 (1+\zeta/R_1)} \frac{\partial A_1}{\partial \alpha_2} - \frac{1}{A_1(1+\zeta/R_1)} \frac{\partial \tau_{12}^{(k)}}{\partial \alpha_1} - \frac{2\tau_{12}^{(k)}}{A_1 A_2 (1+\zeta/R_2)} \frac{\partial A_2}{\partial \alpha_1} \tag{111}$$

These first order differential equations are solved once the boundary conditions are written in each k-th layer of the shell. When $k = 1$, the boundary conditions are derived from the loading conditions at the bottom surface, while for $k \neq 1$ they are modelled from the interlaminar equilibrium conditions [22]:

$$k = 1 \;\Rightarrow\; \begin{cases} \overline{\tau}_{13(ij1)}^{(1)} = q_{1s(ij)}^{(-)} \\ \overline{\tau}_{23(ij1)}^{(1)} = q_{2s(ij)}^{(-)} \end{cases}$$
$$k \neq 1 \;\Rightarrow\; \begin{cases} \overline{\tau}_{13\left(ij\left((k-1)I_Q+1\right)\right)}^{(k)} = \overline{\tau}_{13\left(ij\left((k-1)I_Q\right)\right)}^{(k-1)} \\ \overline{\tau}_{23\left(ij\left((k-1)I_Q+1\right)\right)}^{(k)} = \overline{\tau}_{23\left(ij\left((k-1)I_Q\right)\right)}^{(k-1)} \end{cases} \tag{112}$$

It should be recalled that the doubly-curved shell element is loaded at the top surface; therefore, the equilibrium conditions at $\zeta = h/2$ are $\overline{\tau}_{13(ij(I_Q))}^{(l)} = q_{1(ij)}^{(+)}$ and $\overline{\tau}_{23(ij(I_Q))}^{(l)} = q_{2(ij)}^{(+)}$. As a consequence, the actual through-the-thickness distribution of stresses $\tau_{13}^{(k)}$ and $\tau_{23}^{(k)}$ is evaluated, for each (s_{1i}, s_{2j}), from the following relation [22]:

Table 3
Through-the-thickness distribution, referred to the point located at $(0.25\,L_1, 0.25\,L_2)$ within the physical domain, of the thermo-mechanical configuration variables of a simply-supported rectangular plate subjected to a uniformly-distributed external pressure and thermal flux. Effect of an elastic foundation located at the bottom of the panel. Comparison between 3D FEM results and those obtained from the ELW two-dimensional semi-analytical formulation. The results are provided for the point located at the middle height of each layer of the stacking sequence.

	$\overline{q}_{hu}^{(+)}$		$\overline{q}_{hu}^{(+)}, \overline{q}_{3u}^{(+)}$		$\overline{q}_{hu}^{(+)}, \overline{q}_{3u}^{(+)}, k_{3f}^{(-)}$		$\overline{q}_{hu}^{(+)}, \overline{q}_{3u}^{(+)}, k_{3f}^{(-)}, G_f^{(-)}$
	3D FEM	ELDZL7	3D FEM	ELDZL7	3D FEM	ELDZL7	ELDZL7
Layer 1							
$U_1\ [\times 10^{-5}\mathrm{m}]$	−3.13	−3.10	−6.33	−6.38	−6.13	−6.17	−5.96
$U_2\ [\times 10^{-5}\mathrm{m}]$	−0.71	−0.67	−15.50	−15.58	−14.70	−14.77	−13.92
$U_3\ [\times 10^{-5}\mathrm{m}]$	35.48	35.97	−71.40	−72.39	−65.74	−66.59	−60.56
$\Delta\mathrm{T}\,[\mathrm{K}]$	1.81	1.81	1.81	1.81	1.81	1.81	1.81
Layer 2							
$U_1\ [\times 10^{-5}\mathrm{m}]$	−3.87	−3.87	−3.94	−3.95	−3.95	−3.95	−3.95
$U_2\ [\times 10^{-5}\mathrm{m}]$	−3.26	−3.24	−10.18	−10.22	−9.81	−9.84	−9.45
$U_3\ [\times 10^{-5}\mathrm{m}]$	35.74	36.24	−71.61	−72.61	−65.94	−66.79	−60.75
$\Delta\mathrm{T}\,[\mathrm{K}]$	5.45	5.45	5.45	5.45	5.45	5.45	5.45
Layer 3							
$U_1\ [\times 10^{-5}\mathrm{m}]$	−4.62	−4.65	−1.59	−1.54	−1.79	−1.75	−1.97
$U_2\ [\times 10^{-5}\mathrm{m}]$	−5.80	−5.80	−5.45	−5.45	−5.47	−5.47	−5.50
$U_3\ [\times 10^{-5}\mathrm{m}]$	36.31	36.80	−71.18	−72.18	−65.51	−66.37	−60.32
$\Delta\mathrm{T}\,[\mathrm{K}]$	9.19	9.18	9.19	9.18	9.19	9.18	9.18
Layer 4							
$U_1\ [\times 10^{-5}\mathrm{m}]$	−5.28	−5.33	0.83	0.93	0.41	0.50	0.08
$U_2\ [\times 10^{-5}\mathrm{m}]$	−8.36	−8.38	−0.72	−0.67	−1.14	−1.09	−1.54
$U_3\ [\times 10^{-5}\mathrm{m}]$	37.18	37.67	−70.14	−71.13	−64.48	−65.33	−59.30
$\Delta\mathrm{T}\,[\mathrm{K}]$	13.00	12.99	13.00	12.99	13.00	12.99	13.00

$$\begin{aligned}\tau_{13(ijm)}^{(k)} &= \overline{\tau}_{13(ijm)}^{(k)} + \frac{q_{1(ij)}^{(+)} - \overline{\tau}_{13}^{(l)}{}_{(ij(lI_Q))}}{h}\left(\zeta_m + \frac{h}{2}\right)\\ \tau_{23(ijm)}^{(k)} &= \overline{\tau}_{23(ijm)}^{(k)} + \frac{q_{2(ij)}^{(+)} - \overline{\tau}_{23}^{(l)}{}_{(ij(lI_Q))}}{h}\left(\zeta_m + \frac{h}{2}\right)\end{aligned} \tag{113}$$

with $m = 1, \ldots, lI_Q$. Once the out-of-plane shear stresses are recovered, the normal stress $\sigma_3^{(k)}$ can be derived from the three-dimensional equilibrium equation [22] reported below, where the quantities $\tau_{13}^{(k)}$ and $\tau_{23}^{(k)}$ are known, along with $\sigma_1^{(k)}$ and $\sigma_2^{(k)}$:

$$\begin{aligned}\frac{\partial\sigma_3^{(k)}}{\partial\zeta} + \sigma_3^{(k)}\left(\frac{1}{R_1+\zeta}+\frac{1}{R_2+\zeta}\right) = &-\frac{1}{A_1(1+\zeta/R_1)}\frac{\partial\tau_{13}^{(k)}}{\partial\alpha_1} - \frac{\tau_{13}^{(k)}}{A_1A_2(1+\zeta/R_2)}\frac{\partial A_2}{\partial\alpha_1} +\\ &-\frac{1}{A_2(1+\zeta/R_2)}\frac{\partial\tau_{23}^{(k)}}{\partial\alpha_2} - \frac{\tau_{23}^{(k)}}{A_1A_2(1+\zeta/R_1)}\frac{\partial A_1}{\partial\alpha_2} + \frac{\sigma_1^{(k)}}{R_1+\zeta} + \frac{\sigma_2^{(k)}}{R_2+\zeta}\end{aligned} \tag{114}$$

In the same way, the following balance equation is considered to determine the actual distribution of the out-of-plane heat flux $h_3^{(k)}$:

$$\begin{aligned}\frac{\partial h_3^{(k)}}{\partial\zeta} + h_3^{(k)}\left(\frac{1}{R_1+\zeta}+\frac{1}{R_2+\zeta}\right) = &-\frac{1}{A_1(1+\zeta/R_1)}\frac{\partial h_1^{(k)}}{\partial\alpha_1} - \frac{h_1^{(k)}}{A_1A_2(1+\zeta/R_2)}\frac{\partial A_2}{\partial\alpha_1} +\\ &-\frac{1}{A_2(1+\zeta/R_2)}\frac{\partial h_2^{(k)}}{\partial\alpha_2} - \frac{h_2^{(k)}}{A_1A_2(1+\zeta/R_1)}\frac{\partial A_1}{\partial\alpha_2}\end{aligned} \tag{115}$$

Note that the quantities $h_1^{(k)}$ and $h_2^{(k)}$ occurring in Eqn. (115) have been already derived from Eqn. (110). The solution of the first order differential equations (114)-(115) is obtained by applying the following loading conditions referred to the bottom surface, which serve as the boundary conditions for the problem under consideration [22]:

$$\begin{aligned} k = 1 \;\Rightarrow\; &\begin{cases}\overline{\sigma}_{3(ij1)}^{(1)} = q_{3(ij)}^{(-)}\\ \overline{h}_{3(ij1)}^{(1)} = q_{\mathrm{T}(ij)}^{(-)}\end{cases}\\ k \neq 1 \;\Rightarrow\; &\begin{cases}\overline{\sigma}_{3(ij((k-1)I_T+1))}^{(k)} = \overline{\sigma}_{3(ij((k-1)I_T))}^{(k-1)}\\ \overline{h}_{3(ij((k-1)I_T+1))}^{(k)} = \overline{h}_{3(ij((k-1)I_T))}^{(k-1)}\end{cases}\end{aligned} \tag{116}$$

Following the same approach as in Eqn. (113), the loading conditions at the bottom surface are modelled through the following linear correction of the through-the-thickness distribution of $\sigma_3^{(k)}$ and $h_3^{(k)}$:

$$\begin{aligned}\sigma_{3(ijm)}^{(k)} &= \overline{\sigma}_{3(ijm)}^{(k)} + \frac{q_{3s(ij)}^{(+)} - \overline{\sigma}^{(l)}{}_{3(ij(lI_Q))}}{h}\left(\zeta_m + \frac{h}{2}\right)\\ h_{3(ijm)}^{(k)} &= \overline{h}_{3(ijm)}^{(k)} + \frac{q_{\mathrm{T}(ij)}^{(+)} - \overline{h}_{3(ij(lI_Q))}^{(l)}}{h}\left(\zeta_m + \frac{h}{2}\right)\end{aligned} \tag{117}$$

The thermo-mechanical constitutive relations of Eqn. (82) are now adopted to determine the adjusted dispersions of the out-of-plane primary variables $\gamma_{13}^{(k)}, \gamma_{23}^{(k)}, \varepsilon_3^{(k)}$ and $\vartheta_3^{(k)}$ for each $i = 1,\ldots,I_N, j = 1, \ldots, I_M$ and $m = 1, \ldots, lI_Q$:

$$\begin{aligned}\tau_{13}^{(k)} &= \overline{C}_{44}^{(k)}\gamma_{13}^{(k)}\\ \tau_{23}^{(k)} &= \overline{C}_{55}^{(k)}\gamma_{23}^{(k)}\\ \sigma_3^{(k)} &= \overline{C}_{13}^{(k)}\varepsilon_1^{(k)} + \overline{C}_{23}^{(k)}\varepsilon_2^{(k)} + \overline{C}_{33}^{(k)}\varepsilon_3^{(k)} - \overline{z}_{33}^{(k)}\widehat{\Delta\mathrm{T}}^{(k)}\\ h_3^{(k)} &= \overline{k}_{33}^{(k)}\vartheta_3^{(k)}\end{aligned} \tag{118}$$

In this way, the primary variables $\gamma_{13(ijm)}^{(k)}, \gamma_{23(ijm)}^{(k)}, \varepsilon_{3(ijm)}^{(k)}$ and $\vartheta_{3(ijm)}^{(k)}$ with $i = 1, \ldots, I_N$, $j = 1, \ldots, I_M$ and $m = 1, \ldots, lI_Q$ are derived for any point of the doubly-curved three-dimensional solid from Eqn. (118), leading to the following relations:

Table 4
Through-the-thickness distribution, referred to the point located at $(0.25L_1, 0.25L_2)$ within the physical domain, of the thermo-mechanical primary variables of a simply-supported rectangular plate subjected to a uniformly-distributed external pressure and thermal flux. Effect of an elastic foundation located at the bottom of the panel. Comparison between 3D FEM results and those obtained from the ELW two-dimensional semi-analytical formulation. The results are provided for the point located at the middle height of each layer of the stacking sequence.

	$\overline{q}_{hu}^{(+)}$		$\overline{q}_{hu}^{(+)}, \overline{q}_{3u}^{(+)}$		$\overline{q}_{hu}^{(+)}, \overline{q}_{3u}^{(+)}, k_{3f}^{(-)}$		$\overline{q}_{hu}^{(+)}, \overline{q}_{3u}^{(+)}, k_{3f}^{(-)}, G_f^{(-)}$
	3D FEM	ELDZL7	3D FEM	ELDZL7	3D FEM	ELDZL7	ELDZL7
Layer 1							
$\varepsilon_1\ [\times 10^{-5}]$	5.42	5.40	13.54	13.59	13.20	13.24	12.85
$\varepsilon_2\ [\times 10^{-5}]$	2.87	2.57	51.80	52.35	49.31	49.79	47.13
$\varepsilon_3\ [\times 10^{-5}]$	4.93	5.09	−23.20	−23.52	−22.07	−22.36	−21.15
$\gamma_{12}\ [\times 10^{-5}]$	−4.63	−4.60	−32.89	−32.95	−31.00	−31.04	−29.14
$\gamma_{13}\ [\times 10^{-5}]$	−2.23	−2.03	−1.41	−1.65	−1.18	−1.39	−1.18
$\gamma_{23}\ [\times 10^{-5}]$	0.07	0.05	−3.92	−3.79	−3.67	−3.55	−3.30
ϑ_1 [K/m]	−0.05	−0.06	−0.05	−0.06	−0.05	−0.06	−0.06
ϑ_2 [K/m]	−1.91	−1.89	−1.91	−1.89	−1.91	−1.89	−1.89
ϑ_3 [K/m]	−144.98	−144.56	−144.98	−144.56	−144.98	−144.56	−144.56
Layer 2							
$\varepsilon_1\ [\times 10^{-5}]$	8.40	8.40	8.70	8.70	8.70	8.70	8.70
$\varepsilon_2\ [\times 10^{-5}]$	12.57	12.41	35.17	35.44	34.03	34.26	33.03
$\varepsilon_3\ [\times 10^{-5}]$	16.63	16.68	5.35	5.19	5.64	5.49	5.80
$\gamma_{12}\ [\times 10^{-5}]$	−9.27	−9.25	−17.79	−17.84	−17.23	−17.27	−16.70
$\gamma_{13}\ [\times 10^{-5}]$	−4.26	−3.99	−3.87	−4.32	−3.37	−3.79	−3.33
$\gamma_{23}\ [\times 10^{-5}]$	0.70	0.61	−24.41	−23.99	−22.84	−22.44	−20.83
ϑ_1 [K/m]	−0.15	−0.15	−0.15	−0.15	−0.15	−0.15	−0.15
ϑ_2 [K/m]	−5.54	−5.50	−5.54	−5.50	−5.54	−5.50	−5.50
ϑ_3 [K/m]	−147.24	−146.92	−147.24	−146.92	−147.24	−146.92	−146.92
Layer 3							
$\varepsilon_1\ [\times 10^{-5}]$	11.41	11.43	3.94	3.90	4.28	4.25	4.64
$\varepsilon_2\ [\times 10^{-5}]$	22.24	22.23	21.11	21.08	21.19	21.17	21.25
$\varepsilon_3\ [\times 10^{-5}]$	28.40	28.38	28.98	28.98	28.67	28.66	28.32
$\gamma_{12}\ [\times 10^{-5}]$	−13.71	−13.72	−3.41	−3.40	−4.11	−4.11	−4.82
$\gamma_{13}\ [\times 10^{-5}]$	−2.14	−1.92	−2.81	−3.09	−2.44	−2.70	−2.36
$\gamma_{23}\ [\times 10^{-5}]$	1.03	0.89	−39.95	−39.57	−37.40	−37.03	−34.41
ϑ_1 [K/m]	−0.23	−0.23	−0.23	−0.23	−0.23	−0.23	−0.23
ϑ_2 [K/m]	−8.27	−8.22	−8.27	−8.22	−8.27	−8.22	−8.22
ϑ_3 [K/m]	−150.79	−150.61	−150.79	−150.61	−150.79	−150.61	−150.61
Layer 4							
$\varepsilon_1\ [\times 10^{-5}]$	14.21	14.25	−1.32	−1.39	−0.62	−0.67	0.12
$\varepsilon_2\ [\times 10^{-5}]$	32.11	32.25	7.14	6.80	8.44	8.15	9.55
$\varepsilon_3\ [\times 10^{-5}]$	41.77	41.66	55.25	55.41	54.30	54.43	53.39
$\gamma_{12}\ [\times 10^{-5}]$	−17.94	−17.98	11.16	11.20	9.18	9.20	7.21
$\gamma_{13}\ [\times 10^{-5}]$	0.59	0.67	−0.74	−0.80	−0.60	−0.66	−0.53
$\gamma_{23}\ [\times 10^{-5}]$	0.38	0.30	−21.33	−20.92	−19.96	−19.57	−18.18
ϑ_1 [K/m]	−0.25	−0.26	−0.25	−0.26	−0.25	−0.26	−0.26
ϑ_2 [K/m]	−10.17	−10.11	−10.17	−10.11	−10.17	−10.11	−10.11
ϑ_3 [K/m]	−155.92	−155.90	−155.92	−155.90	−155.92	−155.90	−155.90

$$
\begin{aligned}
\gamma_{13(ijm)}^{(k)} &= \frac{\tau_{13(ijm)}^{(k)}}{\overline{C}_{44}^{(k)}} \\
\gamma_{23(ijm)}^{(k)} &= \frac{\tau_{23(ijm)}^{(k)}}{\overline{C}_{55}^{(k)}} \\
\varepsilon_{3(ijm)}^{(k)} &= \frac{1}{\overline{C}_{33}^{(k)}}\left(\sigma_{3(ijm)}^{(k)} - \overline{C}_{13}^{(k)}\varepsilon_{1(ijm)}^{(k)} - \overline{C}_{23}^{(k)}\varepsilon_{2(ijm)}^{(k)} + -\overline{z}_{33}^{(k)}\widehat{\Delta\mathrm{T}}_{(ijm)}^{(k)}\right) \\
\theta_{3(ijm)}^{(k)} &= \frac{h_{3(ijm)}^{(k)}}{\overline{k}_{33}^{(k)}}
\end{aligned}
\tag{119}
$$

A higher level of accuracy can be reached by evaluating the in-plane stresses, and thermal flux components are determined from the three-dimensional constitutive relationship of Eqn. (82), considering the updated values of the in-plane and out-of-plane primary variables. Then, the entire recovery process is iteratively repeated until a convergence of the through-the-thickness dispersions of the variables is achieved. In this way, the solution of the present model, even though it is based on a two-dimensional formulation, aligns with the predictions of more computationally expensive three-dimensional simulations.

8. Applications and results

In this section, some examples of investigations are presented, where the current formulation is applied to predict the mechanical response of laminated panels of different curvatures in a thermal environment. Various panels are considered, each of them characterized by different curvatures and loading conditions. In addition, the effect of a Winkler-Pasternak elastic foundation is studied. A geometric representation of the panels can be found in Fig. 1, where some information regarding the ELW geometric description of the solid has been added, along with the

Table 5
Through-the-thickness distribution, referred to the point located at $(0.25L_1, 0.25L_2)$ within the physical domain, of the thermo-mechanical secondary variables of a simply-supported rectangular plate subjected to a uniformly-distributed external pressure and thermal flux. Effect of an elastic foundation located at the bottom of the panel. Comparison between 3D FEM results and those obtained from the ELW two-dimensional semi-analytical formulation. The results are provided for the point located at the middle height of each layer of the stacking sequence.

	$\overline{q}^{(+)}_{hu}$		$\overline{q}^{(+)}_{hu}, \overline{q}^{(+)}_{3u}$		$\overline{q}^{(+)}_{hu}, \overline{q}^{(+)}_{3u}, k^{(-)}_{3f}$		$\overline{q}^{(+)}_{hu}, \overline{q}^{(+)}_{3u}, k^{(-)}_{3f}, G^{(-)}_{f}$
	3D FEM	ELDZL7	3D FEM	ELDZL7	3D FEM	ELDZL7	ELDZL7
Layer 1							
$\sigma_1\ [\times 10^5\,\mathrm{N/m^2}]$	11.94	11.60	137.81	138.57	132.23	132.87	126.60
$\sigma_2\ [\times 10^5\,\mathrm{N/m^2}]$	−1.26	−1.53	44.98	45.49	42.49	42.92	40.24
$\sigma_3\ [\times 10^5\,\mathrm{N/m^2}]$	−0.02	−0.02	−0.11	−0.14	−0.44	−0.46	−0.82
$\tau_{12}\ [\times 10^5\,\mathrm{N/m^2}]$	−3.29	−3.27	−23.35	−23.39	−22.01	−22.04	−20.69
$\tau_{13}\ [\times 10^5\,\mathrm{N/m^2}]$	−1.58	−1.44	−1.00	−1.17	−0.83	−0.99	−0.84
$\tau_{23}\ [\times 10^5\,\mathrm{N/m^2}]$	0.05	0.03	−2.43	−2.35	−2.28	−2.21	−2.05
$h_1\ [\mathrm{J/m^2}]$	−0.08	−0.08	−0.08	−0.08	−0.08	−0.08	−0.08
$h_2\ [\mathrm{J/m^2}]$	−0.96	−0.95	−0.96	−0.95	−0.96	−0.95	−0.95
$h_3\ [\mathrm{J/m^2}]$	−72.49	−72.28	−72.49	−72.28	−72.49	−72.28	−72.28
Layer 2							
$\sigma_1\ [\times 10^5\,\mathrm{N/m^2}]$	−5.07	−5.07	0.75	0.82	0.30	0.37	−0.11
$\sigma_2\ [\times 10^5\,\mathrm{N/m^2}]$	−16.28	−18.25	296.87	300.68	280.89	284.20	267.06
$\sigma_3\ [\times 10^5\,\mathrm{N/m^2}]$	−0.12	−0.10	−1.27	−1.29	−1.54	−1.57	−1.86
$\tau_{12}\ [\times 10^5\,\mathrm{N/m^2}]$	−6.58	−6.57	−12.63	−12.66	−12.23	−12.26	−11.86
$\tau_{13}\ [\times 10^5\,\mathrm{N/m^2}]$	−2.65	−2.48	−2.40	−2.68	−2.09	−2.35	−2.07
$\tau_{23}\ [\times 10^5\,\mathrm{N/m^2}]$	0.50	0.43	−17.33	−17.03	−16.22	−15.93	−14.79
$h_1\ [\mathrm{J/m^2}]$	−0.07	−0.08	−0.07	−0.08	−0.07	−0.08	−0.08
$h_2\ [\mathrm{J/m^2}]$	−8.32	−8.25	−8.32	−8.25	−8.32	−8.25	−8.25
$h_3\ [\mathrm{J/m^2}]$	−73.62	−73.46	−73.62	−73.46	−73.62	−73.46	−73.46
Layer 3							
$\sigma_1\ [\times 10^5\,\mathrm{N/m^2}]$	−160.62	−159.98	−266.28	−266.55	−261.54	−261.72	−256.38
$\sigma_2\ [\times 10^5\,\mathrm{N/m^2}]$	−3.85	−3.82	−8.89	−8.90	−8.80	−8.80	−8.69
$\sigma_3\ [\times 10^5\,\mathrm{N/m^2}]$	−0.15	−0.12	−4.16	−4.15	−4.30	−4.29	−4.44
$\tau_{12}\ [\times 10^5\,\mathrm{N/m^2}]$	−9.73	−9.74	−2.42	−2.42	−2.92	−2.92	−3.42
$\tau_{13}\ [\times 10^5\,\mathrm{N/m^2}]$	−1.52	−1.36	−1.99	−2.19	−1.73	−1.92	−1.67
$\tau_{23}\ [\times 10^5\,\mathrm{N/m^2}]$	0.64	0.55	−24.81	−24.57	−23.23	−23.00	−21.37
$h_1\ [\mathrm{J/m^2}]$	−0.34	−0.35	−0.34	−0.35	−0.34	−0.35	−0.35
$h_2\ [\mathrm{J/m^2}]$	−4.13	−4.11	−4.13	−4.11	−4.13	−4.11	−4.11
$h_3\ [\mathrm{J/m^2}]$	−75.39	−75.30	−75.39	−75.30	−75.39	−75.30	−75.30
Layer 4							
$\sigma_1\ [\times 10^5\,\mathrm{N/m^2}]$	−16.63	−16.51	−40.66	−40.77	−39.68	−39.78	−38.69
$\sigma_2\ [\times 10^5\,\mathrm{N/m^2}]$	−10.47	−8.21	−364.02	−368.36	−345.74	−349.51	−329.88
$\sigma_3\ [\times 10^5\,\mathrm{N/m^2}]$	−0.05	−0.03	−6.64	−6.62	−6.66	−6.64	−6.66
$\tau_{12}\ [\times 10^5\,\mathrm{N/m^2}]$	−12.74	−12.77	7.92	7.95	6.52	6.53	5.12
$\tau_{13}\ [\times 10^5\,\mathrm{N/m^2}]$	0.37	0.42	−0.46	−0.50	−0.37	−0.41	−0.33
$\tau_{23}\ [\times 10^5\,\mathrm{N/m^2}]$	0.27	0.21	−15.14	−14.86	−14.17	−13.90	−12.91
$h_1\ [\mathrm{J/m^2}]$	−0.13	−0.13	−0.13	−0.13	−0.13	−0.13	−0.13
$h_2\ [\mathrm{J/m^2}]$	−15.26	−15.16	−15.26	−15.16	−15.26	−15.16	−15.16
$h_3\ [\mathrm{J/m^2}]$	−77.96	−77.95	−77.96	−77.95	−77.96	−77.95	−77.95

stacking sequences for each case.

In all the simulations presented in this study, the lamination schemes are made of Graphite-Epoxy (Gr-Ep) composite material ($\rho^{(k)} = 1450\,\mathrm{kg/m^3}$). The thermo-mechanical elastic properties are taken from Ref. [22] and they are reported below:

$$\begin{aligned}
&\widehat{E}^{(k)}_1 = 137.90\ \mathrm{GPa} && \widehat{G}^{(k)}_{12} = 7.10\ \mathrm{GPa} && \widehat{\nu}^{(k)}_{12} = 0.30\\
&\widehat{E}^{(k)}_2 = 8.96\ \mathrm{GPa} && \widehat{G}^{(k)}_{13} = 7.10\ \mathrm{GPa} && \widehat{\nu}^{(k)}_{13} = 0.30\\
&\widehat{E}^{(k)}_3 = 8.96\ \mathrm{GPa} && \widehat{G}^{(k)}_{23} = 6.21\ \mathrm{GPa} && \widehat{\nu}^{(k)}_{23} = 0.49\\
&k^{(k)}_{11} = 1.50\ \mathrm{J/mK} && k^{(k)}_{22} = 0.50\ \mathrm{J/mK} && k^{(k)}_{33} = 0.50\ \mathrm{J/mK}\\
&a^{(k)}_{11} = 2.50\times 10^{-5}\ 1/\mathrm{K} && a^{(k)}_{22} = 2.50\times 10^{-5}\ 1/\mathrm{K} && a^{(k)}_{33} = 2.50\times 10^{-5}\ 1/\mathrm{K}
\end{aligned} \tag{120}$$

being $\widehat{E}^{(k)}_1, \widehat{E}^{(k)}_2, \widehat{E}^{(k)}_3$ and $\widehat{G}^{(k)}_{12}, \widehat{G}^{(k)}_{13}, \widehat{G}^{(k)}_{23}$ the tensile and shear moduli, respectively, while $\widehat{\nu}^{(k)}_{12}, \widehat{\nu}^{(k)}_{13}, \widehat{\nu}^{(k)}_{23}$ denote the Poisson's coefficients. On the other hand, $k^{(k)}_{11}, k^{(k)}_{22}, k^{(k)}_{33}$ and $a^{(k)}_{11}, a^{(k)}_{22}, a^{(k)}_{33}$ are the non-zero elements of the conductivity matrix and the thermal expansion coefficients of the material in hand, respectively. The derivation of the elements of the mechanical stiffness matrix $\mathbf{\Gamma}^{(k)}_{\mathrm{C}}$ from the orthotropic engineering constants can be found in Ref. [22]. The reference temperature is assumed equal to $\mathrm{T}_0 = 300$ K, while the specific heat is $c^{(k)} = 1256.04\ \mathrm{J/kg\,K}$. Lamination schemes with softcore behavior are obtained through the use of Graphite-Epoxy-soft5 (Gr-Ep-s5) and Graphite-Epoxy-soft10 (Gr-Ep-s10) materials. Their mechanical properties are obtained by scaling of elastic constants of Eqn. (120) by a factor of 5 and 10, respectively, with the exception of the Poisson's coefficients $\widehat{\nu}^{(k)}_{12}, \widehat{\nu}^{(k)}_{13}, \widehat{\nu}^{(k)}_{23}$ and the

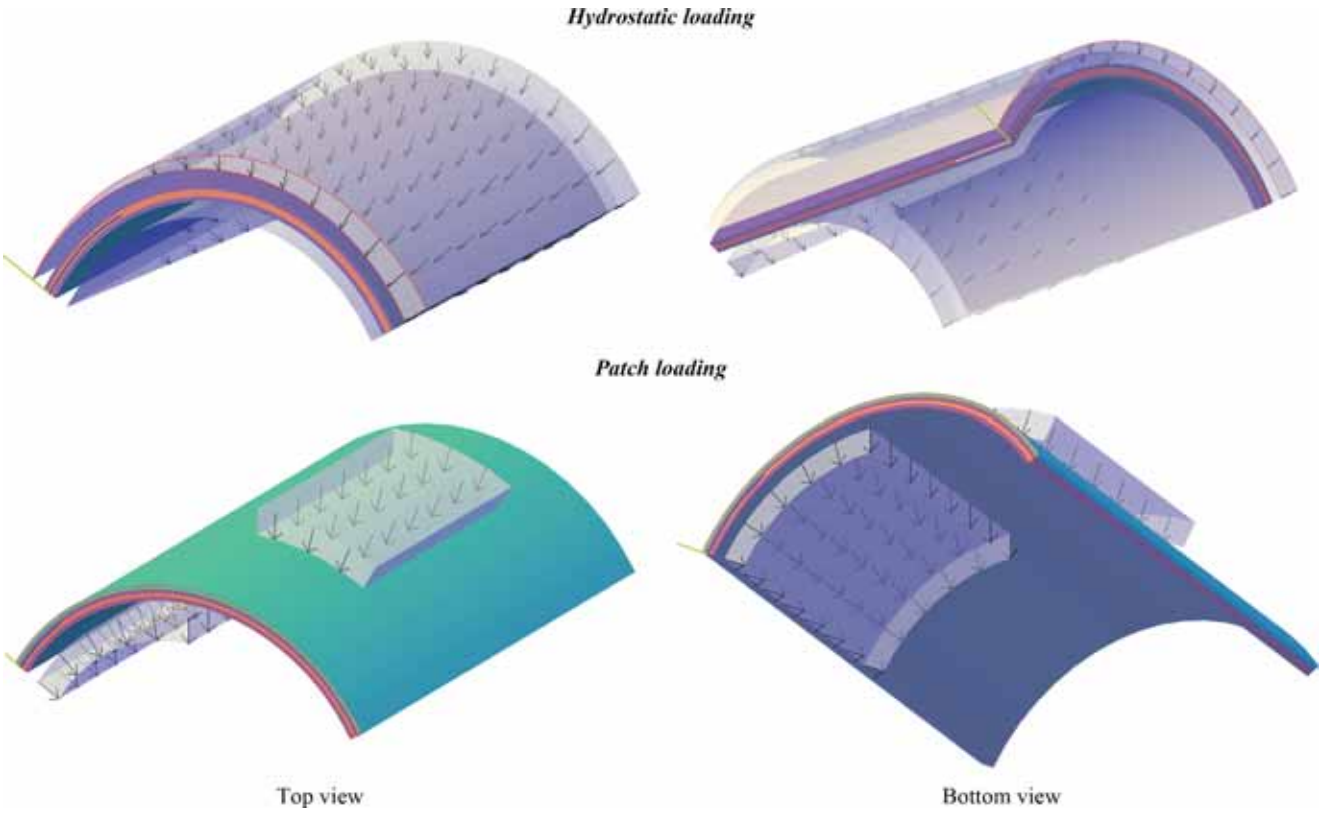

Fig. 10. Different loading conditions considered in the simulations for a laminated cylindrical panel made of four layers of orthotropic composite materials.

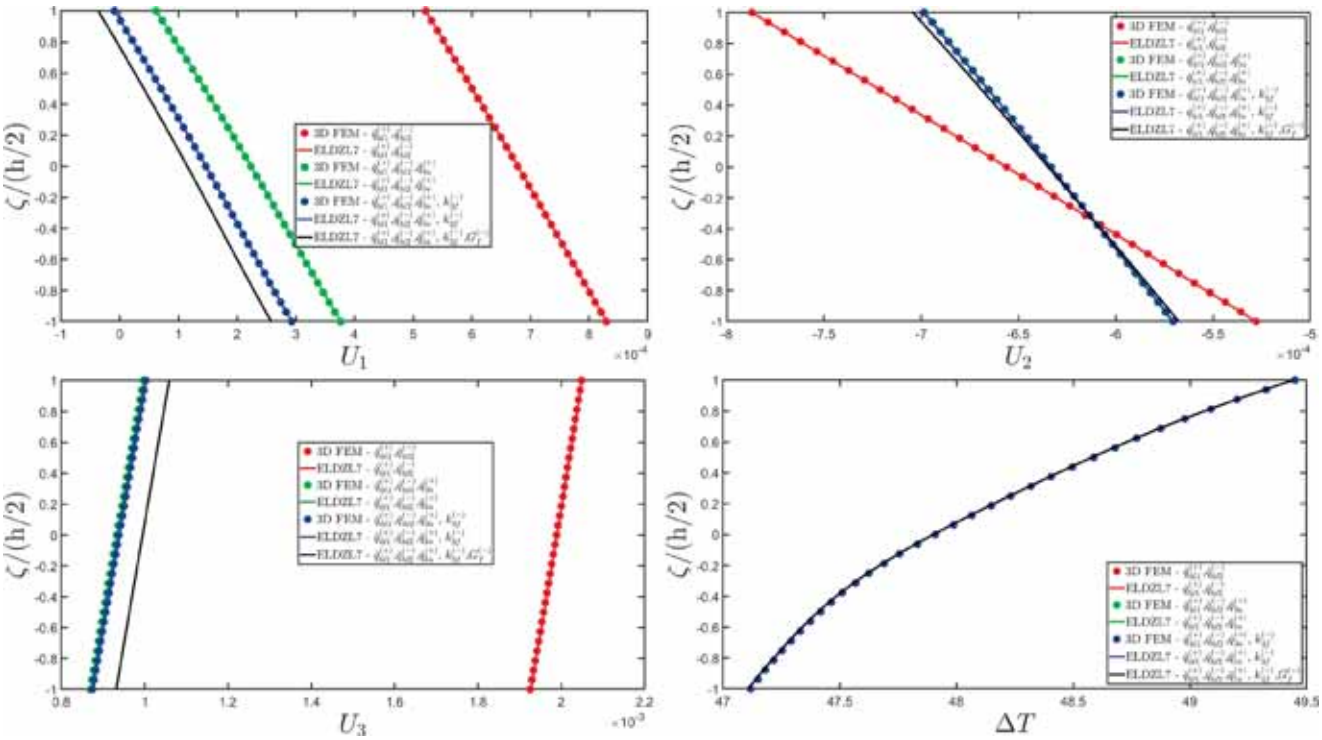

Fig. 11. Three-dimensional displacement field components [m] and temperature distribution [K] of a cylindrical panel subjected to a uniform mechanical pressure of magnitude $\overline{q}_{3u}^{(+)} = -7 \times 10^5$ N/m^2 applied at the top surface. Effect of a Winkler-Pasternak elastic foundation of stiffness $k_{3f}^{(-)} = 5 \times 10^7$ Pa/m and shear modulus equal to $G_f^{(-)} = 5 \times 10^6$ Pa. The structure is subjected to linear thermal fluxes oriented along α_1 and α_2 with magnitudes $\overline{q}_{hu}^{(+)} = -80$ J/m^2 and $\overline{q}_{hu}^{(+)} = -20$ J/m^2 applied at the top and the bottom surface of the panel, respectively, setting $\widetilde{N} = \widetilde{M} = 300$. Visualization of thickness plots at for the point $\left(0.25(\varphi_1^1 - \varphi_1^0), 0.25\, L_2\right)$ of the physical domain.

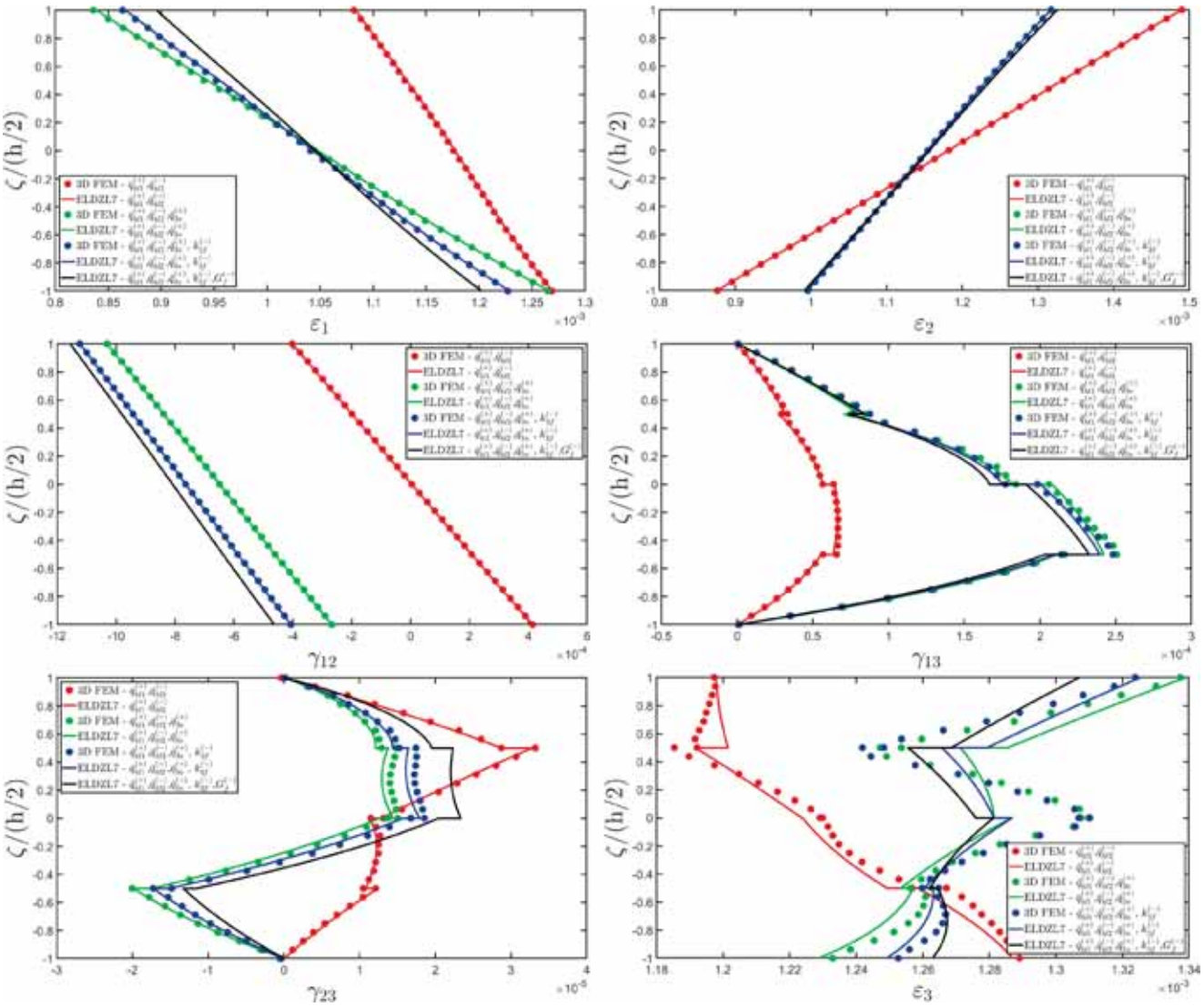

Fig. 12. Three-dimensional strain components of a cylindrical panel subjected to a uniform mechanical pressure of magnitude $\overline{q}_{3u}^{(+)} = -7 \times 10^5$ N/m^2 applied at the top surface. Effect of a Winkler-Pasternak elastic foundation of stiffness $k_{3f}^{(-)} = 5 \times 10^7$ Pa/m and shear modulus equal to $G_f^{(-)} = 5 \times 10^6$ Pa. The structure is subjected to linear thermal fluxes oriented along α_1 and α_2 with magnitudes $\overline{q}_{hu}^{(+)} = -80$ J/m^2 and $\overline{q}_{hu}^{(+)} = -20$ J/m^2 applied at the top and the bottom surface of the panel, respectively, setting $\widetilde{N} = \widetilde{M} = 300$. Visualization of thickness plots at for the point $\left(0.25(\varphi_1^1 - \varphi_1^0), 0.25\, L_2\right)$ of the physical domain.

thermal expansion coefficients $a_{11}^{(k)}, a_{22}^{(k)}, a_{33}^{(k)}$.

Regarding the external loads, it should be noted that, from Eqn. (74) and Eqn. (75), an arbitrary distribution of external loads $q_{1s}^{(+)}, q_{2s}^{(+)}, q_{3s}^{(+)}$, $q_{\mathrm{T}}^{(+)}$ and $q_{1s}^{(-)}, q_{2s}^{(-)}, q_{3s}^{(-)}, q_{\mathrm{T}}^{(-)}$ acting at each point of the top and the bottom surfaces of the three-dimensional solid, respectively, is expanded using the following expression:

$$
\begin{aligned}
q_{1s}^{(\pm)}(s_1,s_2) &= \sum_{n=1}^{\tilde{N}}\sum_{m=1}^{\tilde{M}} Q_{1\lambda nm}^{(\pm)} \cos\left(\frac{n\pi}{L_1}s_1\right) sin\left(\frac{m\pi}{L_2}s_2\right) \\
q_{2s}^{(\pm)}(s_1,s_2) &= \sum_{n=1}^{\tilde{N}}\sum_{m=1}^{\tilde{M}} Q_{2\lambda nm}^{(\pm)} \sin\left(\frac{n\pi}{L_1}s_1\right) \cos\left(\frac{m\pi}{L_2}s_2\right) \\
q_{3s}^{(\pm)}(s_1,s_2) &= \sum_{n=1}^{\tilde{N}}\sum_{m=1}^{\tilde{M}} Q_{3\lambda nm}^{(\pm)} \sin\left(\frac{n\pi}{L_1}s_1\right) sin\left(\frac{m\pi}{L_2}s_2\right) \\
q_{\mathrm{T}s}^{(\pm)}(s_1,s_2) &= \sum_{n=1}^{\tilde{N}}\sum_{m=1}^{\tilde{M}} Q_{\mathrm{T}\lambda nm}^{(\pm)} \sin\left(\frac{n\pi}{L_1}s_1\right) sin\left(\frac{m\pi}{L_2}s_2\right)
\end{aligned}
\tag{121}
$$

where the quantities $Q_{1\lambda nm}^{(\pm)}, Q_{2\lambda nm}^{(\pm)}, Q_{3\lambda nm}^{(\pm)}, Q_{\mathrm{T}\lambda nm}^{(\pm)}$ are the wave amplitudes associated with each n,m. The symbol "λ" denotes the actual distribution of the external forces. In the case of a sinusoidal ($\lambda = s$) dispersion of external loads, the following relation is considered [22]:

$$
Q_{isnm}^{(\pm)} = \overline{q}_{is}^{(\pm)} \tag{122}
$$

with $i = 1,2,3,h$, being $\overline{q}_{is}^{(\pm)}$ the corresponding load amplitude. A uniform ($\lambda = u$) distribution [22] of the external loads is computed as follows:

$$
Q_{iunm}^{(\pm)} = \frac{4\overline{q}_{iu}^{(\pm)}}{\pi^2 nm}(1-\cos(n\pi))(1-\cos(m\pi)) \tag{123}
$$

Similarly, a patch load ($\lambda = p$) centered in the point (s_{10}, s_{20}) within the physical domain, acting on a surface of dimensions $A = 4c_{10}c_{20}$ accounts for the following expression of $Q_{ipnm}^{(\pm)}$ [22]:

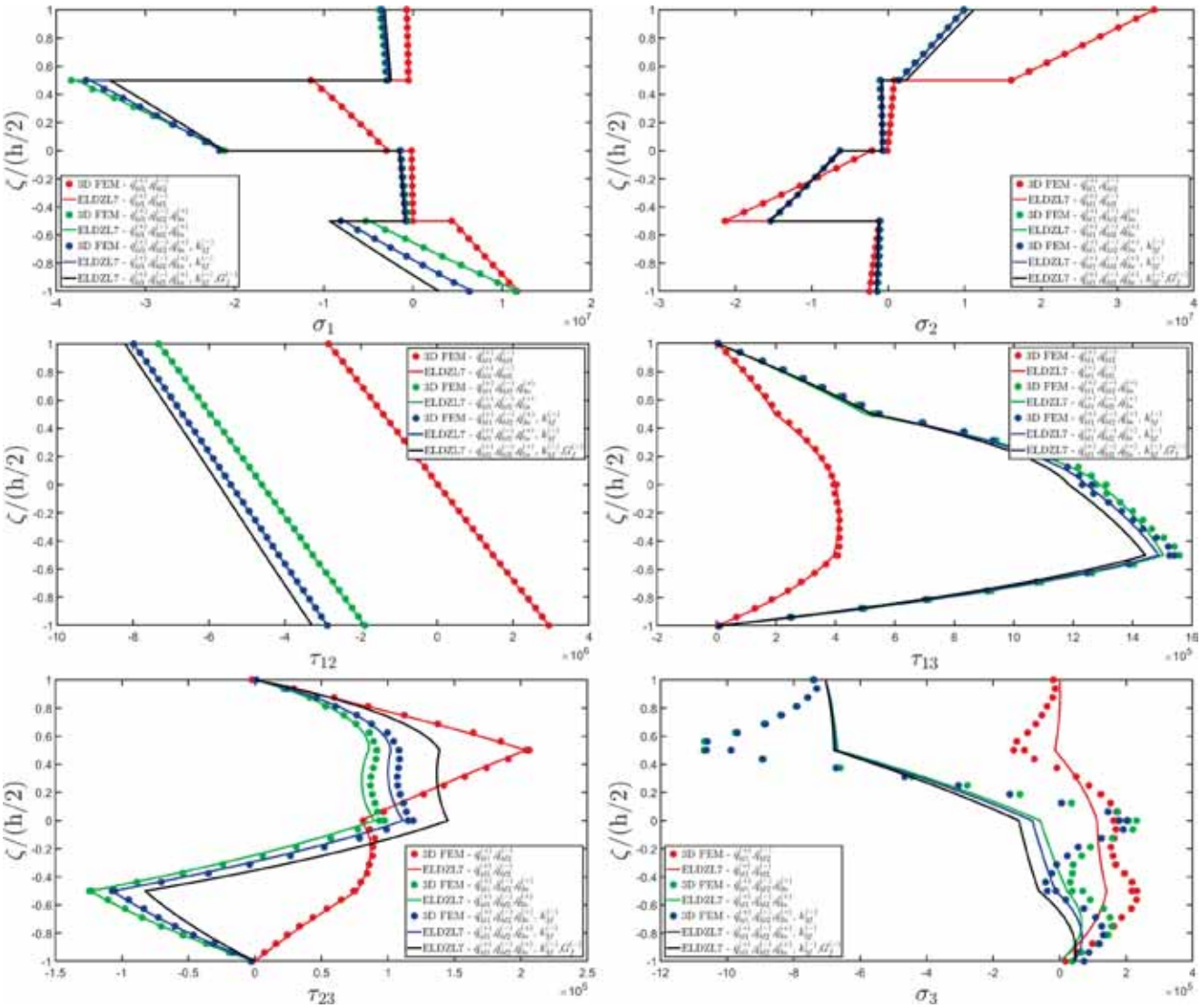

Fig. 13. Three-dimensional stress components [Pa] of a cylindrical panel subjected to a uniform mechanical pressure of magnitude $\overline{q}_{3u}^{(+)} = -7 \times 10^5$ N/m^2 applied at the top surface. Effect of a Winkler-Pasternak elastic foundation of stiffness $k_{3f}^{(-)} = 5 \times 10^7$ Pa/m and shear modulus equal to $G_f^{(-)} = 5 \times 10^6$ Pa. The structure is subjected to linear thermal fluxes oriented along α_1 and α_2 with magnitudes $\overline{q}_{hu}^{(+)} = -80$ J/m^2 and $\overline{q}_{hu}^{(+)} = -20$ J/m^2 applied at the top and the bottom surface of the panel, respectively, setting $\widetilde{N} = \widetilde{M} = 300$. Visualization of thickness plots at for the point $\left(0.25(\varphi_1^1 - \varphi_1^0), 0.25\, L_2\right)$ of the physical domain.

$$Q_{ipnm}^{(\pm)} = \frac{16\overline{q}_{ip}^{(\pm)}}{\pi^2 nm} \sin\left(\frac{n\pi s_{10}}{L_1}\right) \sin\left(\frac{m\pi s_{20}}{L_2}\right) \sin\left(\frac{n\pi c_{10}}{L_1}\right) \sin\left(\frac{m\pi c_{20}}{L_2}\right) \tag{124}$$

A hydrostatic loading ($\lambda = h$) along the α_1 principal direction is expanded as [22]:

$$Q_{ihnm}^{(\pm)} = -\frac{4\overline{q}_{ih}^{(\pm)}}{\pi^2 nm} \cos(n\pi)(1 - \cos(m\pi)) \tag{125}$$

Finally, a hydrostatic load along α_2 [22] is embedded in the present semi-analytical formulation through the relation reported below:

$$Q_{ihnm}^{(\pm)} = -\frac{4\overline{q}_{ih}^{(\pm)}}{\pi^2 nm} (1 - \cos(n\pi)) \cos(m\pi) \tag{126}$$

The first two preliminary examples aim to validate the proposed model and the implemented numerical techniques. The first example focuses on the bending response of a SSSS rectangular plate with geometric sizes $L_1 = 2.00$ m and $L_2 = 1.20$ m, subjected to a sinusoidal pressure of magnitude $Q_{3snm}^{(+)} = -1 \times 10^5$ N/m^2 with $\widetilde{N} = \widetilde{M} = 1$ applied at the top surface. The structure consists of three layers with thicknesses $h_1 = h_3 = 0.03$ m and $h_2 = 0.04$ m. Two different lamination schemes are considered: the first one accounts for three laminae of Gr-Ep material with (0 / 90 / 0), while in the second one the central core of the panel is made of Gr-Ep-s5. The vertical deflection of the central point of the plate, located at $s_1 = L_1/2$, $s_2 = L_2/2$ and $\zeta = 0$, is evaluated from the present model employing various displacement field assumptions. The results are reported in Table 1 and Table 2 for the two different configurations of the stacking sequence of the plate. To validate the results, a closed-form solution is found employing the same kinematic field assumptions as those adopted in the numerical simulation. In addition, the vertical deflection of the plate is evaluated from a computationally demanding three-dimensional FEM model developed with a commercial software. The numerical simulations employing various higher order ELW kinematic fields are performed with both the GDQ method and the F-GDQ method based a CGL computational grid. For further details on

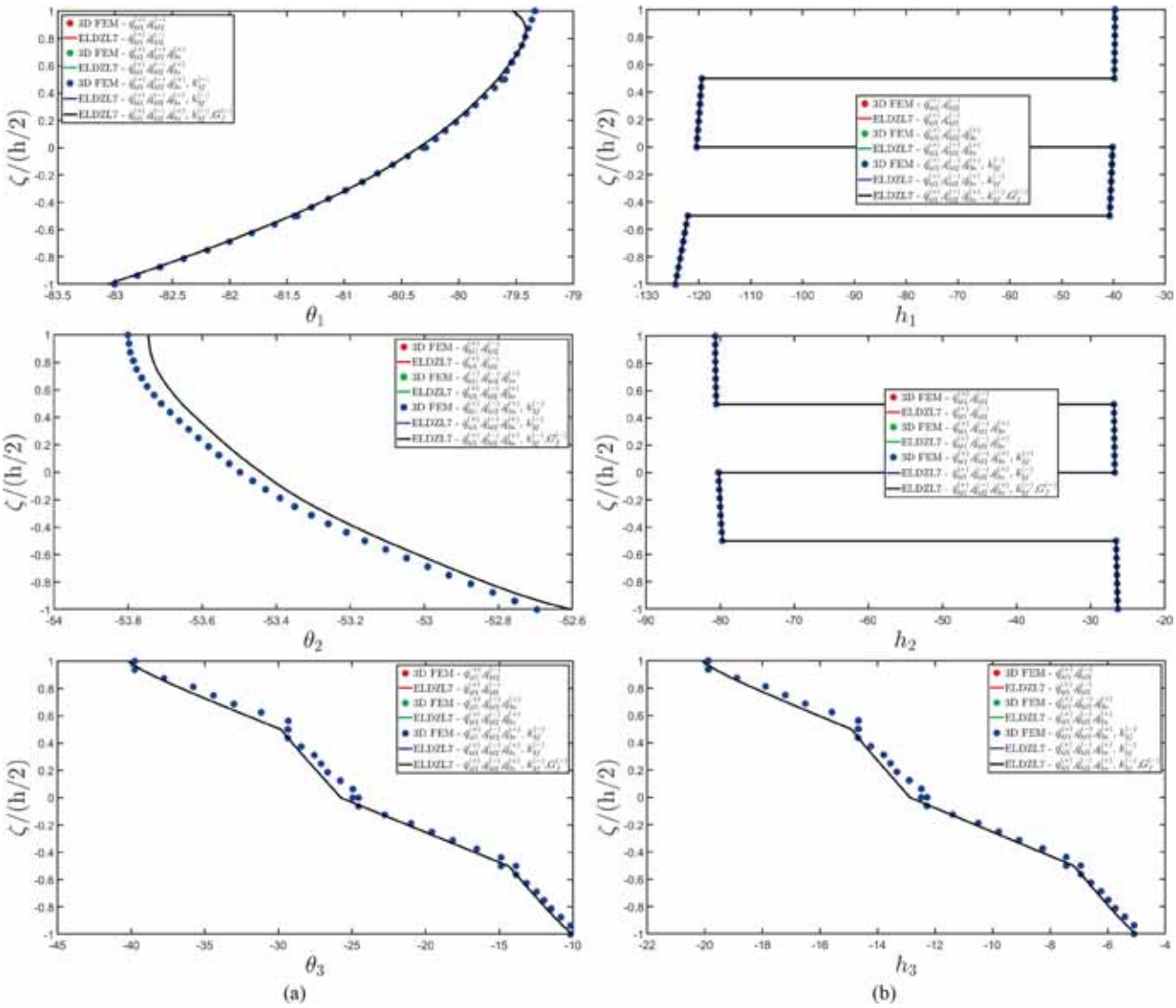

Fig. 14. Three-dimensional thermal gradient components (a) and heat flux components (b), expressed in [J/m^2], of a cylindrical panel subjected to a uniform mechanical pressure of magnitude $\overline{q}_{3u}^{(+)} = -7 \times 10^5$ N/m^2 applied at the top surface. Effect of a Winkler-Pasternak elastic foundation of stiffness $k_{3f}^{(-)} = 5 \times 10^7$ Pa/m and shear modulus equal to $G_f^{(-)} = 5 \times 10^6$ Pa. The structure is subjected to linear thermal fluxes oriented along α_1 and α_2 with magnitudes $\overline{q}_{hu}^{(+)} = -80$ J/m^2 and $\overline{q}_{hu}^{(+)} = -20$ J/m^2 applied at the top and the bottom surface of the panel, respectively, setting $\widetilde{N} = \widetilde{M} = 300$. Visualization of thickness plots at for the point $\left(0.25(\varphi_1^1 - \varphi_1^0), 0.25 L_2\right)$ of the physical domain.

this numerical model, the interested reader should refer to [56]. The static response of the panel is evaluated for different sizes of the CGL grid employing various higher order theories. In order to check the convergence of results, the percentage error parameters $e_{\%1}$ and $e_{\%2}$ are introduced, defined as follows:

$$e_{\%1} = \left| \frac{w_{DQ} - w_{exact}}{w_{exact}} \right| \times 100\% \qquad e_{\%2} = \left| \frac{w_{DQ} - w_{FEM}}{w_{FEM}} \right| \times 100\% \tag{127}$$

In particular, w_{FEM} is the vertical deflection obtained from the 3D FEM simulation, while w_{exact} denotes the predictions from the analytical model employing various higher order kinematic equations. Finally, w_{DQ} accounts for the outcomes of the ELW formulation for the mechanical case employing both the GDQ and F-GDQ numerical techniques. In Fig. 2, these two quantities are derived for the values reported in Table 1 and Table 2, showing the convergence of the numerical methods for various higher order theories. Note that both the GDQ and F-GDQ simulations provide very low discrepancies with respect to the analytical solutions and the 3D FEM results. More specifically, the same numerical predictions are provided for different values of $I_N = I_M$, showing the excellent stability of these numerical techniques. For both configurations of the lamination schemes, the convergence analysis is performed with various kinematic field assumptions, and the lowest values of $e_{\%1}$ and $e_{\%2}$ are observed when higher order ELW theories are selected, especially in the configuration without the softcore.

The second example aims to verify the accuracy of the model in predicting the three-dimensional response of a SSSS rectangular plate for the mechanical elasticity case. The plate, with dimensions $L_1 =$

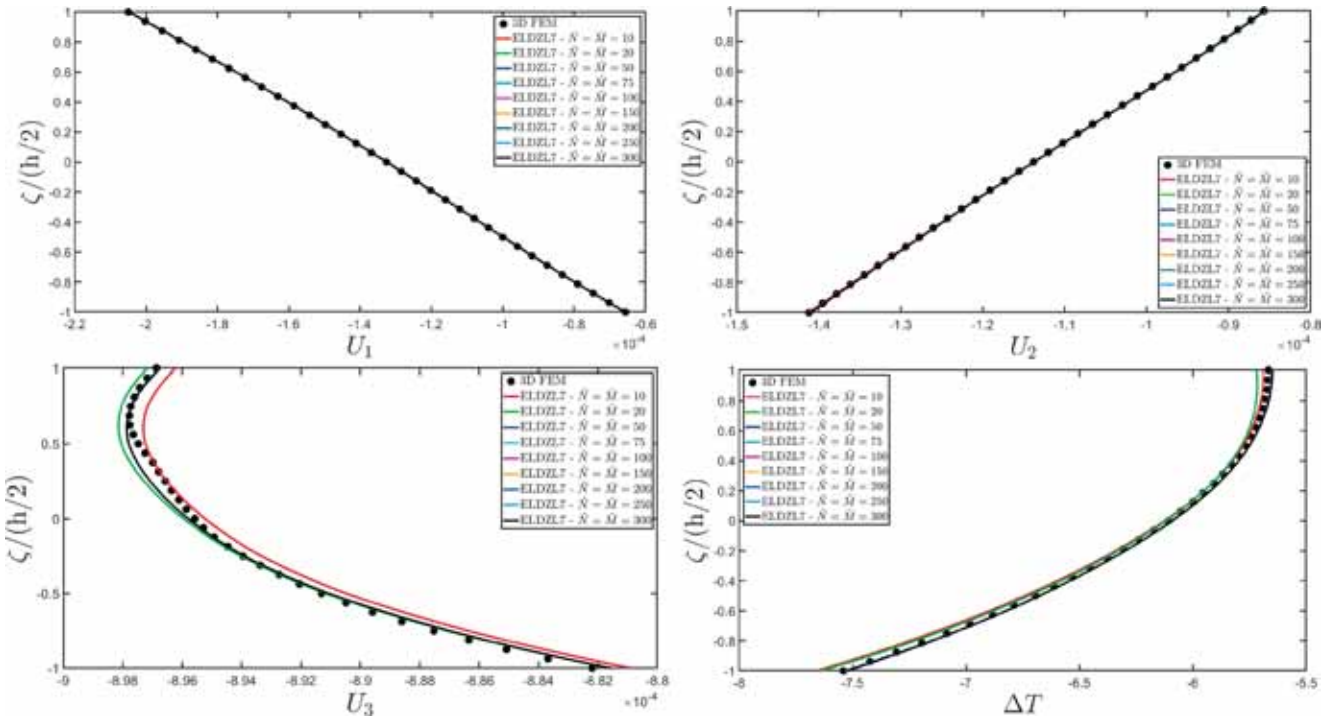

Fig. 15. Three-dimensional displacement field components [m] and temperature distribution [K] of a cylindrical panel subjected to a uniform mechanical pressure of magnitude $\overline{q}_{3u}^{(+)} = -7 \times 10^5$ N/m^2 applied at the top surface lying on a Winkler elastic foundation of stiffness $k_{3f}^{(-)} = 5 \times 10^7$ Pa/m employing various wave numbers $\widetilde{N}$,$\widetilde{M}$. A patch thermal flux of magnitude $\overline{q}_{hp}^{(+)} = -80$ J/m^2 is applied at the top surface, whose governing parameters are $(s_{10}, s_{20}) = \left(0.75(\varphi_1^1 - \varphi_1^0), 0.5L_2\right)$ and $(c_{10}, c_{20}) = \left(0.125(\varphi_1^1 - \varphi_1^0), 0.25L_2\right)$. Another patch thermal flux of magnitude $\overline{q}_{hp}^{(-)} = -20$ J/m^2 and governing parameters $(s_{10}, s_{20}) = \left(0.25(\varphi_1^1 - \varphi_1^0), 0.25L_2\right)$ and $(c_{10}, c_{20}) = \left(0.25(\varphi_1^1 - \varphi_1^0), 0.25L_2\right)$ is applied at the bottom surface of the panel. Visualization of thickness plots at for the point $\left(0.25(\varphi_1^1 - \varphi_1^0), 0.25L_2\right)$ of the physical domain.

2.00 m and $L_2 = 1.00$ m, consists of four layers of Gr-Ep with $h_1 = h_2 = h_3 = h_4 = 0.025$ m, setting a cross-ply lamination scheme with (0 / 90 / 0/ 90). The loading conditions consist in a prescribed value of the displacement field components at the top skin of the plate employing a sinusoidal dispersion of prescribed values of $u_1^{(\tau)}, u_2^{(\tau)}, u_3^{(\tau)}$ for $\tau = N$ with $\widetilde{N} = \widetilde{M} = 1$, according to Eqn. (16) and Eqn. (73). The wave amplitudes of the distributions are set equal to $\overline{U}_{1s}^{(+)} = \overline{U}_{2s}^{(+)} = \overline{U}_{3s}^{(+)} = -1 \times 10^{-3}$ m. Furthermore, a uniformly-distributed Winkler foundation is applied at the bottom surface, according to Eqn. (57). Various load cases are considered. In the first simulation, a prescribed value of $\overline{U}_{1s}^{(+)}$ is applied, and a spring stiffness equal to $k_{3f}^{(-)} = 5 \times 10^7$ Pa/m is considered. In the second and third load cases, sinusoidal distributions of $u_2^{(N)}$ and $u_3^{(N)}$ are considered with $\widetilde{N} = \widetilde{M} = 1$. Finally, a sinusoidal dispersion of each displacement field component is modelled in the same simulation for the last load case. The stiffness of the Winkler foundation is set equal to $k_{3f}^{(-)} = 5 \times 10^9$ Pa/m. Thickness plots are provided for the point located at $(0.25L_1, 0.25L_2)$ and represented in Figs. 3–5. For each case study, the results are successfully compared to those ones obtained from a refined 3D-FEM simulation, developed with a commercial software, consisting of 439,215 DOFs. As can be seen from Fig. 3, the present two-dimensional closed-form solution of the mechanical elasticity problem with $N = 7$, together with the zigzag function, predicts well the three-dimensional response of the panel for all load cases, even in the out-of-plane principal direction. As visible in Fig. 3, which collects the thickness plots of the displacement field components, when an in-plane displacement field component is prescribed, the panel tends to bend upwards, whereas it bends downwards when the out-of-plane displacement field is enforced at the top surface. Referring to the three-dimensional strain components represented in Fig. 4, it can be shown that the out-of-plane strain components $\gamma_{13}, \gamma_{23}, \varepsilon_3$ are characterized by a piecewise through-the-thickness profiles, due to the fact that a different orientation is assigned to each lamina of the stacking sequence. This aspect becomes more evident in Fig. 5, where the through-the-thickness profile of the three-dimensional stress components are provided. It can be seen that highest magnitudes of in-plane stresses are obtained for layers with $\vartheta = 0$. Furthermore, the effect of the presence of the Winkler foundation is evident in the distribution of the normal stress σ_3, since external actions induced by the springs at the bottom surface are balanced by an additional stress along the thickness direction.

Next example presents the thermo-mechanical response of a rectangular plate with dimensions $L_1 = 2.00$ m and $L_2 = 1.00$ m made of four Gr-Ep layers of thickness $h_1 = h_2 = h_3 = h_4 = 0.025$ m with (0 / 90 / 0/ 90). A uniform external pressure of magnitude $\overline{q}_{3u}^{(+)} = -7 \times 10^5$ N/m^2 and a uniformly-distributed heat flux $\overline{q}_{hu}^{(+)} = -80$ J/m^2 are considered, both applied at $\zeta = h/2$. An elastic foundation is present at the bottom surface modelled with either the Winkler ($k_{3f}^{(-)} = 5 \times 10^7$ Pa/m) and Winkler-Pasternak models with $k_{3f}^{(-)} = 5 \times 10^7$ Pa/m and $G_f^{(-)} = 5 \times 10^6$ Pa. Furthermore, a null value of temperature variation is prescribed at the bottom surface of the plate. The thickness plots, evaluated with the ELDZL7 theory with $\widetilde{N} = \widetilde{M} = 300$, are provided for the point located at $(0.25L_1, 0.25L_2)$ within the physical domain, and they are plotted in Figs. 6–9. Furthermore, the

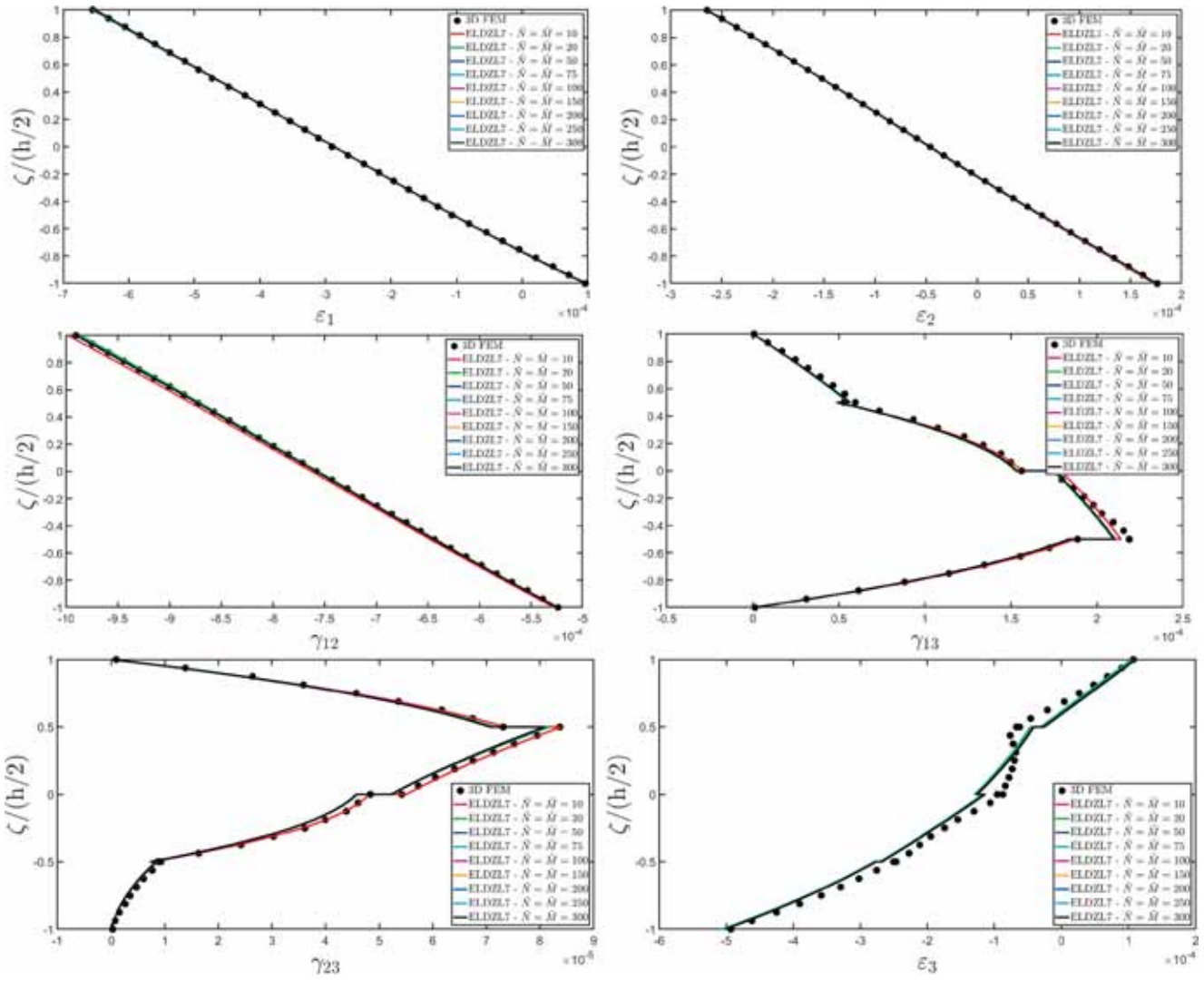

Fig. 16. Three-dimensional strain components of a cylindrical panel subjected to a uniform mechanical pressure of magnitude $\overline{q}_{3u}^{(+)} = -7 \times 10^5$ N/m^2 applied at the top surface lying on a Winkler elastic foundation of stiffness $k_{3f}^{(-)} = 5 \times 10^7$ Pa/m employing various wave numbers $\widetilde{N}, \widetilde{M}$. A patch thermal flux of magnitude $\overline{q}_{hp}^{(+)} = -80$ J/m^2 is applied at the top surface, whose governing parameters are $(s_{10}, s_{20}) = \left(0.75(\varphi_1^1 - \varphi_1^0), 0.5L_2\right)$ and $(c_{10}, c_{20}) = \left(0.125(\varphi_1^1 - \varphi_1^0), 0.25L_2\right)$. Another patch thermal flux of magnitude $\overline{q}_{hp}^{(-)} = -20$ J/m^2 and governing parameters $(s_{10}, s_{20}) = \left(0.25(\varphi_1^1 - \varphi_1^0), 0.25L_2\right)$ and $(c_{10}, c_{20}) = \left(0.25(\varphi_1^1 - \varphi_1^0), 0.25L_2\right)$ is applied at the bottom surface of the panel. Visualization of thickness plots at for the point $\left(0.25(\varphi_1^1 - \varphi_1^0), 0.25\,L_2\right)$ of the physical domain.

numerical results regarding configuration, primary and secondary variables are summarised in Table 3, Table 4 and Table 5, respectively, for a futher comparison. The response of the panel, derived from the present model, is compared to the results of a 3D FEM simulation, showing an excellent agreement between the two models. In a first simulation, the mechanical response of the structural component subjected to the external pressure is considered. Then, the coupled thermo-mechanical response is calculated under the influence of the thermal flux, as well as the elastic foundation. Finally, the shear stiffness of the foundation is evaluated with the ELW theory following the Winkler-Pasternak model. As can be seen from Fig. 6, when a shear layer is added, a minor vertical deflection is observed due to the additional stiffness of the structural system. Furthermore, a slight variation of the in-plane displacement field components is found. A linear profile of the temperature variation is found in all load cases. The three-dimensional strain components of Fig. 7 clearly show that the plate bends upward when a negative thermal flux is applied at the top surface; therefore, the deflection induced by the mechanical surface traction is completely balanced by the stresses induced by a temperature variation within the solid. In Fig. 8 the three-dimensional stress components are reported for all load cases, showing, above all, that different profiles are obtained when Winkler and Winkler-Pasternak theories are used to model the elastic foundation. In all cases, the recovery profile provides the exact through-the-thickness distribution of these quantities under the effect of the external mechanical pressures, thus allowing one to derive the numerical predictions of a refined three-dimensional simulation with a reduced computational cost. Thanks to the recovery procedure applied to a multifield problem, the present model predicts with a high level of accuracy the profile, within each lamina, of both in-plane and out-of-plane temperature gradient components and thermal flux components, all of them derived from a thermo-mechanical two-dimensional simulation (Fig. 9).

In next example of investigation, a cylindrical panel is studied, made of four layers of Gr-Ep material with $(0\,/\,90\,/\,0\,/\,90)$ as lamination

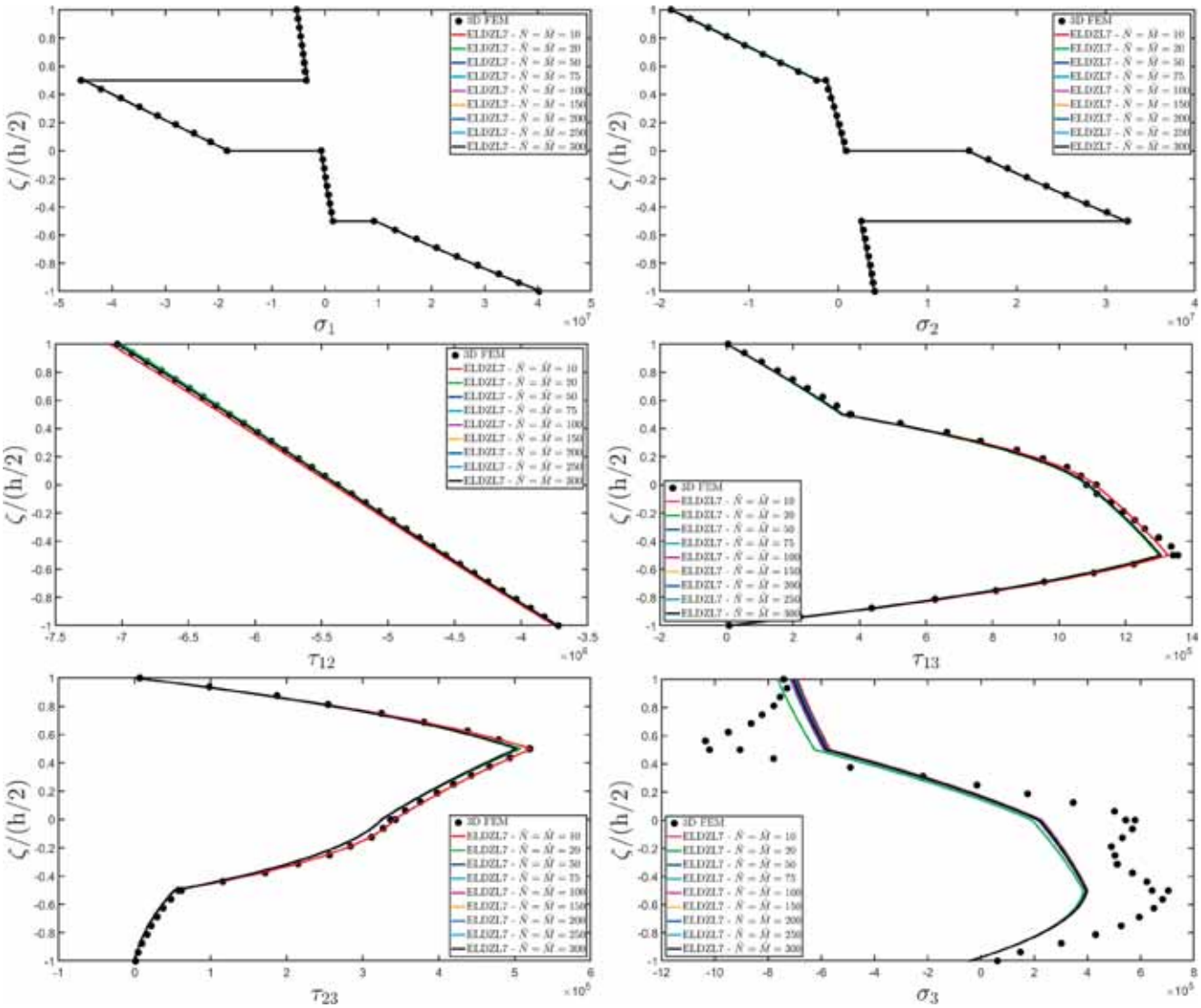

Fig. 17. Three-dimensional stress components [Pa] of a cylindrical panel subjected to a uniform mechanical pressure of magnitude $\overline{q}_{3u}^{(+)} = -7 \times 10^5$ N/m^2 applied at the top surface lying on a Winkler elastic foundation of stiffness $k_{3f}^{(-)} = 5 \times 10^7$ Pa/m employing various wave numbers $\widetilde{N}, \widetilde{M}$. A patch thermal flux of magnitude $\overline{q}_{hp}^{(+)} = -80$ J/m^2 is applied at the top surface, whose governing parameters are $(s_{10}, s_{20}) = \left(0.75(\varphi_1^1 - \varphi_1^0), 0.5L_2\right)$ and $(c_{10}, c_{20}) = \left(0.125(\varphi_1^1 - \varphi_1^0), 0.25L_2\right)$. Another patch thermal flux of magnitude $\overline{q}_{hp}^{(-)} = -20$ J/m^2 and governing parameters $(s_{10}, s_{20}) = \left(0.25(\varphi_1^1 - \varphi_1^0), 0.25L_2\right)$ and $(c_{10}, c_{20}) = \left(0.25(\varphi_1^1 - \varphi_1^0), 0.25L_2\right)$ is applied at the bottom surface of the panel. Visualization of thickness plots at for the point $\left(0.25(\varphi_1^1 - \varphi_1^0), 0.25\,L_2\right)$ of the physical domain.

scheme, while the thicknesses of the laminae are set equal to $h_1 = h_2 = h_3 = h_4 = 0.025$ m. The structure lies on an elastic foundation, modelled with the Winkler-Pasternak theory, setting $k_{3f}^{(-)} = 5 \times 10^7$ Pa/m and $G_f^{(-)} = 5 \times 10^6$ Pa. A uniformly-distributed external pressure of magnitude $\overline{q}_{3u}^{(+)} = 5 \times 10^7$ N/m^2 is applied to the panel at the top surface. The thermal loads consist of two thermal fluxes of magnitude $\overline{q}_{hu}^{(+)} = -80$ J/m^2 and $\overline{q}_{hu}^{(-)} = -20$ J/m^2 applied at the top and bottom surfaces, respectively. More specifically, the former flux is linearly distributed along α_1, whereas the latter accounts for an hydrostatic distribution along α_2. In other words, thermal flux loads are expanded according to Eqn. (125) and Eqn. (126). Another loading condition is studied, in which the same thermal fluxes are uniformly distributed in specific regions of the top and bottom surfaces according to expansion of Eqn. (124) for patch loads. For this distribution, the governing parameters $(s_{10}, s_{20}) = \left(0.75(\varphi_1^1 - \varphi_1^0), 0.5L_2\right)$ and $(c_{10}, c_{20}) = \left(0.125(\varphi_1^1 - \varphi_1^0), 0.25L_2\right)$ are adopted for the thermal flux applied at the top surface, while $(s_{10}, s_{20}) = \left(0.25(\varphi_1^1 - \varphi_1^0), 0.25L_2\right)$ and $(c_{10}, c_{20}) = \left(0.25(\varphi_1^1 - \varphi_1^0), 0.25L_2\right)$ are used at the bottom surface of the panel. For the sake of clarity, a three-dimensional representation of the thermal loading conditions can be found in Fig. 10. The thickness plots are calculated at $\left(0.25(\varphi_1^1 - \varphi_1^0), 0.25L_2\right)$, and they are collected in Figs. 11–14 for the first load case, while the results of the second load case are represented in Figs. 15–18.

It should be noted from Fig. 11 that, for the selected lamination scheme, when two hydrostatic thermal fluxes are considered the temperature variation deviates from the classical linear distribution typically adopted in uncoupled models that can be found in literature. In addition, a linear profile is observed for the out-of-plane displacement

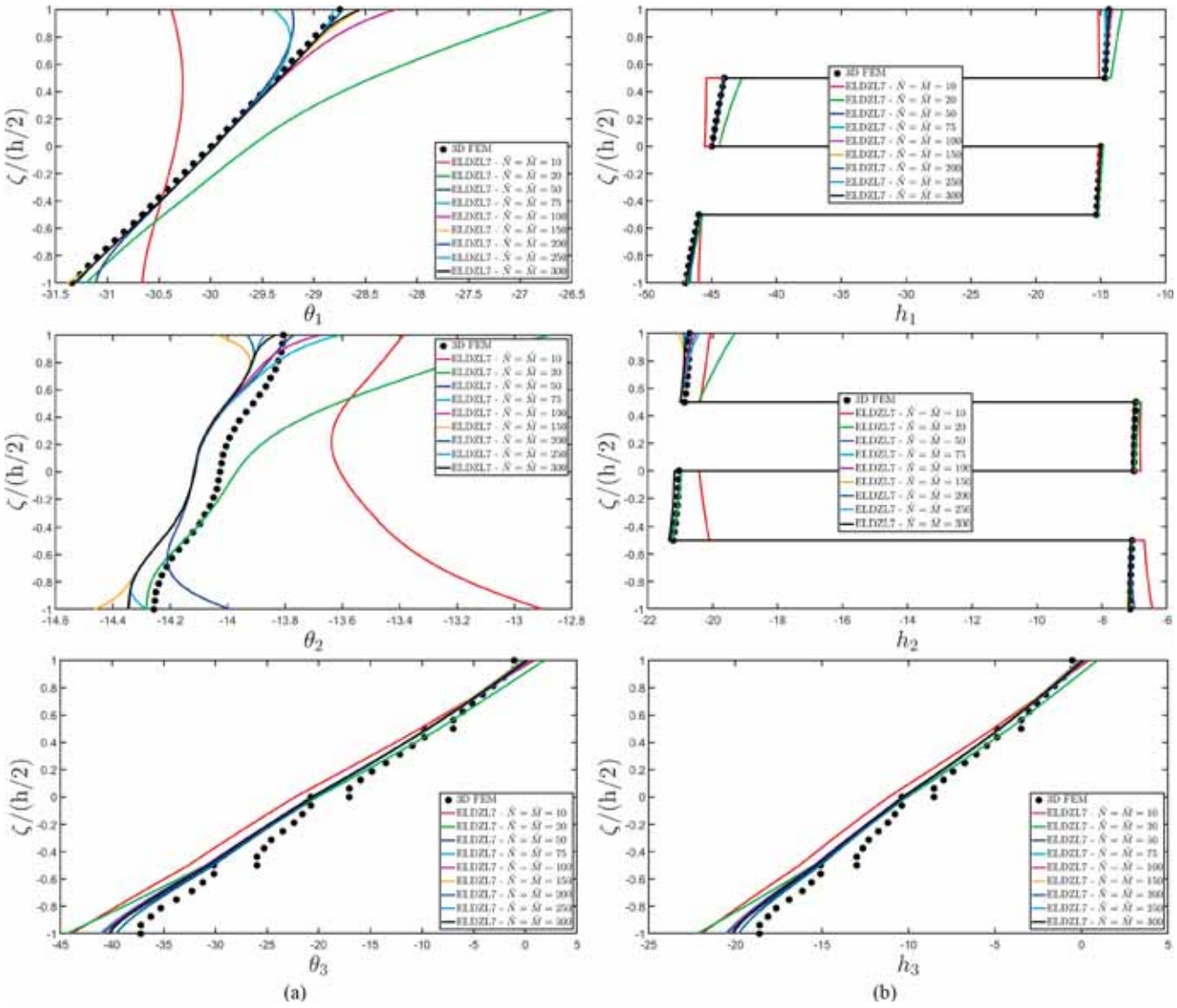

Fig. 18. Three-dimensional thermal gradient components (a) and heat flux components (b), expressed in [J/m^2], of a cylindrical panel subjected to a uniform mechanical pressure of magnitude $\overline{q}_{3u}^{(+)} = -7 \times 10^5$ N/m^2 applied at the top surface lying on a Winkler elastic foundation of stiffness $k_{3f}^{(-)} = 5 \times 10^7$ Pa/m employing various wave numbers $\widetilde{N}, \widetilde{M}$. A patch thermal flux of magnitude $\overline{q}_{hp}^{(+)} = -80$ J/m^2 is applied at the top surface, whose governing parameters are $(s_{10}, s_{20}) = \left(0.75(\varphi_1^1 - \varphi_1^0), 0.5L_2\right)$ and $(c_{10}, c_{20}) = \left(0.125(\varphi_1^1 - \varphi_1^0), 0.25L_2\right)$. Another patch thermal flux of magnitude $\overline{q}_{hp}^{(-)} = -20$ J/m^2 and governing parameters $(s_{10}, s_{20}) = \left(0.25(\varphi_1^1 - \varphi_1^0), 0.25L_2\right)$ and $(c_{10}, c_{20}) = \left(0.25(\varphi_1^1 - \varphi_1^0), 0.25L_2\right)$ is applied at the bottom surface of the panel. Visualization of thickness plots at for the point $\left(0.25(\varphi_1^1 - \varphi_1^0), 0.25\,L_2\right)$ of the physical domain.

field component. Even though the mechanical load is downward-oriented, the presence of curvature, together with the cross-ply lamination scheme, leads to an upward bending of the structure at the investigated point. Finally, the shear stiffness of the elastic foundation moves the distribution of both U_1 and U_3. The three-dimensional strain components of Fig. 12 show that the deformation of the structure induces different piecewise profiles, especially in out-of-plane strain components, for all loading conditions. In particular, the introduction of a thermal load can vary the slope of the strain distribution, as seen, for example, in the thickness plots of γ_{23} and ε_3. Similar considerations can be made for the through-the-thickness dispersion of the stress components of Fig. 13. In-plane stresses are distributed, for each load case, with a linear or piecewise linear profile. On the other hand, higher magnitudes of out-of-plane stress components are observed when both mechanical and thermal loads are applied to the structural component, especially in the case of τ_{13} and σ_3. Finally, different slopes of τ_{23} profile are seen with respect to more complicated load cases when only thermal loads are applied to the structure under consideration. It should be noted that the same distribution of the three-dimensional temperature gradient components and the thermal flux components is obtained in all load cases using either the present semi-analytical model and a 3D FEM simulation, as clearly shown in Fig. 14.

Referring to the load case in which the thermal loads are applied according to the patch load expansion, it should be noted that the predictions of the present theory converge rapidly to the numerical results of a coupled three-dimensional thermo-mechanical FEM model, espe-

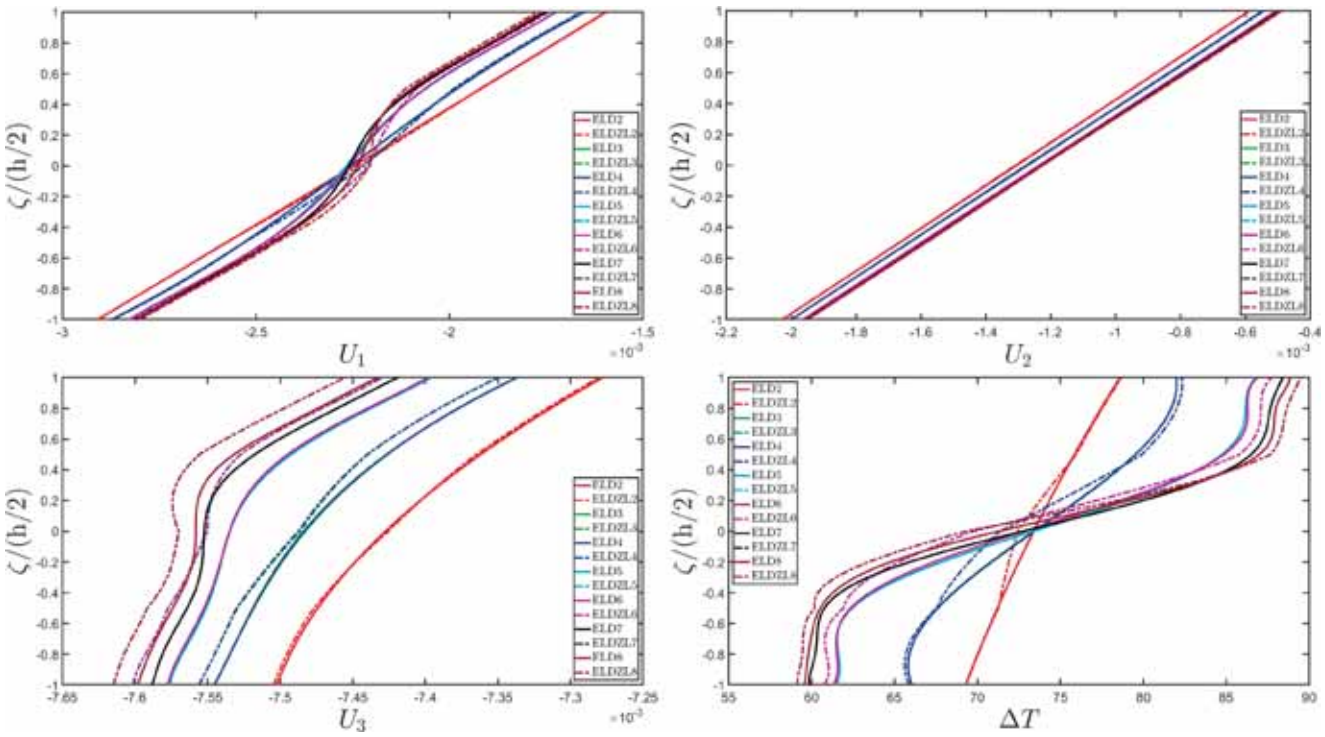

Fig. 19. Three-dimensional displacement field components [m] and temperature distribution [K] of a shallow spherical panel lying on an elastic foundation subjected to external sinusoidal pressures with $\widetilde{N} = \widetilde{M} = 1$ of magnitudes $\overline{q}_{1s}^{(+)} = \overline{q}_{2s}^{(+)} = 7 \times 10^5$ N/m^2 and $\overline{q}_{3s}^{(+)} = -7 \times 10^6$ N/m^2, along with sinusoidal distributions of thermal fluxes with $\widetilde{N} = \widetilde{M} = 1$ of magnitudes $\overline{q}_{hs}^{(+)} = -80$ J/m^2 and $\overline{q}_{hs}^{(-)} = -20$ J/m^2, applied at $\zeta = h/2$ and $\zeta = -h/2$, respectively. The structure is located on a Winkler-Pasternak elastic foundation of stiffnesses $k_{1f}^{(-)} = k_{2f}^{(-)} = 5 \times 10^7$ Pa/m and $k_{3f}^{(-)} = 1 \times 10^8$ Pa/m, whose shear modulus is set equal to $G_f^{(-)} = 5 \times 10^6$ Pa. Visualization of thickness plots at the point $\left(0.25(\varphi_1^1 - \varphi_1^0), 0.25(\vartheta_1^1 - \vartheta_1^0)\right)$ of the physical domain employing different higher order kinematic expansions, together with the zigzag function.

cially for the mechanical quantities. As can be seen from Fig. 15, only ten waves are needed to derive correctly the in-plane displacement field components, and a high level of accuracy is observed for U_3 and ΔT three-dimensional configuration variables. Note that in this case the structure bends downwards with a linear profile of in-plane displacement field components, while a parabolic profile is seen for U_3. In the same way, a very high convergence rate of results can be observed in all three-dimensional strain components of Fig. 16. Note that the 3D FEM results can be well predicted by the present two-dimensional ELW model because higher order theories are embedded in the formulation, resulting in a non-uniform value of ε_3. Looking at the distributions of the three-dimensional stress components of Fig. 17, it can be shown that the present higher order model predicts accurately the 3D-FEM results in each point of the three-dimensional solid for both in-plane and out-of-plane variables. With particular reference to the profile of σ_3 normal stress, all curves converge to the same region near $\zeta = h/2$ and $\zeta = -h/2$ since the recovery post-processing procedure allows the model to fulfil the three-dimensional balance equations along the thickness direction. In this way, a similar profile to that one obtained from the 3D FEM simulation is found. Finally, in Fig. 18 we provide the thickness plots of the three-dimensional primary and secondary variables of the thermal conduction problem. Unlike the mechanical case, the convergence to the three-dimensional solution is seen only with higher values of $\widetilde{N}, \widetilde{M}$. The thickness plots are provided in a region where the adiabatic thermal condition is enforced at the top surface, since a null value of the external flux is considered here, while a nonzero heat flux is applied at the bottom surface. As a consequence, the thickness plot of the temperature gradient component of Fig. 18 assumes a null value at the top surface, and a vertical profile of the temperature variation of Fig. 15 is observed near the top surface of the cylinder.

At this point, the thermo-mechanical response of a laminated shallow spherical panel of radius $R_1 = R_2 = R = 3$ m is studied. The structure is made of four layers of equal thickness $h_1 = h_2 = h_3 = h_4 = 0.025$ m made of composite materials, including a central softcore region. The two external layers are made of Gr-Ep, while the second lamina is made of Gr-Ep-s5. The third layer is made of Gr-Ep-s10. External loads are distributed with a sinusoidal dispersion characterized by $\widetilde{N} = \widetilde{M} = 1$. A Winkler-Pasternak foundation is present at the bottom surface with a uniform distribution of linear elastic springs. The stiffness of the linear springs oriented along α_1, α_2 is set equal to $k_{1f}^{(-)} = k_{2f}^{(-)} = 5 \times 10^7$ Pa/m, while the stiffness of the linear springs oriented along the thickness direction is $k_{3f}^{(-)} = 5 \times 10^8$ Pa/m. Finally, the shear modulus of the foundation is set to $G_f^{(-)} = 5 \times 10^6$ Pa. Sinusoidally-distributed mechanical loads are applied at the top surface, with magnitudes $\overline{q}_{1s}^{(+)} = \overline{q}_{2s}^{(+)} = 7 \times 10^5$ N/m^2, and $\overline{q}_{3s}^{(+)} = -7 \times 10^6$ N/m^2. As far as the thermal loads is concerned, two sinusoidal distributions of external thermal fluxes are applied at the top and bottom of the shell with $\overline{q}_{hs}^{(+)} = -80$ J/m^2 and $\overline{q}_{hs}^{(-)} = -20$ J/m^2. The results are calculated using different higher order theories, and the thickness plots are provided for the point $\left(0.25(\varphi_1^1 - \varphi_1^0), 0.25(\vartheta_1^1 - \vartheta_1^0)\right)$, all collected in Figs. 19–22. The through-the-thickness distribution of the three-dimensional configuration variables in Fig. 19 shows that the

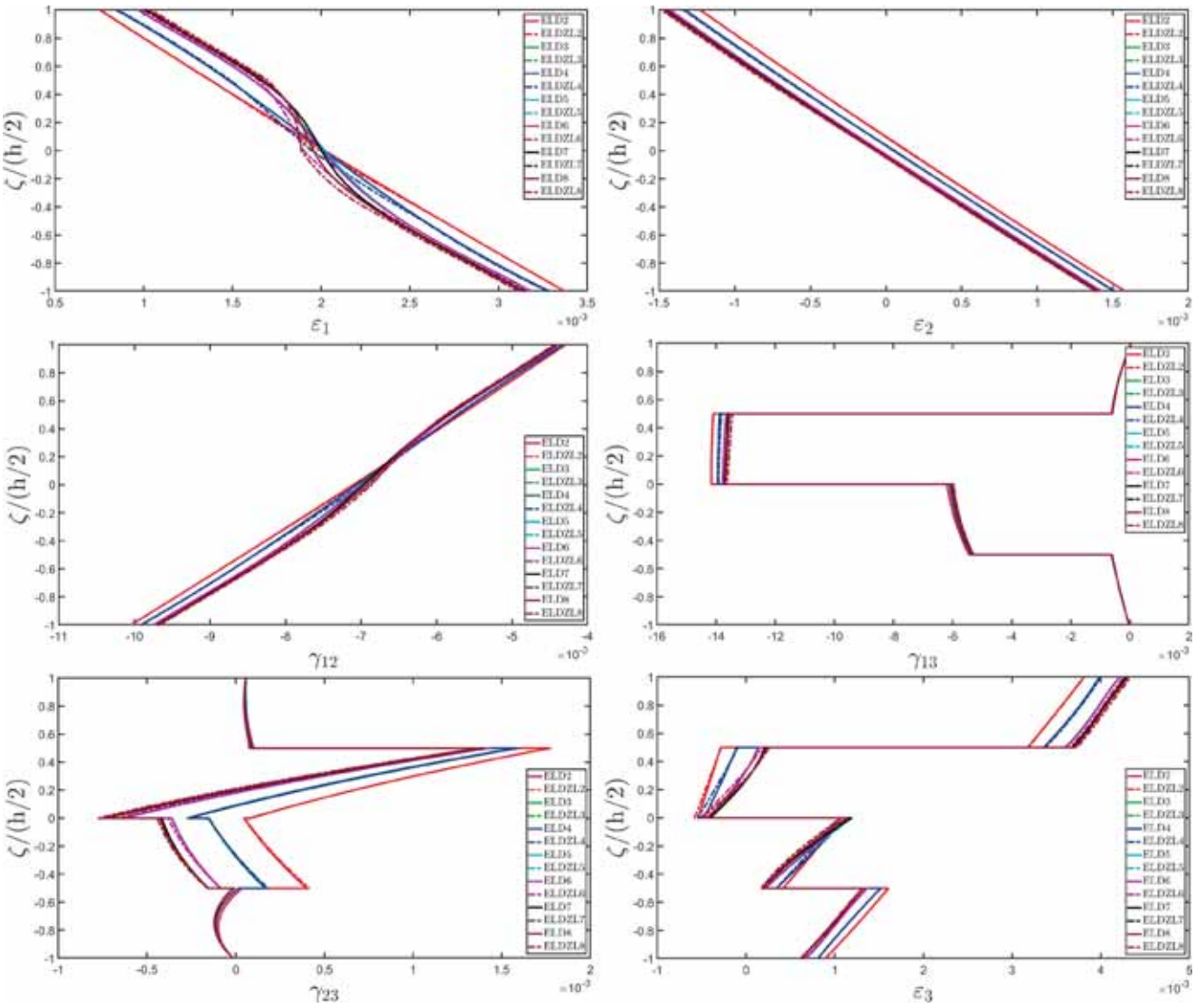

Fig. 20. Three-dimensional strain components of a shallow spherical panel lying on an elastic foundation subjected to external sinusoidal pressures with $\widetilde{N} = \widetilde{M} = 1$ of magnitudes $\overline{q}_{1s}^{(+)} = \overline{q}_{2s}^{(+)} = 7 \times 10^5$ N/m^2 and $\overline{q}_{3s}^{(+)} = -7 \times 10^6$ N/m^2, along with sinusoidal distributions of thermal fluxes with $\widetilde{N} = \widetilde{M} = 1$ of magnitudes $\overline{q}_{hs}^{(+)} = -80$ J/m^2 and $\overline{q}_{hs}^{(-)} = -20$ J/m^2, applied at $\zeta = h/2$ and $\zeta = -h/2$, respectively. The structure is located on a Winkler-Pasternak elastic foundation of stiffnesses $k_{1f}^{(-)} = k_{2f}^{(-)} = 5 \times 10^7$ Pa/m and $k_{3f}^{(-)} = 1 \times 10^8$ Pa/m, whose shear modulus is set equal to $G_f^{(-)} = 5 \times 10^6$ Pa. Visualization of thickness plots at the point $\left(0.25(\varphi_1^1 - \varphi_1^0), 0.25(\vartheta_1^1 - \vartheta_1^0)\right)$ of the physical domain employing different higher order kinematic expansions, together with the zigzag function.

lamination scheme of the structure is characterized by a meaningful softcore behavior for both the mechanical and thermal cases. A nonlinear profile of the displacement field components and temperature variation is obtained in each layer, and the adoption of a zigzag function within the ELW kinematic assumption provides a slope change at the interface between two adjacent laminae. For this reason, a convergence of results is seen as the kinematic expansion order increases, indicating that the thermo-mechanical response of the present panel cannot be predicted with classical two-dimensional theories, because higher order theories are essential. This issue becomes more evident in Fig. 20, which shows the thickness plots of the three-dimensional strain components. In-plane strains are characterized by a slope change of the profile, while a piecewise distribution is observed for the out-of-plane strain components.

As far as the three-dimensional stress components is concerned, Fig. 21 shows that the model exhibits a high convergence rate to a particular through-the-thickness profile of in-plane stress components. However, lower order theories provide different results when compared to those obtained from other ELW theories, especially for the out-of-plane shear stress τ_{23}. It is observed that the adoption of zigzag function leads to different profiles of the configuration variables for a given kinematic expansion order, while similar results are provided for primary and secondary variables. Fig. 22 illustrates the three-dimensional temperature gradient components and the thermal flux components. The adoption of higher order theories enables the prediction of a nonlinear profile for the in-plane temperature gradient components. Furthermore, the figure shows that the adoption of the ELW zigzag function introduces variations in the profile of the in-plane primary and secondary variables.

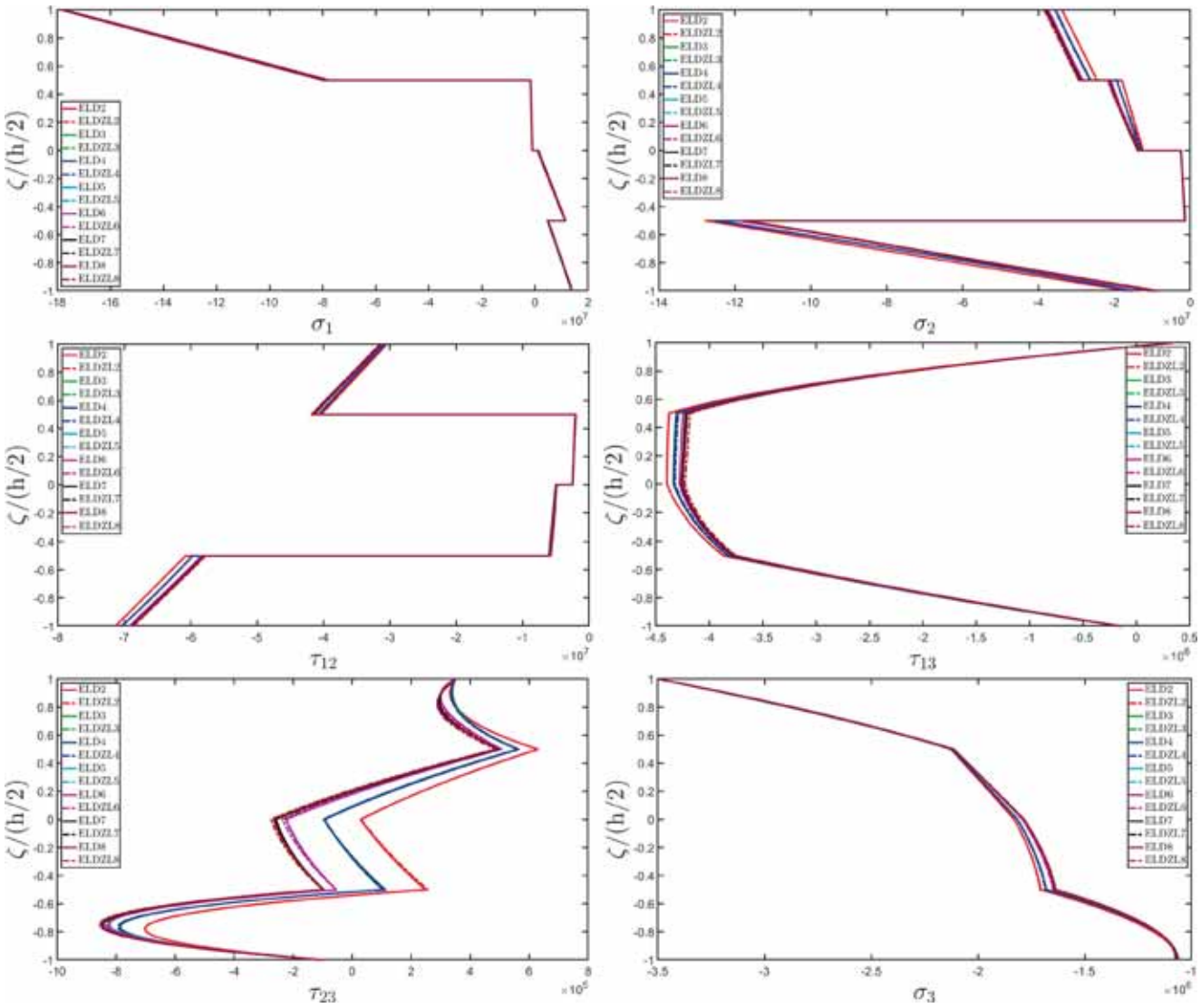

Fig. 21. Three-dimensional stress components [Pa] of a shallow spherical panel lying on an elastic foundation subjected to external sinusoidal pressures with $\widetilde{N} = \widetilde{M} = 1$ of magnitudes $\overline{q}_{1s}^{(+)} = \overline{q}_{2s}^{(+)} = 7 \times 10^5$ N/m^2 and $\overline{q}_{3s}^{(+)} = -7 \times 10^6$ N/m^2, along with sinusoidal distributions of thermal fluxes with $\widetilde{N} = \widetilde{M} = 1$ of magnitudes $\overline{q}_{hs}^{(+)} = -80$ J/m^2 and $\overline{q}_{hs}^{(-)} = -20$ J/m^2, applied at $\zeta = h/2$ and $\zeta = -h/2$, respectively. The structure is located on a Winkler-Pasternak elastic foundation of stiffnesses $k_{1f}^{(-)} = k_{2f}^{(-)} = 5 \times 10^7$ Pa/m and $k_{3f}^{(-)} = 1 \times 10^8$ Pa/m, whose shear modulus is set equal to $G_f^{(-)} = 5 \times 10^6$ Pa. Visualization of thickness plots at the point $\left(0.25(\varphi_1^1 - \varphi_1^0), 0.25(\vartheta_1^1 - \vartheta_1^0)\right)$ of the physical domain employing different higher order kinematic expansions, together with the zigzag function.

Furthermore, the recovery procedure ensures the fulfillment of the thermal balance equations along the thickness direction in all distributions. All the h_3 curves converge to the same point at the top and bottom surfaces, and the value assumed by this secondary variable in those regions is equal to that of the external loads at the point where the thickness plot is derived.

9. Conclusions

In the present manuscript, the stationary thermo-mechanical response of laminated curved panels is investigated using higher order theories. The fundamental equations are derived from a stationary configuration of the Helmholtz free energy and are expressed in curvilinear principal coordinates within a unified formulation. Configuration variables are described using higher order thickness functions, following the ELW approach. Mechanical and thermal external actions are applied as external pressures and thermal fluxes or prescribed values of each configuration variable. A semi-analytical solution is derived, and the three-dimensional thermo-mechanical response is calculated from the ELW model using a computationally efficient recovery procedure. After some preliminary examples where the model is employed to derive the numerical predictions coming from refined three-dimensional simulations, some interesting results are presented, in which it is shown that the present model is capable of predicting accurately the mechanical response of curved and layered structures in a thermal environment, including the effect of an external thermal load in terms of prescribed temperature and thermal flux. The presented semi-analytical theory is valuable not only for validating numerical models but also for providing

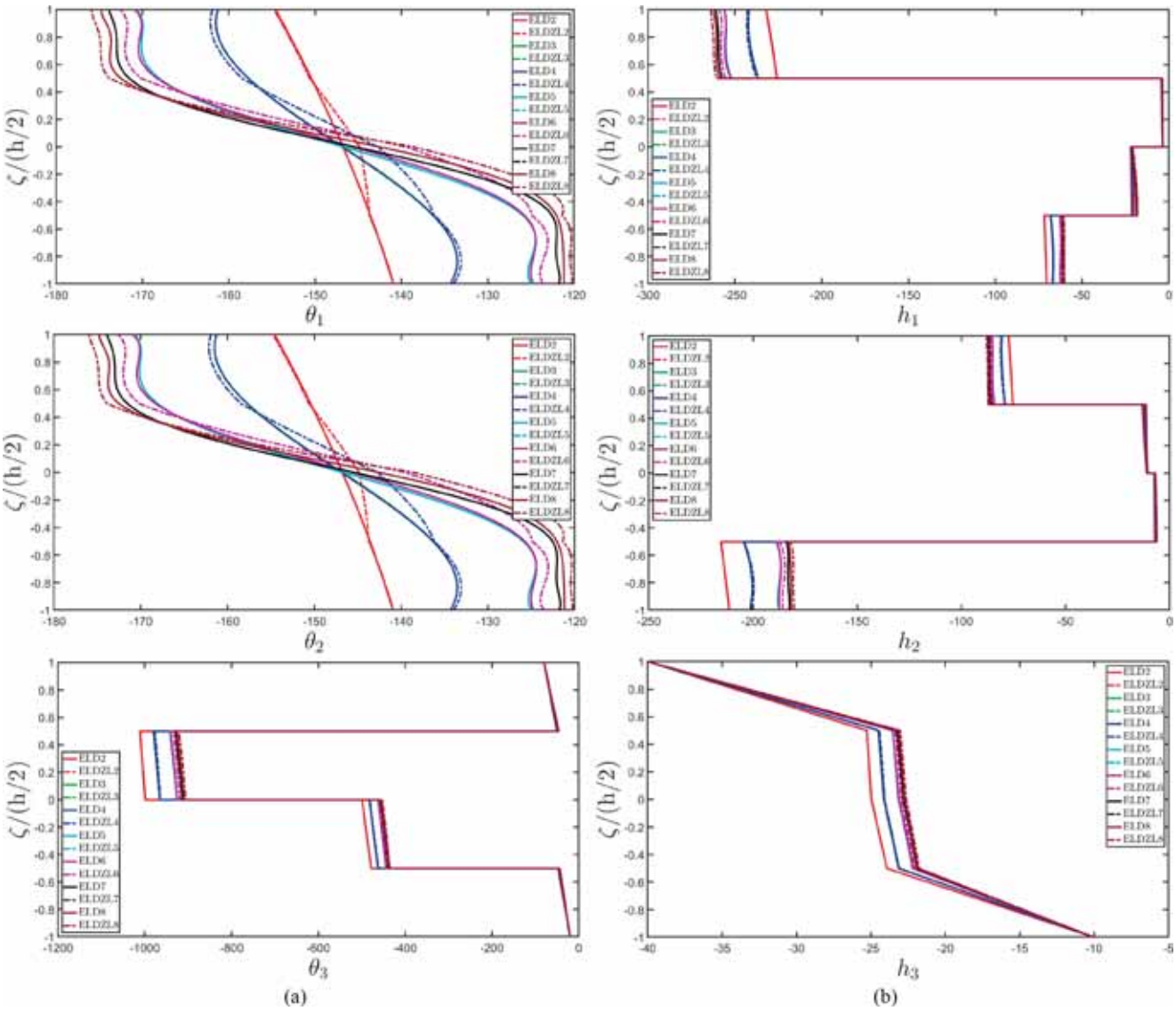

Fig. 22. Three-dimensional thermal gradient components (a) and heat flux components (b), expressed in [J/m^2], of a shallow spherical panel lying on an elastic foundation subjected to external sinusoidal pressures with $\widetilde{N} = \widetilde{M} = 1$ of magnitudes $\overline{q}_{1s}^{(+)} = \overline{q}_{2s}^{(+)} = 7 \times 10^5$ N/m^2 and $\overline{q}_{3s}^{(+)} = -7 \times 10^6$ N/m^2, along with sinusoidal distributions of thermal fluxes with $\widetilde{N} = \widetilde{M} = 1$ of magnitudes $\overline{q}_{hs}^{(+)} = -80$ J/m^2 and $\overline{q}_{hs}^{(-)} = -20$ J/m^2, applied at $\zeta = h/2$ and $\zeta = -h/2$, respectively. The structure is located on a Winkler-Pasternak elastic foundation of stiffnesses $k_{1f}^{(-)} = k_{2f}^{(-)} = 5 \times 10^7$ Pa/m and $k_{3f}^{(-)} = 1 \times 10^8$ Pa/m, whose shear modulus is set equal to $G_f^{(-)} = 5 \times 10^6$ Pa. Visualization of thickness plots at the point $\left(0.25(\varphi_1^1 - \varphi_1^0), 0.25(\vartheta_1^1 - \vartheta_1^0)\right)$ of the physical domain employing different higher order kinematic expansions, together with the zigzag function.

some numerical predictions during the design process.

CRediT authorship contribution statement

Francesco Tornabene: Writing – review & editing, Writing – original draft, Validation, Supervision, Software, Methodology, Investigation, Formal analysis, Data curation, Conceptualization. **Matteo Viscoti:** Writing – original draft, Validation, Investigation, Data curation. **Rossana Dimitri:** Writing – review & editing, Validation, Supervision, Methodology, Investigation, Formal analysis, Data curation.

Declaration of competing interest

The authors declare that they have no known competing financial interests or personal relationships that could have appeared to influence the work reported in this paper.

Data availability

No data was used for the research described in the article.

Appendix I

In the present Appendix each element of the vector $\mathbf{\Sigma}^{(\tau)\alpha_i}$ is written explicitly in terms of the configuration variables of the present formulation belonging to the vector $\boldsymbol{\delta}^{(\eta)}$ with $\eta = 0, \ldots, N+1$. The same procedure can be found in a compact matrix form in Eqn. (53).

$$N_1^{(\tau)\alpha_i} = \sum_{\eta=0}^{N+1} \left(\left(\frac{A_{11(20)}^{(\tau\eta)[00]\alpha_i\alpha_1}}{A_1} \frac{\partial}{\partial\alpha_1} + \frac{A_{12(11)}^{(\tau\eta)[00]\alpha_i\alpha_1}}{A_1 A_2} \frac{\partial A_2}{\partial\alpha_1} - \frac{A_{16(20)}^{(\tau\eta)[00]\alpha_i\alpha_1}}{A_1 A_2} \frac{\partial A_1}{\partial\alpha_2} + \frac{A_{16(11)}^{(\tau\eta)[00]\alpha_i\alpha_1}}{A_2} \frac{\partial}{\partial\alpha_2} - \frac{A_{14(20)}^{(\tau\eta)[00]\alpha_i\alpha_1}}{R_1} + A_{14(10)}^{(\tau\eta)[01]\alpha_i\alpha_1} \right) u_1^{(\eta)} + \right.$$

$$+ \left(\frac{A_{11(20)}^{(\tau\eta)[00]\alpha_i\alpha_2}}{A_1 A_2} \frac{\partial A_1}{\partial\alpha_2} + \frac{A_{12(11)}^{(\tau\eta)[00]\alpha_i\alpha_2}}{A_2} \frac{\partial}{\partial\alpha_2} + \frac{A_{16(20)}^{(\tau\eta)[00]\alpha_i\alpha_2}}{A_1} \frac{\partial}{\partial\alpha_1} - \frac{A_{16(11)}^{(\tau\eta)[00]\alpha_i\alpha_2}}{A_1 A_2} \frac{\partial A_2}{\partial\alpha_1} - \frac{A_{15(11)}^{(\tau\eta)[00]\alpha_i\alpha_2}}{R_2} + A_{15(10)}^{(\tau\eta)[01]\alpha_i\alpha_2} \right) u_2^{(\eta)} +$$

$$\left. + \left(\frac{A_{11(20)}^{(\tau\eta)[00]\alpha_i\alpha_3}}{R_1} + \frac{A_{12(11)}^{(\tau\eta)[00]\alpha_i\alpha_3}}{R_2} + \frac{A_{14(20)}^{(\tau\eta)[00]\alpha_i\alpha_3}}{A_1} \frac{\partial}{\partial\alpha_1} + \frac{A_{15(11)}^{(\tau\eta)[00]\alpha_i\alpha_3}}{A_2} \frac{\partial}{\partial\alpha_2} + A_{13(10)}^{(\tau\eta)[01]\alpha_i\alpha_3} \right) u_3^{(\eta)} - Z_{11(10)}^{(\tau\eta)[00]\alpha_i\alpha_4} \xi^{(\eta)} \right)$$

$$N_2^{(\tau)\alpha_i} = \sum_{\eta=0}^{N+1} \left(\left(\frac{A_{12(11)}^{(\tau\eta)[00]\alpha_i\alpha_1}}{A_1} \frac{\partial}{\partial\alpha_1} + \frac{A_{22(02)}^{(\tau\eta)[00]\alpha_i\alpha_1}}{A_1 A_2} \frac{\partial A_2}{\partial\alpha_1} - \frac{A_{26(11)}^{(\tau\eta)[00]\alpha_i\alpha_1}}{A_1 A_2} \frac{\partial A_1}{\partial\alpha_2} + \frac{A_{26(02)}^{(\tau\eta)[00]\alpha_i\alpha_1}}{A_2} \frac{\partial}{\partial\alpha_2} - \frac{A_{24(11)}^{(\tau\eta)[00]\alpha_i\alpha_1}}{R_1} + A_{24(01)}^{(\tau\eta)[01]\alpha_i\alpha_1} \right) u_1^{(\eta)} + \right.$$

$$+ \left(\frac{A_{12(11)}^{(\tau\eta)[00]\alpha_i\alpha_2}}{A_1 A_2} \frac{\partial A_1}{\partial\alpha_2} + \frac{A_{22(02)}^{(\tau\eta)[00]\alpha_i\alpha_2}}{A_2} \frac{\partial}{\partial\alpha_2} + \frac{A_{26(11)}^{(\tau\eta)[00]\alpha_i\alpha_2}}{A_1} \frac{\partial}{\partial\alpha_1} - \frac{A_{26(02)}^{(\tau\eta)[00]\alpha_i\alpha_2}}{A_1 A_2} \frac{\partial A_2}{\partial\alpha_1} - \frac{A_{25(02)}^{(\tau\eta)[00]\alpha_i\alpha_2}}{R_2} + A_{25(01)}^{(\tau\eta)[01]\alpha_i\alpha_2} \right) u_2^{(\eta)} +$$

$$\left. + \left(\frac{A_{12(11)}^{(\tau\eta)[00]\alpha_i\alpha_3}}{R_1} + \frac{A_{22(02)}^{(\tau\eta)[00]\alpha_i\alpha_3}}{R_2} + \frac{A_{24(11)}^{(\tau\eta)[00]\alpha_i\alpha_3}}{A_1} \frac{\partial}{\partial\alpha_1} + \frac{A_{25(02)}^{(\tau\eta)[00]\alpha_i\alpha_3}}{A_2} \frac{\partial}{\partial\alpha_2} + A_{23(01)}^{(\tau\eta)[01]\alpha_i\alpha_3} \right) u_3^{(\eta)} - Z_{22(01)}^{(\tau\eta)[00]\alpha_i\alpha_4} \xi^{(\eta)} \right)$$

$$N_{12}^{(\tau)\alpha_i} = \sum_{\eta=0}^{N+1} \left(\left(\frac{A_{16(20)}^{(\tau\eta)[00]\alpha_i\alpha_1}}{A_1} \frac{\partial}{\partial\alpha_1} + \frac{A_{26(11)}^{(\tau\eta)[00]\alpha_i\alpha_1}}{A_1 A_2} \frac{\partial A_2}{\partial\alpha_1} - \frac{A_{66(20)}^{(\tau\eta)[00]\alpha_i\alpha_1}}{A_1 A_2} \frac{\partial A_1}{\partial\alpha_2} + \frac{A_{66(11)}^{(\tau\eta)[00]\alpha_i\alpha_1}}{A_2} \frac{\partial}{\partial\alpha_2} - \frac{A_{46(20)}^{(\tau\eta)[00]\alpha_i\alpha_1}}{R_1} + A_{46(10)}^{(\tau\eta)[01]\alpha_i\alpha_1} \right) u_1^{(\eta)} + \right.$$

$$+ \left(\frac{A_{16(20)}^{(\tau\eta)[00]\alpha_i\alpha_2}}{A_1 A_2} \frac{\partial A_1}{\partial\alpha_2} + \frac{A_{26(11)}^{(\tau\eta)[00]\alpha_i\alpha_2}}{A_2} \frac{\partial}{\partial\alpha_2} + \frac{A_{66(20)}^{(\tau\eta)[00]\alpha_i\alpha_2}}{A_1} \frac{\partial}{\partial\alpha_1} - \frac{A_{66(11)}^{(\tau\eta)[00]\alpha_i\alpha_2}}{A_1 A_2} \frac{\partial A_2}{\partial\alpha_1} - \frac{A_{56(11)}^{(\tau\eta)[00]\alpha_i\alpha_2}}{R_2} + A_{56(10)}^{(\tau\eta)[01]\alpha_i\alpha_2} \right) u_2^{(\eta)} +$$

$$\left. + \left(\frac{A_{16(20)}^{(\tau\eta)[00]\alpha_i\alpha_3}}{R_1} + \frac{A_{26(11)}^{(\tau\eta)[00]\alpha_i\alpha_3}}{R_2} + \frac{A_{46(20)}^{(\tau\eta)[00]\alpha_i\alpha_3}}{A_1} \frac{\partial}{\partial\alpha_1} + \frac{A_{56(11)}^{(\tau\eta)[00]\alpha_i\alpha_3}}{A_2} \frac{\partial}{\partial\alpha_2} + A_{36(10)}^{(\tau\eta)[01]\alpha_i\alpha_3} \right) u_3^{(\eta)} - Z_{12(10)}^{(\tau\eta)[00]\alpha_i\alpha_4} \xi^{(\eta)} \right)$$

$$N_{21}^{(\tau)\alpha_i} = \sum_{\eta=0}^{N+1} \left(\left(\frac{A_{16(11)}^{(\tau\eta)[00]\alpha_i\alpha_1}}{A_1} \frac{\partial}{\partial\alpha_1} + \frac{A_{26(02)}^{(\tau\eta)[00]\alpha_i\alpha_1}}{A_1 A_2} \frac{\partial A_2}{\partial\alpha_1} - \frac{A_{66(11)}^{(\tau\eta)[00]\alpha_i\alpha_1}}{A_1 A_2} \frac{\partial A_1}{\partial\alpha_2} + \frac{A_{66(02)}^{(\tau\eta)[00]\alpha_i\alpha_1}}{A_2} \frac{\partial}{\partial\alpha_2} - \frac{A_{46(11)}^{(\tau\eta)[00]\alpha_i\alpha_1}}{R_1} + A_{46(01)}^{(\tau\eta)[01]\alpha_i\alpha_1} \right) u_1^{(\eta)} + \right.$$

$$+ \left(\frac{A_{16(11)}^{(\tau\eta)[00]\alpha_i\alpha_2}}{A_1 A_2} \frac{\partial A_1}{\partial\alpha_2} + \frac{A_{26(02)}^{(\tau\eta)[00]\alpha_i\alpha_2}}{A_2} \frac{\partial}{\partial\alpha_2} + \frac{A_{66(11)}^{(\tau\eta)[00]\alpha_i\alpha_2}}{A_1} \frac{\partial}{\partial\alpha_1} - \frac{A_{66(02)}^{(\tau\eta)[00]\alpha_i\alpha_2}}{A_1 A_2} \frac{\partial A_2}{\partial\alpha_1} - \frac{A_{56(02)}^{(\tau\eta)[00]\alpha_i\alpha_2}}{R_2} + A_{56(01)}^{(\tau\eta)[01]\alpha_i\alpha_2} \right) u_2^{(\eta)} +$$

$$\left. + \left(\frac{A_{16(11)}^{(\tau\eta)[00]\alpha_i\alpha_3}}{R_1} + \frac{A_{26(02)}^{(\tau\eta)[00]\alpha_i\alpha_3}}{R_2} + \frac{A_{46(11)}^{(\tau\eta)[00]\alpha_i\alpha_3}}{A_1} \frac{\partial}{\partial\alpha_1} + \frac{A_{56(02)}^{(\tau\eta)[00]\alpha_i\alpha_3}}{A_2} \frac{\partial}{\partial\alpha_2} + A_{36(01)}^{(\tau\eta)[01]\alpha_i\alpha_3} \right) u_3^{(\eta)} - Z_{12(01)}^{(\tau\eta)[00]\alpha_i\alpha_4} \xi^{(\tau)} \right)$$

$$T_1^{(\tau)\alpha_i} = \sum_{\eta=0}^{N+1} \left(\left(\frac{A_{14(20)}^{(\tau\eta)[00]\alpha_i\alpha_1}}{A_1} \frac{\partial}{\partial\alpha_1} + \frac{A_{24(11)}^{(\tau\eta)[00]\alpha_i\alpha_1}}{A_1 A_2} \frac{\partial A_2}{\partial\alpha_1} - \frac{A_{46(20)}^{(\tau\eta)[00]\alpha_i\alpha_1}}{A_1 A_2} \frac{\partial A_1}{\partial\alpha_2} + \frac{A_{46(11)}^{(\tau\eta)[00]\alpha_i\alpha_1}}{A_2} \frac{\partial}{\partial\alpha_2} - \frac{A_{44(20)}^{(\tau\eta)[00]\alpha_i\alpha_1}}{R_1} + A_{44(10)}^{(\tau\eta)[01]\alpha_i\alpha_1} \right) u_1^{(\eta)} + \right.$$

$$+ \left(\frac{A_{14(20)}^{(\tau\eta)[00]\alpha_i\alpha_2}}{A_1 A_2} \frac{\partial A_1}{\partial\alpha_2} + \frac{A_{24(11)}^{(\tau\eta)[00]\alpha_i\alpha_2}}{A_2} \frac{\partial}{\partial\alpha_2} + \frac{A_{46(20)}^{(\tau\eta)[00]\alpha_i\alpha_2}}{A_1} \frac{\partial}{\partial\alpha_1} - \frac{A_{46(11)}^{(\tau\eta)[00]\alpha_i\alpha_2}}{A_1 A_2} \frac{\partial A_2}{\partial\alpha_1} - \frac{A_{45(11)}^{(\tau\eta)[00]\alpha_i\alpha_2}}{R_2} + A_{45(10)}^{(\tau\eta)[01]\alpha_i\alpha_2} \right) u_2^{(\eta)} +$$

$$\left. + \left(\frac{A_{14(20)}^{(\tau\eta)[00]\alpha_i\alpha_3}}{R_1} + \frac{A_{24(11)}^{(\tau\eta)[00]\alpha_i\alpha_3}}{R_2} + \frac{A_{44(20)}^{(\tau\eta)[00]\alpha_i\alpha_3}}{A_1} \frac{\partial}{\partial\alpha_1} + \frac{A_{45(11)}^{(\tau\eta)[00]\alpha_i\alpha_3}}{A_2} \frac{\partial}{\partial\alpha_2} + A_{34(10)}^{(\tau\eta)[01]\alpha_i\alpha_3} \right) u_3^{(\eta)} - Z_{13(10)}^{(\tau\eta)[00]\alpha_i\alpha_4} \xi^{(\eta)} \right)$$

$$T_2^{(\tau)\alpha_i} = \sum_{\eta=0}^{N+1} \left(\left(\frac{A_{15(11)}^{(\tau\eta)[00]\alpha_i\alpha_1}}{A_1} \frac{\partial}{\partial\alpha_1} + \frac{A_{25(02)}^{(\tau\eta)[00]\alpha_i\alpha_1}}{A_1 A_2} \frac{\partial A_2}{\partial\alpha_1} - \frac{A_{56(11)}^{(\tau\eta)[00]\alpha_i\alpha_1}}{A_1 A_2} \frac{\partial A_1}{\partial\alpha_2} + \frac{A_{56(02)}^{(\tau\eta)[00]\alpha_i\alpha_1}}{A_2} \frac{\partial}{\partial\alpha_2} - \frac{A_{45(11)}^{(\tau\eta)[00]\alpha_i\alpha_1}}{R_1} + A_{45(01)}^{(\tau\eta)[01]\alpha_i\alpha_1} \right) u_1^{(\eta)} + \right.$$

$$+ \left(\frac{A_{15(11)}^{(\tau\eta)[00]\alpha_i\alpha_2}}{A_1 A_2} \frac{\partial A_1}{\partial\alpha_2} + \frac{A_{25(02)}^{(\tau\eta)[00]\alpha_i\alpha_2}}{A_2} \frac{\partial}{\partial\alpha_2} + \frac{A_{56(11)}^{(\tau\eta)[00]\alpha_i\alpha_2}}{A_1} \frac{\partial}{\partial\alpha_1} - \frac{A_{56(02)}^{(\tau\eta)[00]\alpha_i\alpha_2}}{A_1 A_2} \frac{\partial A_2}{\partial\alpha_1} - \frac{A_{55(02)}^{(\tau\eta)[00]\alpha_i\alpha_2}}{R_2} + A_{55(01)}^{(\tau\eta)[01]\alpha_i\alpha_2} \right) u_2^{(\eta)} +$$

$$\left. + \left(\frac{A_{15(11)}^{(\tau\eta)[00]\alpha_i\alpha_3}}{R_1} + \frac{A_{25(02)}^{(\tau\eta)[00]\alpha_i\alpha_3}}{R_2} + \frac{A_{45(11)}^{(\tau\eta)[00]\alpha_i\alpha_3}}{A_1} \frac{\partial}{\partial\alpha_1} + \frac{A_{55(02)}^{(\tau\eta)[00]\alpha_i\alpha_3}}{A_2} \frac{\partial}{\partial\alpha_2} + A_{35(01)}^{(\tau\eta)[01]\alpha_i\alpha_3} \right) u_3^{(\eta)} - Z_{23(01)}^{(\tau\eta)[00]\alpha_i\alpha_4} \xi^{(\eta)} \right)$$

$$P_1^{(\tau)\alpha_i} = \sum_{\eta=0}^{N+1} \left(\left(\frac{A_{14(10)}^{(\tau\eta)[10]\alpha_i\alpha_1}}{A_1} \frac{\partial}{\partial\alpha_1} + \frac{A_{24(01)}^{(\tau\eta)[10]\alpha_i\alpha_1}}{A_1 A_2} \frac{\partial A_2}{\partial\alpha_1} - \frac{A_{46(10)}^{(\tau\eta)[10]\alpha_i\alpha_1}}{A_1 A_2} \frac{\partial A_1}{\partial\alpha_2} + \frac{A_{46(01)}^{(\tau\eta)[10]\alpha_i\alpha_1}}{A_2} \frac{\partial}{\partial\alpha_2} - \frac{A_{44(10)}^{(\tau\eta)[10]\alpha_i\alpha_1}}{R_1} + A_{44(00)}^{(\tau\eta)[11]\alpha_i\alpha_1} \right) u_1^{(\eta)} + \right.$$

$$+\left(\frac{A^{(\tau\eta)[10|\alpha_i\alpha_2}_{14(10)}}{A_1A_2}\frac{\partial A_1}{\partial\alpha_2}+\frac{A^{(\tau\eta)[10|\alpha_i\alpha_2}_{24(01)}}{A_2}\frac{\partial}{\partial\alpha_2}+\frac{A^{(\tau\eta)[10|\alpha_i\alpha_2}_{46(10)}}{A_1}\frac{\partial}{\partial\alpha_1}-\frac{A^{(\tau\eta)[10|\alpha_i\alpha_2}_{46(01)}}{A_1A_2}\frac{\partial A_2}{\partial\alpha_1}-\frac{A^{(\tau\eta)[10|\alpha_i\alpha_2}_{45(01)}}{R_2}+A^{(\tau\eta)[11|\alpha_i\alpha_2}_{45(00)}\right)u_2^{(\eta)}+$$

$$+\left(\frac{A^{(\tau\eta)[10|\alpha_i\alpha_3}_{14(10)}}{R_1}+\frac{A^{(\tau\eta)[10|\alpha_i\alpha_3}_{24(01)}}{R_2}+\frac{A^{(\tau\eta)[10|\alpha_i\alpha_3}_{44(10)}}{A_1}\frac{\partial}{\partial\alpha_1}+\frac{A^{(\tau\eta)[10|\alpha_i\alpha_3}_{45(01)}}{A_2}\frac{\partial}{\partial\alpha_2}+A^{(\tau\eta)[11|\alpha_i\alpha_3}_{34(00)}\right)u_3^{(\eta)}-Z^{(\tau\eta)[10|\alpha_i\alpha_4}_{13(00)}\xi^{(\eta)}\Bigg)$$

$$P_2^{(\tau)\alpha_i}=\sum_{\eta=0}^{N+1}\Bigg(\left(\frac{A^{(\tau\eta)[10|\alpha_i\alpha_1}_{15(10)}}{A_1}\frac{\partial}{\partial\alpha_1}+\frac{A^{(\tau\eta)[10|\alpha_i\alpha_1}_{25(01)}}{A_1A_2}\frac{\partial A_2}{\partial\alpha_1}-\frac{A^{(\tau\eta)[10|\alpha_i\alpha_1}_{56(10)}}{A_1A_2}\frac{\partial A_1}{\partial\alpha_2}+\frac{A^{(\tau\eta)[10|\alpha_i\alpha_1}_{56(01)}}{A_2}\frac{\partial}{\partial\alpha_2}-\frac{A^{(\tau\eta)[10|\alpha_i\alpha_1}_{45(10)}}{R_1}+A^{(\tau\eta)[11|\alpha_i\alpha_1}_{45(00)}\right)u_1^{(\eta)}+$$

$$+\left(\frac{A^{(\tau\eta)[10|\alpha_i\alpha_2}_{15(10)}}{A_1A_2}\frac{\partial A_1}{\partial\alpha_2}+\frac{A^{(\tau\eta)[10|\alpha_i\alpha_2}_{25(01)}}{A_2}\frac{\partial}{\partial\alpha_2}+\frac{A^{(\tau\eta)[10|\alpha_i\alpha_2}_{56(10)}}{A_1}\frac{\partial}{\partial\alpha_1}-\frac{A^{(\tau\eta)[10|\alpha_i\alpha_2}_{56(01)}}{A_1A_2}\frac{\partial A_2}{\partial\alpha_1}-\frac{A^{(\tau\eta)[10|\alpha_i\alpha_2}_{55(01)}}{R_2}+A^{(\tau\eta)[11|\alpha_i\alpha_2}_{55(00)}\right)u_2^{(\eta)}+$$

$$+\left(\frac{A^{(\tau\eta)[10|\alpha_i\alpha_3}_{15(10)}}{R_1}+\frac{A^{(\tau\eta)[10|\alpha_i\alpha_3}_{25(01)}}{R_2}+\frac{A^{(\tau\eta)[10|\alpha_i\alpha_3}_{45(10)}}{A_1}\frac{\partial}{\partial\alpha_1}+\frac{A^{(\tau\eta)[10|\alpha_i\alpha_3}_{55(01)}}{A_2}\frac{\partial}{\partial\alpha_2}+A^{(\tau\eta)[11|\alpha_i\alpha_3}_{35(00)}\right)u_3^{(\eta)}-Z^{(\tau\eta)[10|\alpha_i\alpha_4}_{23(00)}\xi^{(\eta)}\Bigg)$$

$$S_3^{(\tau)\alpha_i}=\sum_{\eta=0}^{N+1}\Bigg(\left(\frac{A^{(\tau\eta)[10|\alpha_i\alpha_1}_{13(10)}}{A_1}\frac{\partial}{\partial\alpha_1}+\frac{A^{(\tau\eta)[10|\alpha_i\alpha_1}_{23(01)}}{A_1A_2}\frac{\partial A_2}{\partial\alpha_1}-\frac{A^{(\tau\eta)[10|\alpha_i\alpha_1}_{36(10)}}{A_1A_2}\frac{\partial A_1}{\partial\alpha_2}+\frac{A^{(\tau\eta)[10|\alpha_i\alpha_1}_{36(01)}}{A_2}\frac{\partial}{\partial\alpha_2}-\frac{A^{(\tau\eta)[10|\alpha_i\alpha_1}_{34(10)}}{R_1}+A^{(\tau\eta)[11|\alpha_i\alpha_1}_{34(00)}\right)u_1^{(\eta)}+$$

$$+\left(\frac{A^{(\tau\eta)[10|\alpha_i\alpha_2}_{13(10)}}{A_1A_2}\frac{\partial A_1}{\partial\alpha_2}+\frac{A^{(\tau\eta)[10|\alpha_i\alpha_2}_{23(01)}}{A_2}\frac{\partial}{\partial\alpha_2}+\frac{A^{(\tau\eta)[10|\alpha_i\alpha_2}_{36(10)}}{A_1}\frac{\partial}{\partial\alpha_1}-\frac{A^{(\tau\eta)[10|\alpha_i\alpha_2}_{36(01)}}{A_1A_2}\frac{\partial A_2}{\partial\alpha_1}-\frac{A^{(\tau\eta)[10|\alpha_i\alpha_2}_{35(01)}}{R_2}+A^{(\tau\eta)[11|\alpha_i\alpha_2}_{35(00)}\right)u_2^{(\eta)}+$$

$$+\left(\frac{A^{(\tau\eta)[10|\alpha_i\alpha_3}_{13(10)}}{R_1}+\frac{A^{(\tau\eta)[10|\alpha_i\alpha_3}_{23(01)}}{R_2}+\frac{A^{(\tau\eta)[10|\alpha_i\alpha_3}_{34(10)}}{A_1}\frac{\partial}{\partial\alpha_1}+\frac{A^{(\tau\eta)[10|\alpha_i\alpha_3}_{35(01)}}{A_2}\frac{\partial}{\partial\alpha_2}+A^{(\tau\eta)[11|\alpha_i\alpha_3}_{33(00)}\right)u_3^{(\eta)}-Z^{(\tau\eta)[10|\alpha_i\alpha_4}_{33(00)}\xi^{(\eta)}\Bigg)$$

$$E^{(\tau)\alpha_i}=\sum_{\eta=0}^{N+1}\Bigg(\left(\frac{Z^{(\tau\eta)[00|\alpha_i\alpha_1}_{11(10)}}{A_1}\frac{\partial}{\partial\alpha_1}+\frac{Z^{(\tau\eta)[00|\alpha_i\alpha_1}_{22(01)}}{A_1A_2}\frac{\partial A_2}{\partial\alpha_1}-\frac{Z^{(\tau\eta)[00|\alpha_i\alpha_1}_{12(10)}}{A_1A_2}\frac{\partial A_1}{\partial\alpha_2}+\frac{Z^{(\tau\eta)[00|\alpha_i\alpha_1}_{12(01)}}{A_2}\frac{\partial}{\partial\alpha_2}-\frac{Z^{(\tau\eta)[00|\alpha_i\alpha_1}_{13(10)}}{R_1}+Z^{(\tau\eta)[01|\alpha_i\alpha_1}_{13(00)}\right)u_1^{(\eta)}+$$

$$+\left(\frac{Z^{(\tau\eta)[00|\alpha_i\alpha_2}_{11(10)}}{A_1A_2}\frac{\partial A_1}{\partial\alpha_2}+\frac{Z^{(\tau\eta)[00|\alpha_i\alpha_2}_{22(01)}}{A_2}\frac{\partial}{\partial\alpha_2}+\frac{Z^{(\tau\eta)[00|\alpha_i\alpha_2}_{12(10)}}{A_1}\frac{\partial}{\partial\alpha_1}-\frac{Z^{(\tau\eta)[00|\alpha_i\alpha_2}_{12(01)}}{A_1A_2}\frac{\partial A_2}{\partial\alpha_1}-\frac{Z^{(\tau\eta)[00|\alpha_i\alpha_2}_{23(01)}}{R_2}+Z^{(\tau\eta)[01|\alpha_i\alpha_2}_{23(00)}\right)u_2^{(\eta)}+$$

$$+\left(\frac{Z^{(\tau\eta)[00|\alpha_i\alpha_3}_{11(10)}}{R_1}+\frac{Z^{(\tau\eta)[00|\alpha_i\alpha_3}_{22(01)}}{R_2}+\frac{Z^{(\tau\eta)[00|\alpha_i\alpha_3}_{13(10)}}{A_1}\frac{\partial}{\partial\alpha_1}+\frac{Z^{(\tau\eta)[00|\alpha_i\alpha_3}_{23(01)}}{A_2}\frac{\partial}{\partial\alpha_2}+Z^{(\tau\eta)[01|\alpha_i\alpha_3}_{33(00)}\right)u_3^{(\eta)}+C^{(\tau\eta)[00|\alpha_i\alpha_4}_{11(00)}\xi^{(\eta)}\Bigg)$$

$$H_1^{(\tau)\alpha_i}=-\sum_{\eta=0}^{N+1}\left(\frac{K^{(\tau\eta)[00|\alpha_i\alpha_4}_{11(20)}}{A_1}\frac{\partial}{\partial\alpha_1}+\frac{K^{(\tau\eta)[00|\alpha_i\alpha_4}_{12(11)}}{A_2}\frac{\partial}{\partial\alpha_2}+K^{(\tau\eta)[01|\alpha_i\alpha_4}_{13(10)}\right)\xi^{(\eta)}$$

$$H_2^{(\tau)\alpha_i}=-\sum_{\eta=0}^{N+1}\left(\frac{K^{(\tau\eta)[00|\alpha_i\alpha_4}_{12(11)}}{A_1}\frac{\partial}{\partial\alpha_1}+\frac{K^{(\tau\eta)[00|\alpha_i\alpha_4}_{22(02)}}{A_2}\frac{\partial}{\partial\alpha_2}+K^{(\tau\eta)[01|\alpha_i\alpha_4}_{23(01)}\right)\xi^{(\eta)}$$

$$H_3^{(\tau)\alpha_i}=-\sum_{\eta=0}^{N+1}\left(\frac{K^{(\tau\eta)[10|\alpha_i\alpha_4}_{13(10)}}{A_1}\frac{\partial}{\partial\alpha_1}+\frac{K^{(\tau\eta)[10|\alpha_i\alpha_4}_{23(01)}}{A_2}\frac{\partial}{\partial\alpha_2}+K^{(\tau\eta)[11|\alpha_i\alpha_4}_{33(00)}\right)\xi^{(\eta)} \tag{A.1}$$

Appendix I. I

In the present section the complete expression can be found of the semi-analytical fundamental coefficients $\widetilde{L}_{ijnm}^{(\tau\eta)\alpha_i\alpha_j}$ with $i,j=1,\ldots,4$ belonging to the matrix of Eqn. (84).

$$\widetilde{L}_{11nm}^{(\tau\eta)\alpha_1\alpha_1}=-A^{(\tau\eta)[00|\alpha_1\alpha_1}_{11(20)}\left(\frac{n\pi}{L_1}\right)^2-A^{(\tau\eta)[00|\alpha_1\alpha_1}_{66(02)}\left(\frac{m\pi}{L_2}\right)^2-\frac{A^{(\tau\eta)[00|\alpha_1\alpha_1}_{44(20)}}{R_1^2}+\frac{A^{(\tau\eta)[01|\alpha_1\alpha_1}_{44(10)}+A^{(\tau\eta)[10|\alpha_1\alpha_1}_{44(10)}}{R_1}-A^{(\tau\eta)[11|\alpha_1\alpha_1}_{44(00)}$$

$$\widetilde{L}_{12nm}^{(\tau\eta)\alpha_1\alpha_2}=-\left(A^{(\tau\eta)[00|\alpha_1\alpha_2}_{12(11)}+A^{(\tau\eta)[00|\alpha_1\alpha_2}_{66(11)}\right)\left(\frac{n\pi}{L_1}\right)\left(\frac{m\pi}{L_2}\right)$$

$$\widetilde{L}_{13nm}^{(\tau\eta)\alpha_1\alpha_3}=\left(A^{(\tau\eta)[01|\alpha_1\alpha_3}_{13(10)}-A^{(\tau\eta)[10|\alpha_1\alpha_3}_{44(10)}+\frac{A^{(\tau\eta)[00|\alpha_1\alpha_3}_{11(20)}+A^{(\tau\eta)[00|\alpha_1\alpha_3}_{44(20)}}{R_1}+\frac{A^{(\tau\eta)[00|\alpha_1\alpha_3}_{12(11)}}{R_2}\right)\left(\frac{n\pi}{L_1}\right)$$

$$\widetilde{L}_{14nm}^{(\tau\eta)\alpha_1\alpha_4}=-Z^{(\tau\eta)[00|\alpha_1\alpha_4}_{11(10)}\left(\frac{n\pi}{L_1}\right)$$

$$\widetilde{L}_{21nm}^{(\tau\eta)\alpha_2\alpha_1} = -\left(A_{12(11)}^{(\tau\eta)[00]\alpha_2\alpha_1} + A_{66(11)}^{(\tau\eta)[00]\alpha_2\alpha_1}\right)\left(\frac{n\pi}{L_1}\right)\left(\frac{m\pi}{L_2}\right)$$

$$\widetilde{L}_{22nm}^{(\tau\eta)\alpha_2\alpha_2} = -A_{66(20)}^{(\tau\eta)[00]\alpha_2\alpha_2}\left(\frac{n\pi}{L_1}\right)^2 - A_{22(02)}^{(\tau\eta)[00]\alpha_2\alpha_2}\left(\frac{m\pi}{L_2}\right)^2 - \frac{A_{55(02)}^{(\tau\eta)[00]\alpha_2\alpha_2}}{R_2^2} + \frac{A_{55(01)}^{(\tau\eta)[01]\alpha_2\alpha_2} + A_{55(01)}^{(\tau\eta)[10]\alpha_2\alpha_2}}{R_2} - A_{55(00)}^{(\tau\eta)[11]\alpha_2\alpha_2}$$

$$\widetilde{L}_{23nm}^{(\tau\eta)\alpha_2\alpha_3} = \left(A_{23(01)}^{(\tau\eta)[01]\alpha_2\alpha_3} - A_{55(01)}^{(\tau\eta)[10]\alpha_2\alpha_3} + \frac{A_{22(02)}^{(\tau\eta)[00]\alpha_2\alpha_3} + A_{55(02)}^{(\tau\eta)[00]\alpha_2\alpha_3}}{R_2} + \frac{A_{12(11)}^{(\tau\eta)[00]\alpha_2\alpha_3}}{R_1}\right)\left(\frac{m\pi}{L_2}\right)$$

$$\widetilde{L}_{24nm}^{(\tau\eta)\alpha_2\alpha_4} = -Z_{22(01)}^{(\tau\eta)[00]\alpha_2\alpha_4}\left(\frac{m\pi}{L_2}\right)$$

$$\widetilde{L}_{31nm}^{(\tau\eta)\alpha_3\alpha_1} = \left(A_{13(10)}^{(\tau\eta)[10]\alpha_3\alpha_1} - A_{44(10)}^{(\tau\eta)[01]\alpha_3\alpha_1} + \frac{A_{11(20)}^{(\tau\eta)[00]\alpha_3\alpha_1} + A_{44(20)}^{(\tau\eta)[00]\alpha_3\alpha_1}}{R_1} + \frac{A_{12(11)}^{(\tau\eta)[00]\alpha_3\alpha_1}}{R_2}\right)\left(\frac{n\pi}{L_1}\right)$$

$$\widetilde{L}_{32nm}^{(\tau\eta)\alpha_3\alpha_2} = \left(A_{23(01)}^{(\tau\eta)[10]\alpha_3\alpha_2} - A_{55(01)}^{(\tau\eta)[01]\alpha_3\alpha_2} + \frac{A_{12(11)}^{(\tau\eta)[00]\alpha_3\alpha_2}}{R_1} + \frac{A_{22(02)}^{(\tau\eta)[00]\alpha_3\alpha_2} + A_{55(02)}^{(\tau\eta)[00]\alpha_3\alpha_2}}{R_2}\right)\left(\frac{m\pi}{L_2}\right)$$

$$\widetilde{L}_{33nm}^{(\tau\eta)\alpha_3\alpha_3} = -A_{44(20)}^{(\tau\eta)[00]\alpha_3\alpha_3}\left(\frac{n\pi}{L_1}\right)^2 - A_{55(02)}^{(\tau\eta)[00]\alpha_3\alpha_3}\left(\frac{m\pi}{L_2}\right)^2 - \frac{A_{11(20)}^{(\tau\eta)[00]\alpha_3\alpha_3}}{R_1^2} - \frac{A_{22(02)}^{(\tau\eta)[00]\alpha_3\alpha_3}}{R_2^2} - \frac{2A_{12(11)}^{(\tau\eta)[00]\alpha_3\alpha_3}}{R_1R_2} + \\ - \frac{A_{13(10)}^{(\tau\eta)[01]\alpha_3\alpha_3} + A_{13(10)}^{(\tau\eta)[10]\alpha_3\alpha_3}}{R_1} - \frac{A_{23(01)}^{(\tau\eta)[01]\alpha_3\alpha_3} + A_{23(01)}^{(\tau\eta)[10]\alpha_3\alpha_3}}{R_2} - A_{33(00)}^{(\tau\eta)[11]\alpha_3\alpha_3}$$

$$\widetilde{L}_{34nm}^{(\tau\eta)\alpha_3\alpha_4} = \frac{Z_{11(10)}^{(\tau\eta)[00]\alpha_3\alpha_4}}{R_1} + \frac{Z_{22(01)}^{(\tau\eta)[00]\alpha_3\alpha_4}}{R_2} + Z_{33(00)}^{(\tau\eta)[10]\alpha_3\alpha_4}$$

$$\widetilde{L}_{41nm}^{(\tau\eta)\alpha_4\alpha_1} = 0$$

$$\widetilde{L}_{42nm}^{(\tau\eta)\alpha_4\alpha_2} = 0$$

$$\widetilde{L}_{43nm}^{(\tau\eta)\alpha_4\alpha_3} = 0$$

$$\widetilde{L}_{44nm}^{(\tau\eta)\alpha_4\alpha_4} = K_{11(20)}^{(\tau\eta)[00]\alpha_4\alpha_4}\left(\frac{n\pi}{L_1}\right)^2 + K_{22(02)}^{(\tau\eta)[00]\alpha_4\alpha_4}\left(\frac{m\pi}{L_2}\right)^2 + K_{33(00)}^{(\tau\eta)[11]\alpha_4\alpha_4} \tag{A.2}$$

References

[1] Tzou HS. Piezoelectric shells: distributed sensing and control of continua. Kluwer Academic Publishers; 1993.
[2] Chee CY, Tong L, Steven GP. A review on the modelling of piezoelectric sensors and actuators incorporated in intelligent structures. J Intell Mater Syst Struct 1998;9:3–19.
[3] Chen Z, Akbarzadeh A. Advanced thermal stress analysis of smart materials and structures. Berlin: Springer; 2020.
[4] Brischetto S. Hygrothermal loading effects in bending analysis of multilayered composite plates. Comput Model Eng Sci 2012;88:367–417.
[5] Reddy JN, Barbosa JI. On vibration suppression of magnetostrictive beams. Smart Mater Struct 2000;9:49.
[6] Ikeda T. Fundamentals of piezoelectricity. Oxford University Press; 1996.
[7] Takenaka K. Negative thermal expansion materials: technological key for control of thermal expansion. Sci Technol Adv Mater 2012;13(2012):013001.
[8] Reddy JN. Mechanics of laminated composite plates and shells: theory and analysis. Boca Raton: CRC Press; 2003.
[9] Noor AK, Malik M. An assessment of five modeling approaches for thermo-mechanical stress analysis of laminated composite panels. Comput Mech 2000;25:43–58.
[10] Holzapfel GA. Nonlinear solid mechanics: a continuum approach for engineering science. John Wiley & Sons; 2002.
[11] Brischetto S, Torre R. Thermo-elastic analysis of multilayered plates and shells based on 1D and 3D heat conduction problems. Compos Struct 2018;206:326–53.
[12] Sayyad AS, Shinde BM, Ghugal YM. Thermoelastic bending analysis of laminated composite plates according to various shear deformation theories, open. Engineering 2014;5:18–30.
[13] He JF. Thermoelastic analysis of laminated plates including transverse shear deformation effects. Compos Struct 1995;30:51–9.
[14] Brischetto S, Torre R, Cesare D. Three-dimensional coupling between elastic and thermal fields in the static analysis of multilayered composite shells. Comput Model Eng Sci 2023;136:1–44.
[15] Cetkovic M. Thermo-mechanical bending of laminated composite and sandwich plates using layerwise displacement model. Compos Struct 2015;125:388–99.
[16] Albarody TMB, Al-Kayiem HH. Dynamic analysis of laminated composite thermo-magneto-electro-elastic shells. J Mech Sci Technol 2014;28:4877–91.
[17] Joshan YS, Neeraj G, Singh BN. Analytical modelling for thermo-mechanical analysis of cross-ply and angle-ply laminated composite plates. Aerosp Sci Technol 2017;70:137–51.
[18] Vinyas M, Kattimani SC. Hygrothermal analysis of magneto-electro-elastic plate using 3D finite element analysis. Compos Struct 2017;180:617–37.
[19] Moayedi H, et al. Application of nonlocal strain–stress gradient theory and GDQEM for thermo-vibration responses of a laminated composite nanoshell. Eng Comput 2021;37:3359–74.
[20] Liu B, et al. Three-dimensional thermo-mechanical solutions of cross-ply laminated plates and shells by a differential quadrature hierarchical finite element method. Compos Struct 2019;208:711–24.
[21] Panda SK, Katariya PV. Stability and free vibration behaviour of laminated composite panels under thermo-mechanical loading, international journal of. Applied and Computational Mathematics 2015;1:475–90.
[22] Tornabene F. Hygro-thermo-magneto-electro-elastic theory of anisotropic doubly-curved shells. Bologna: Esculapio; 2023.
[23] Khare RK, Kant T, Garg AK. Closed-form thermo-mechanical solutions of higher-order theories of cross-ply laminated shallow shells. Compos Struct 2003;59:313–40.
[24] Tornabene F, Viscoti M, Dimitri R. Effect of porosity on the modal response of doubly-curved laminated shell structures made of functionally graded materials employing higher order theories. Structures 2024;60:105848.
[25] Panduro RMR, Mantari JL. Hygro-thermo-mechanical behavior of classical composites using a new trigonometrical shear strain shape function and a compact layerwise approach. Compos Struct 2017;160:378–91.

[26] Wu Z, Chen W, Ren X. Refined global–local higher-order theory for angle-ply laminated plates under thermo-mechanical loads and finite element model. Compos Struct 2009;88:643–58.
[27] Liew KM, Pan ZZ, Zhang LW. An overview of layerwise theories for composite laminates and structures: development, numerical implementation and application. Compos Struct 2019;216:240–59.
[28] Brischetto S, Carrera E. Thermal stress analysis by refined multilayered composite shell theories. J Therm Stresses 2008;32:165–86.
[29] Tornabene F, Viscoti M, Dimitri R. Generalized higher order layerwise theory for the dynamic study of anisotropic doubly-curved shells with a mapped geometry. Eng Anal Bound Elem 2022;134:147–83.
[30] Reddy JN. An evaluation of equivalent-single-layer and layerwise theories of composite laminates. Compos Struct 1993;25:21–35.
[31] Tornabene F, Fantuzzi N, Bacciocchi M, Reddy JN. An equivalent layer-wise approach for the free vibration analysis of thick and thin laminated and sandwich shells. Appl Sci 2016;7:17.
[32] Icardi U, Sola F. Assessment of recent zig-Zag theories for laminated and sandwich structures. Compos B Eng 2016;97:26–52.
[33] Murakami H. Laminated composite plate theory with improved in-plane responses. ASME Journal of Applied Mechanics 1986;53:661–6.
[34] Tornabene F, Viscoti M, Dimitri R. On the importance of the recovery procedure in the semi-analytical solution for the static analysis of curved laminated panels: comparison with 3D finite elements. Materials 2024;17:588.
[35] Gherlone M. On the use of zigzag functions in equivalent single layer theories for laminated composite and sandwich beams: a comparative study and some observations on external weak layers. J Appl Mech 2013;80:061004.
[36] Tessler A, Di Sciuva M, Gherlone M. Refined zigzag theory for laminated composite and sandwich plates. NASA Technical Publication; 2009. 20090007494.
[37] Tessler A, Di Sciuva M, Gherlone M. A consistent refinement of first-order shear deformation theory for laminated composite and sandwich plates using improved zigzag kinematics. J Mech Mater Struct 2010;5:341–67.
[38] Washizu K. Variational methods in Elasticity & Plasticity. Oxford: Pergamon Press; 1975.
[39] Reddy JN. A generalization of two-dimensional theories of laminated composite plates. Communications in Applied Numerical Methods 1987;3:173–80.
[40] Wang CM, Reddy JN, Lee KH. Shear deformable beams and plates: relationships with classical solutions. Amsterdam: Elsevier; 2000.
[41] Tornabene F, Viscoti M, Dimitri R, Reddy JN. Higher order theories for the vibration study of doubly-curved anisotropic shells with a variable thickness and isogeometric mapped geometry. Compos Struct 2021;267:113829.
[42] Mantari JL, Soares CG. Analysis of isotropic and multilayered plates and shells by using a generalized higher-order shear deformation theory. Compos Struct 2012;94:2640–56.
[43] Carslaw HS, Jaeger JC. Conduction of heat in solids. Oxford University Press; 1947.
[44] Landau LD, Lifshitz EM. The classical theory of fields. Oxford: Pergamon Press; 1951.
[45] Gaskell DR. Introduction to the thermodynamics of materials. New York: Taylor & Francis; 2003.
[46] G.C. Sih, J.G. Michopoulos, S.C. Chou, Hygrothermoelasticity, Martinus Nijhoff Publishers, 1986.
[47] Incropera FP, DeWitt DP, Bergman TL, Lavine AS. Fundamentals of heat and mass transfer. John Wiley & Sons; 1996.
[48] Pagano NJ. Exact solutions for composite laminates in cylindrical bending. J Compos Mater 1969;3:398–411.
[49] Pagano NJ. Exact solutions for rectangular bidirectional composites and sandwich plates. J Compos Mater 1970;4:20–34.
[50] Thai HT, Kim SE. Analytical solution of a two variable refined plate theory for bending analysis of orthotropic levy-type plates. Int J Mech Sci 2012;54:269–76.
[51] Brischetto S. Exact elasticity solution for natural frequencies of functionally graded simply-supported structures, computer modeling in engineering. Science 2013;95:391–430.
[52] Groh RMJ, Weaver PM. Static inconsistencies in certain axiomatic higher-order shear deformation theories for beams, plates and shells. Compos Struct 2015;120:231–45.
[53] Tornabene F, Reddy JN. FGM and laminated doubly-curved and degenerate shells resting on nonlinear elastic foundations: a GDQ solution for static analysis with a posteriori stress and strain recovery. J Indian Inst Sci 2013;93:635–88.
[54] Tornabene F, Viscoti M, Dimitri R. Static analysis of doubly-curved shell structures of smart materials and arbitrary shape subjected to general loads employing higher order theories and generalized differential quadrature method, computer methods in engineering. Science 2022:22210.
[55] Tornabene F, Viscoti M, Dimitri R. Static analysis of anisotropic doubly-curved shell subjected to concentrated loads employing higher order layer-wise theories, computer methods in engineering. Science 2022:22237.
[56] Tornabene F. Generalized differential and integral quadrature. Bologna: Esculapio; 2023.
[57] Bert CW, Malik M. Differential quadrature method in computational mechanics: a review. Appl Mech Rev 1996;49:1–28.
[58] Shu C, Richards BE. Application of generalized differential quadrature to solve two-dimensional incompressible navier-stokes equations. Int J Numer Meth Fluids 1992;15:791–8.
[59] Shu C. Differential quadrature and its application in engineering. Berlin Heidelberg: Springer Science & Business Media; 2012.
[60] Reddy JN. Introduction to the finite element method. New York: McGraw-Hill Education; 2019.
[61] Zienkiewicz OC, Taylor RL. The finite element method: solid mechanics, Vol. 2. New York: McGraw-Hill; 1967.
[62] Tornabene F, Viscoti M, Dimitri R, Rosati L. Dynamic analysis of anisotropic doubly-curved shells with general boundary conditions, variable thickness and arbitrary shape. Compos Struct 2023;309:116542.
[63] Du H, Lim MK, Lin R. Application of generalized differential quadrature method to structural problems. Int J Numer Meth Eng 1994;37:1881–96.
[64] Striz AG, Wang X, Bert CW. Harmonic differential quadrature method and applications to analysis of structural components. Acta Mech 1995;111:85–94.
[65] Civalek Ö. Application of differential quadrature (DQ) and harmonic differential quadrature (HDQ) for buckling analysis of thin isotropic plates and elastic columns. Eng Struct 2004;26:171–86.
[66] Shu C, Xue H. Explicit computation of weighting coefficients in the harmonic differential quadrature. J Sound Vib 1997;204:549–55.
[67] Chen W, Wang X, Zhong T. The structure of weighting coefficient matrices of harmonic differential quadrature and its applications. Commun Numer Methods Eng 1996;12:455–9.
[68] Shu C, Chen W, Xue H, Du H. Numerical study of grid distribution effect on accuracy of DQ analysis of beams and plates by error estimation of derivative approximation. Int J Numer Meth Eng 2001;51:159–79.
[69] Shu C, Chen W. On optimal selection of interior points for applying discretized boundary conditions in DQ vibration analysis of beams and plates. J Sound Vib 1999;222:239–57.
[70] Tornabene F, Viscoti M, Dimitri R. Free vibration analysis of laminated doubly-curved shells with arbitrary material orientation distribution employing higher order theories and differential quadrature method. Eng Anal Bound Elem 2023;152:397–445.
[71] Alibeigloo A, Emtehani A. Static and free vibration analyses of carbon nanotube-reinforced composite plate using differential quadrature method. Meccanica 2015;50:61–76.
[72] Tornabene F, Viscoti M, Dimitri R. Equivalent Layer-Wise Theory for the Hygro-Thermo-Magneto-Electro-Elastic Analysis of Laminated Curved Shells. Thin-Walled Struct 2024. https://doi.org/10.1016/j.tws.2024.111751.
[73] Sobhy M. Differential quadrature method for magneto-hygrothermal bending of functionally graded graphene/Al sandwich-curved beams with honeycomb core via a new higher-order theory. J Sandw Struct Mater 2021;23:1662–700.
[74] Fung T. Solving initial value problems by differential quadrature method—part 1: first-order equations. Int J Numer Meth Eng 2001;50:1411–27.
[75] Tornabene F, Dimitri R. A numerical study of the seismic response of arched and vaulted structures made of isotropic or composite materials. Eng Struct 2018;159:332–66.
[76] Chen CN. Extended GDQ and related discrete element analysis methods for transient analyses of continuum mechanics problems. Comput Math Appl 2004;47:91–9.
[77] Bellman R, Casti J. Differential quadrature and long-term integration. J Math Anal Appl 1971;34:235–8.
[78] Liu GR, Wu TY. Application of generalized differential quadrature rule in blasius and onsager equations. Int J Numer Meth Eng 2001;52:1013–27.
[79] Xing Y, Liu B. A differential quadrature analysis of dynamic and quasi-static magneto-thermo-elastic stresses in a conducting rectangular plate subjected to an arbitrary variation of magnetic field. Int J Eng Sci 2010;48:1944–60.
[80] Dai T, Dai HL, Liu ZY. Multi-field mechanical behavior of a rotating porous FGMEE circular disk with variable thickness under hygrothermal environment. Compos Struct 2019;210:641–56.
[81] Mohammadimehr M, Salemi M, Navi BR. Bending, buckling, and free vibration analysis of MSGT microcomposite Reddy plate reinforced by FG-SWCNTs with temperature-dependent material properties under hydro-thermo-mechanical loadings using DQM. Compos Struct 2016;138:361–80.
[82] Mohammadimehr M, Emdadi M, Afshari H, Navi BR. Bending, buckling and vibration analyses of MSGT microcomposite circular-annular sandwich plate under hydro-thermo-magneto-mechanical loadings using DQM. International Journal of Smart and Nano Materials 2018;9:233–60.
[83] Hong CC. Transient responses of magnetostrictive plates by using the GDQ method. European Journal of Mechanics-A/Solids 2010;29:1015–21.
[84] Malik M, Bert CW, Kukreti AR. Differential quadrature solution of uniformly loaded circular plate resting on elastic half-space. WIT Trans Eng Sci 1993;1:385–96.
[85] Tornabene F, Viscoti M, Dimitri R. Static analysis of anisotropic doubly-curved shells with arbitrary geometry and variable thickness resting on a Winkler-pasternak support and subjected to general loads. Eng Anal Bound Elem 2022;140:618–73.
[86] Bouderba B, Houari MSA, Tounsi A. Thermomechanical bending response of FGM thick plates resting on Winkler-pasternak elastic foundations. Steel Compos Struct 2013;14:85–104.